Title: The Role of Molecular Mobility in Governing the Physical Stability of Amorphous Pharmaceuticals

Author: Karolina Adrjanowicz

University of Silesia

Department of Mathematics, Physics and Chemistry

Karolina Adrjanowicz

The Role of Molecular Mobility in Governing the Physical Stability of Amorphous Pharmaceuticals

Ph. D. thesis

Supervisor: Prof. Marian Paluch

Katowice 2012

INNOWACYJNA GOSPODARKA
NARODOWA STRATEGIA SPÓJNOŚCI

FNP
Fundacja na rzecz Nauki Polskiej

UNIA EUROPEJSKA
EUROPEJSKI FUNDUSZ
ROZWOJU REGIONALNEGO

ACKNOWLEDGEMENTS

The research described in this Ph. D. dissertation was financially supported by the Foundation for Polish Science, within the TEAM project entitled "From Study of Molecular Dynamics in Amorphous Medicines at Ambient and Elevated Pressure to Novel Applications in Pharmacy" (Contract No. TEAM/2008–1/6), co-financed by the EU European Regional Development Fund. Moreover, I wish to thank people who have supported me over a stretch of four years of my Ph. D. studies.

Firstly, I wish to give special thanks to my supervisor, Profesor Marian Paluch, who has been a faithful source of wisdom, creative ideas and constructuve criticism. I am grateful for sharing his time in plenty of interesting and inspiring discussions, thus allowing me to benefit from his broad experience and knowledge.

I am also indebted to many of my peers from Dielectric Spectroscopy Group for providing a pleasant working atmosphere, fruitful discussions, and collaboration in conducting experiments.

Finally, I wish to thank my family for everlasting support and their commitment supporting me at the best and the worst of times.

TABLE OF CONTENTS

PREFACE **5**

1. AMORPHOUS SOLIDS **11**

1.1. General information about the amorphous state 11

1.2. Preparation of amorphous materials 13

1.2.1. Physical methods of amorphization 14

1.2.2. Chemical methods of amorphization 17

1.2.3. Effect of preparation method and water content on physical stability of amorphous materials 17

2. SUPERCOOLED LIQUIDS AND GLASSES **19**

2.1. Phenomenology of the glass transition 19

2.2. Models of the glass transition 22

2.2.1. Free-Volume models 23

2.2.2. Entropy models 23

2.2.3. Two Order Parameter Model (TOP) 24

3. MOLECULAR DYNAMICS IN SUPERCOOLED AND GLASSY STATES **25**

3.1. Theoretical backgrounds of dielectric response in supercooled liquids 26

3.1.1. Dielectric Polarization in time-dependent electric field 26

3.1.2. Debye and Non-Debye Relaxations 28

3.1.3. Relaxation versus Retardation 31

3.2. Slow dynamics - Structural relaxation 32

3.2.1. Temperature dependence of the structural relaxation time above T_g 32

3.2.2. Temperature dependence of the structural relaxation time below T_g 37

3.2.3. Dynamics of supercooled liquids at high pressure 39

3.3. Excess wing and Secondary relaxations 42

4. EXPERIMENTAL **46**

4.1. Experimental Methods 46

4.1.1. Dielectric Spectroscopy (DS) 46

4.1.2. Differential Scanning Calorimetry (DSC) 49

4.1.3. The X-ray diffraction (XRD) 50

4.2. Description of investigated materials and applied amorphization methods 52

5. ANALYSIS AND PRESENTATION OF EXPERIMENTAL RESUTS OBTAINED AT ATMOSPHERIC PRESSURE 57
5.1. Do dynamical properties of amorphous materials depends on the preparation method? . 57
5.1.1. Telmisartan 57
5.1.2. Antibiotics 62
5.2. How to predict the time scale of structural relaxation below T_g ? 67
5.2.1. Telmisartan 68
5.3. What Governs the Physical Stability of Amorphous Pharmaceuticals? Global Mobility, Local Mobility or Maybe Something Else? 75
5.3.1. DNA and RNA nucleosides 75
5.3.2. Glucose derivatives 90
5.3.3. Antibiotics 97
6. ANALYSIS AND PRESENTATION OF EXPERIMENTAL RESUTS OBTAINED AT ELEVATED PRESSURE 101
6.1. What is the effect of pressure on molecular dynamics and crystallization kinetics of Ibuprofen? 101
7. CONCLUSION 114
REFERENCES 119

PREFACE

According to statistics, over 80% of drugs are being sold in solid dosage forms. About 40% of examined drug candidates turned out to be poorly water-soluble, which results in their insufficient bioavailability [1]. Unfortunately, despite years of research Active Pharmaceutical Ingredients (APIs) belonging to the second (low solubility, high permeability) and fourth class (low solubility, low permeability) of the Biopharmaceutical Classification System (BCS) are still the most challenging molecules for modern pharmacy [2]. Solubility issue is a major concern in the case of drugs used in chronic diseases such as cardiovascular, psychiatric and rheumatological [3], resulting in necessity of frequent administration pharmaceuticals with increased API dose, rising medical treatment costs and causing unwanted side effects. Since solubility is one of the most important physicochemical properties in pharmaceutical product design, diverse attempts have been made to improve it. This include changing drugs into better soluble hydrochloric salts, the usage of polymeric matrixes, cyclodextrins and micronization [4, 5, 6].

Typically, solid dosage form contains a well-defined crystalline from of API. This is very rational procedure, because crystalline materials are generally physically and chemically stable during product shelf life. Moreover, it is very easy to develop repeatable way of their synthesis and analysis. Unfortunately, in most cases the crystalline form of drug has insufficient or unsatisfactory water-solubility in physiological pH range, as stability and solubility go in opposite directions.

One of the most promising methods for improving solubility as well as dissolution profile of poorly water-soluble drugs is preparation pharmaceutically active substances in the amorphous form. It is established, that solubility as well as dissolution rate of amorphous APIs in water are orders of magnitude greater than crystalline counterparts, which might result in significant improvement of their bioavailability [7, 8, 9]. The advantages of amorphous state given in terms of better solubility and dissolution rate are well presented in Table I and Figure I. It is also worth mentioning that properly designed tablets' formulations with amorphous form of API might have better direct compression parameters [10].

The enhanced solubility of amorphous drugs stems from specific thermodynamic properties of the amorphous state. The enthalpy, entropy and free energy of amorphous solid are always higher than its crystalline counterpart, and this higher free energy results in greater solubility of amorphous pharmaceuticals. However, preparation of active substances in the amorphous

state entails als considerable risks. Firstly, the amorphous state is an out of equilibrium state and tends to revert to thermodynamically stable crystalline form over the time course of processing, storage, and use of the product [11, 12]. As a consequence, the advantages given in terms of better solubility and bioavailability are completely lost. Secondly, as a result of greater chemical reactivity the amorphous pharmaceuticals are prone to chemical degradation [13]. This might result in altering the indented therapeutic effect of the drug. Thus, the main challenge in working with amorphous APIs involves thorough identification and understanding of the critical factors responsible for chemical instability and recrystallization from the amorphous state. If that succeed, fully aware stabilization protocol will be finally designed.

Table I. Solubility of crystalline and amorphous forms of Azithromycin. Data were taken from [14].

Solubility (mg/ml)	water		Acetate buffer 4.5		0.1N HCl	
	cryst.	amorph.	cryst.	amorph.	cryst.	amorph.
37° C	0.03	0.12	13.8	23.5	5.5	7.9

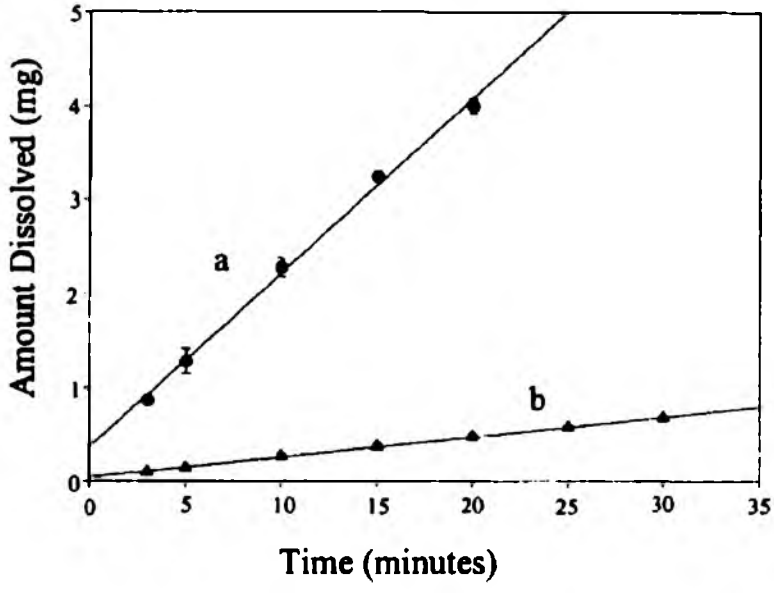

Figure I. Intrinsic dissolution rates of ritonavir in 0.1 N HCl at 37°C: (a) amorphous (0.3 mg/cm^2 – min), (b) crystalline (0.03 mg/cm^2 – min). Reprinted from [15].

One thing must be made clear before we proceed further. Terms: 'pharmaceutical', 'drug' or 'medicine' refer to the final dosage form that contains not only Active Pharmaceutical Ingredients, but also excipients such as: blinders, lubricants, sweeteners or colors. However, in the context of discussed issues only the former ones are being prepared in the amorphous state. In this work I will use alternative terms 'amorphous pharmaceuticals' and 'amorphous drugs', as they are commonly used in scientific jargon. Anyway, one should bear in mind that both mentioned above terms will refer only to 'amorphous form of API'.

Herein, it is worth mentioning that within last years significant progress has been made in exploring our knowledge about stability of amorphous materials. However, there is still much to do, since the entire recrystallization phenomenon cannot be simply explained. Another hindrance is great number of parameters affecting physical stability of amorphous materials. The principal factors that have significant influence on crystallization from the amorphous state are: degree of molecular mobility, thermodynamic factor, amount of water content (the presence of water usually favors crystallization), amorphization method, addition of surfactants (or excipients), mechanical stress [16, 17, 18]. More so, in order to thoroughly analyze physical stability of amorphous solids it is necessary to consider many other aspects which may also affect nucleation and crystal growth rate such as specific surface area (the larger surface area the greater physical instability of the amorphous material) and surface mobility [19, 20].

Many investigators dealing with amorphous systems admit that molecular mobility seems to be the key parameter affecting their physical and chemical stability [21, 22, 23]. This way of thinking is justified, because molecules need to rearrange in order to incorporate into crystal lattice. However, in the literature there are no systematic and qualitative studies on that issue. As a results, many important questions are still not answered. For example, *is it possible to predict long-term stability of amorphous APIs basing only on their molecular mobility?* Another, very important aspect is *whether dynamical properties of amorphous materials depend on preparation way, or irrespectively of the amorphization technique we get the same amorphous solid with identical molecular dynamics.* And finally, the most hotly debated one - *what governs the physical stability of amorphous materials? Is it the global mobility associated with structural relaxation, local mobility of intermolecular origin (Johari-Goldstein secondary relaxation) or maybe other parameters of much greater importance?*

In this work to address the above questions I have made an attempt to study the molecular dynamics of different pharmaceutically important substances by means of Broadband Dielectric Spectroscopy (BDS). Dielectric spectroscopy was chosen as the main experimental technique, because it enables observation of relaxation processes of different molecular origin that appear in the supercooled liquid and glassy states in the wide range of frequencies, temperatures and even elevated pressure. Herein, it is worth noticing that the effect of pressure on molecular dynamics might be significant and by application of pressure in studying dynamical properties of glass-formers completely new and valuable information can be gained [24]. Thus, in my studies I have also performed high-pressure experiments on selected drug substance. There is a big need to perform these types of experiments, because firstly there is no systematic studies on the effect of pressure on amorphous pharmaceuticals and secondly pressure can affect both, molecular dynamics and thermodynamic properties of the glass-forming materials, for example: molecular packing, thermal expansion behavior, fragility and so on. Moreover, as speculated very recently by Hajime Tanaka pressure is the only thermodynamic variable that actually controls crystallization abilities of glass-formers [25]. Hence, in this Ph. D. dissertation I have also tried to address the following fundamental questions: *What is the effect of pressure on molecular dynamics and crystallization kinetics of glass-forming materials? Is it possible to obtain highly-stable glass by compression of liquid at high temperature?* or *Does increased pressure inhibit crystallization of glass-formers?* In order to answer these questions, I have performed pioneering isostructural crystallization kinetics experiments, at different T and P combinations while keeping the structural relaxation time.

As the supporting techniques, I have used Differential Scanning Calorimetry (DSC) and X-Ray Powder Diffraction (XRD). The former technique was used to evaluate the basic thermodynamic properties of investigated materials, while the latter one to verify their long-term stability.

This work is structured as follows: Chapter 1 gives an introduction to the amorphous state and amorphization methods. In Chapter 2 phenomenology of the glass transition and glass transition models are briefly described. The backgrounds of molecular dynamics in supercooled and glassy states are given in Chapter 3. The principles of experimental techniques, preparation methods and brief characterization of examined compounds can be found in Chapter 4. Chapters 5 and 6 present the experimental results from studies at ambient

and elevated pressure, respectively. Finally, Chapter 7 summarizes obtained results and gives perspective on future studies.

Results presented in this theses have been published in the following publications of mine:

1. Adrjanowicz K., Wojnarowska Z., Wlodarczyk P., Kaminski K., Paluch M., Mazgalski J., 2009, *Molecular mobility in liquid and glassy states of Telmisartan (TEL) studied by Broadband Dielectric Spectroscopy*, Eur. J. Pharm. Sci. 38, 395

2. Adrjanowicz K., Kaminski K., Paluch M., Wlodarczyk P., Grzybowska K., Wojnarowska Z., Hawelek L., Sawicki W., Lepek P., Lunio R., 2010, *Dielectric relaxation studies and dissolution behavior of amorphous verapamil hydrochloride*, J. Pharm. Sci. 99(2):828-39

3. Adrjanowicz K., Kaminski K., Wojnarowska Z., Dulski M., Hawelek L., Pawlus S., Paluch M., 2010, *Dielectric Relaxation and Crystallization Kinetics of Ibuprofen at Ambient and Elevated Pressure*, J. Phys. Chem. B, 114 (19), pp 6579–6593

4. Adrjanowicz K., Paluch M., Ngai K. L., 2010, *Determining the structural relaxation times deep in the glassy state of the pharmaceutical Telmisartan*, J. Phys.: Condens. Matter, 22, 125902

5. Adrjanowicz K., Grzybowska K., Kaminski K., Hawelek L., Paluch M., Zakowiecki D., 2011, *Comprehensive studies on physical and chemical stability in liquid and glassy states of Telmisartan (TEL): Solubility advantages given by cryomilled and quenched material*, Phil. Magazine, 91, 1926-1948

6. Adrjanowicz K., Wojnarowska Z., Paluch M., Piontek J., 2011, *Thermodynamic scaling of molecular dynamics in supercooled ibuprofen*, J. Phys. Chem. B, 11(16) 4559-67

7. Adrjanowicz K., Kaminski K., Grzybowska K., Hawelek L., Paluch M., Gruszka I., Zakowiecki D., Sawicki W., Lepek P., Kamysz W., Guzik L., 2011, *Effect of Cryogrinding on Chemical Stability of the Sparingly Water-Soluble Drug Furosemide*, Pharmaceutical Research 2011, 28, 3220-3236

8. Kaminski K., Adrjanowicz K., Wojnarowska Z., Paluch M., Kaminska E., Kasprzycka A., 2011, *Do intermolecular interactions control crystallization abilities of glass forming liquids?* J. Phys. Chem. B. 115 (40), pp 11537–11547

9. Adrjanowicz K., Grzybowski A., Kaminski K., Paluch M., 2011, *Temperature and Volume Effect on the Molecular Dynamics of Supercooled Ibuprofen at Ambient and Elevated Pressure*, Mol. Pharmaceutics, *8* (5), pp 1975–1979

10. Adrjanowicz K., Wojnarowska Z., Grzybowska K., Hawelek L., Kaminski K., Paluch M., Kasprzycka A., Walczak K., *Molecular dynamics and crystallization phenomenon of supercooled and glassy DNA and RNA nucleosides: β-adenosine, β-thymidine and β-uridine,* Phys. Rev. E 2011, 84, 051507

11. Adrjanowicz, K.; Paluch, M.; Kaminski, K.; Ngai, K. L.; Yu, L.; *Study of dynamics and crystallization kinetics of ROY at ambient and elevated pressure* J. Chem. Phys (accepted for publication)

12. Adrjanowicz, K.; Kaminski, K.; Grzybowska, K.; Hawelek, L.; Zakowiecki, D.; Cal, K.;, Tarnacka, M.; *Molecular Dynamics in Supercooled Liquid and Glassy State of Antibiotics: Azithromycin, Clarithromycin and Roxithromycin Studied by Dielectric Spectroscopy. Advantages Given by the Amorphous State,* Mol. Pharmaceutics 2012, Just Accepted Manuscript, DOI: 10.1021/mp300067r

13. Adrjanowicz K., Paluch M., *Mielenie jako alternatywna metoda otrzymywania substancji leczniczych w formie amorficznej*, Farmacja Polska, 2011, 6, 384-393 (in polish)

CHAPTER 1

AMORPHOUS SOLIDS

Within the last 30 years there has been observed a growing interest in the amorphous solids and a large number of the proposed futuristic and next-generation materials turned out to be amorphous. This include amorphous semiconductors, ceramics and metallic glasses [26, 27]. The latter one are even supposed to be stronger and tougher than steel. However, amorphous materials are not something new. They are known and used by human beings for thousands of years. Although the best example of amorphous solid is window glass made from silica, the amorphous or glassy behavior can be found for much wider group of materials starting from ceramics, polymers, metals to soft matter and biological systems. Glassy formation is also ubiquitous in nature, allowing preservation of numerous insects and small organisms in extremely cold or dehydrated conditions [28]. Food and pharmaceuticals are sometimes unintentionally prepare in the amorphous state during manufacturing processing. When improvement of solubility and bioavailability is desired, pharmaceutically important substances are deliberately formed in the amorphous state.

1.1. General information about the amorphous state

To begin with, amorphous materials are bona fide solids and share the essential attributes of the solid state as crystals. However, there is a fundamental difference between the amorphous and crystalline states. In perfect crystals, atoms are arranged in a pattern that repeats periodically in three dimension to an infinite extent. In amorphous solids, long-range order is absent and there is no translational periodicity, as that known for crystals. This fundamental difference is evident at a first glance in Figure 1.1.

The lack of long-range order, or periodicity, characteristic for amorphous solid is clearly visible in X-ray diffraction patterns, where instead of sharp Bragg's peaks produced by crystalline sample, a broad hallo pattern is observed (Figure 1.2). However, it doesn't mean complete lack of order, because in amorphous materials there can still be found medium-range ordering (of the order of 5-20 Å) and short-range ordering (of the order of a few Å) [29]. What is more, in amorphous solids degree of local order might be very high. This is what they have in common with crystals, high degree of short range order [30]. The

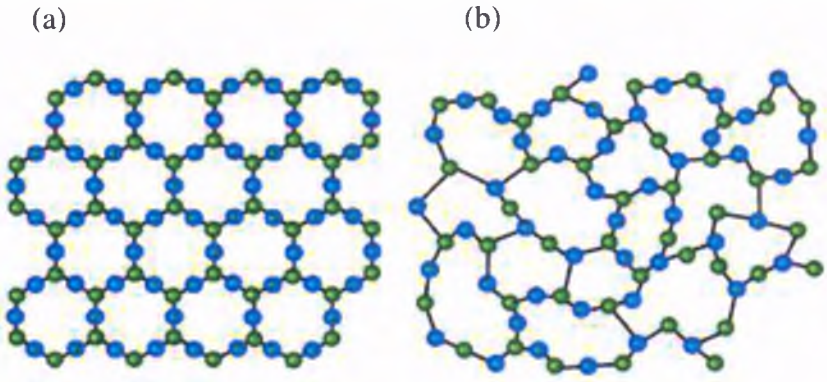

Figure 1.1. Schematic sketches illustrating differences in atomic arrangements in (a) crystalline and (b) amorphous solids. Figure was taken from [31].

amorphous state is also thermodynamically less stable than the corresponding crystalline state (i.e. it possesses a greater free energy). As a result amorphous materials revert to thermodynamically stable crystalline form. It is only the matter of time scale of this transition, which depends mainly on storage temperature and humidity conditions.

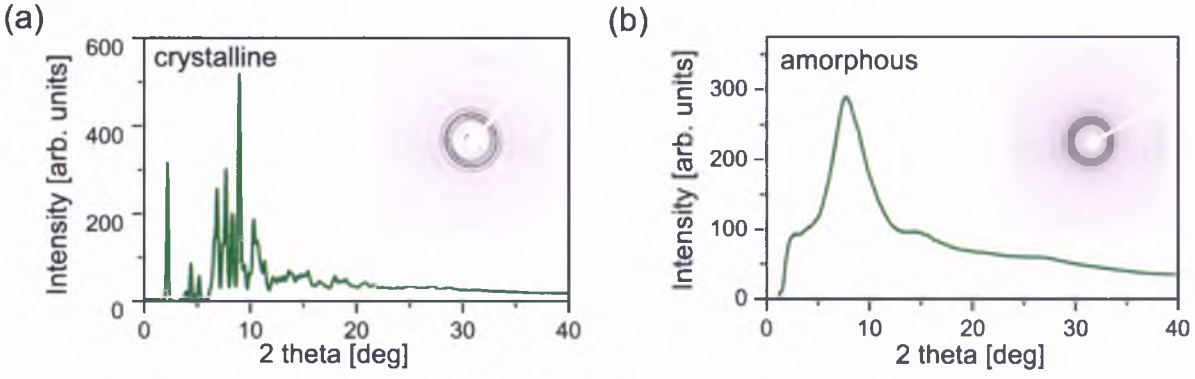

Figure 1.2. X-ray powder diffraction patterns for (a) amorphous and (b) crystalline solids.

Herein, it should be noted that term 'amorphous solid' is the general one that applies to any solid having a non-periodic atom array. The term 'glass' is conventionally reserved for an amorphous solid prepared by rapid quenching of a melt (vitrification process). Sometimes both terms 'amorphous' and 'glass' are used synonymously. However, one must be bear in mind that glasses are just sub-set of amorphous materials. All glasses are amorphous, but not all amorphous solids are necessarily glasses [29].

1.2. Preparation of amorphous materials

For a very long time it was thought that only limited number of materials can be prepared in the amorphous state. Now, we know that amorphous state is ubiquitous and glass-forming ability is almost universal property of condensed matter. Accordingly to Turnbull's viewpoint *'nearly all materials can, if cooled fast enough and far enough, be prepared as amorphous solid'* [32]. Vitrification process is the oldest established method of producing an amorphous solid. However, over the past 50 years many amorphous systems have been prepared using various methods, other than traditional liquid-cooling. Alternative techniques for producing amorphous materials are schematically presented in Figure 1.3.

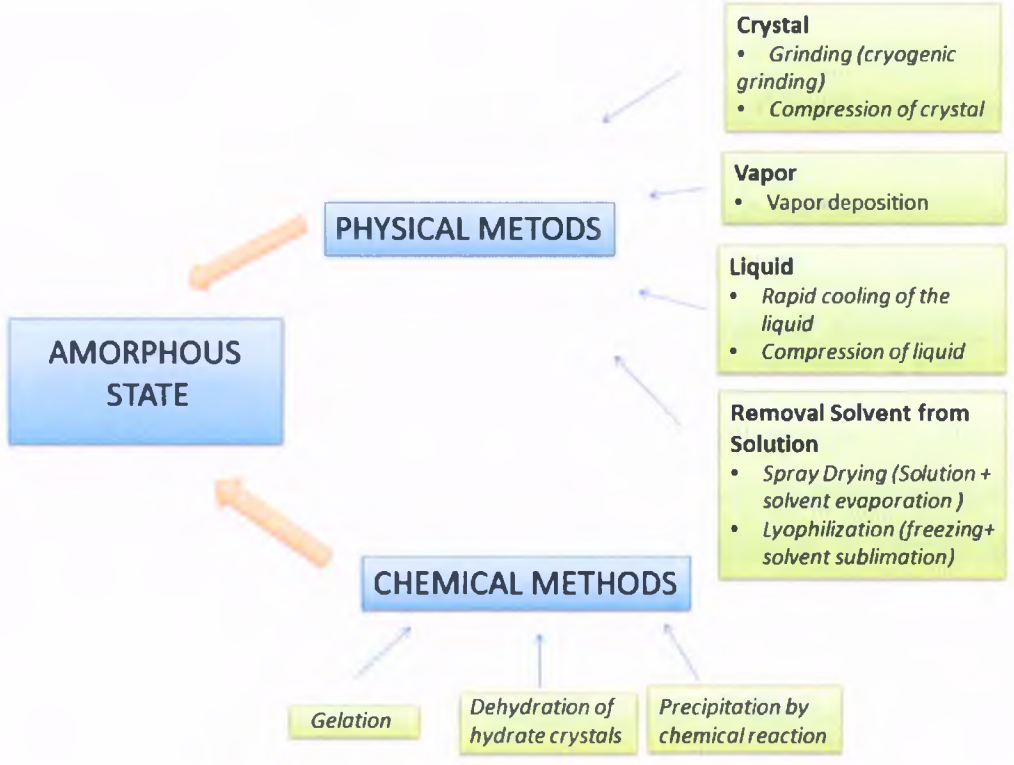

Figure 1.3. Various methods of formation of amorphous materials.

Generally, amorphization methods can be divided into two categories: physical and chemical. The essential difference between both methods is that in physical processes the composition of substances does not change during the formation process. The chemical methods accompany necessarily some changes in chemical potential of the system [33]. The physical methods are (1) rapid cooling of liquid, (2) compression of liquid, (3) deposition of vapor onto a cold substance, (4) freeze-drying, (5) spray-drying, (6) compression of crystal,

(7) mechanical milling. The chemical methods are: (8) gelation, (9) precipitation by chemical reaction, (10) dehydration of hydrate crystals.

It is worth noticing that given above amorphization methods list is not complete, because there are also other ways of preparation amorphous solids such as laser glazing, particle bombardment onto crystals and so on. However, there are not as common in pharmaceutical industry as that mentioned above. Both physical and chemical methods of amorphization will be briefly described below.

1.2.1. Physical methods of amorphization

1. The rapid cooling of the liquid – is the most familiar method. Developed in recent days hyper-quenching method with the cooling rate 10^6 $K \cdot s^{-1}$ allowed amorphization even water or metals which possess strong crystallization abilities [33].

2. Compression of liquid is a quite new technique. The basic of this method lies in the simple rule that pressurization of liquid gives the same effect as cooling of liquid. Thus, the amorphous state obtained as a result of liquid compression will be called in the further part of this work as a glassy state.

3. Vapor deposition is very important and powerful method. The starting compound is vaporized and the material is collected on a substrate kept at a temperature far below the hypothetical glass transition temperature T_g. Cold substrate causes atoms to be 'frozen' in the random positions at which they arrive.

4. Freeze-drying (or lyophilization) is a drying process in which solvent, typically water, is first frozen and then removed by sublimation under low pressure. The process consists of 3 main stages: freezing, primary- and secondary drying. After complete solidification in the first stage, the shelf temperature is slightly increased to supply heat for the sublimation of ice. The secondary drying includes removal of water from the solute phase by desorption at temperatures above room temperature.

5. Spray drying is a transformation of feed from a fluid state into a dried particulate form by spraying the feed into a hot drying medium.

6. Compression of crystal is very promising method allowing obtaining the amorphous state without passing the liquid state. The transformation crystalline to amorphous solid occurs when the free energy of crystal is raised above that of the amorphous state. High energy supplied to crystal in the form of compression is used to destroy the neatly ordered arrangements [33].

7. Mechanical milling - amorphization proceeds as a result of extended mechanical treatment of crystalline solid in a mill. Grinding is very useful method, particularly for compounds undergoing thermal degradation at the melting point, so it is impossible to prepare amorphous state by quenching of the liquid. It is also very suitable when examined material is poorly soluble in polar and non-polar solvents, so there is enormous problem associated with preparation homogeneous solutions for freeze- and spray-drying techniques.

Grinding of various types of crystalline materials can be performed at room temperature in a traditional ball-mill, or in a newly developed cryogenic impact milling devices immersed in liquid nitrogen (then it is called cryogrinding). Cryogrinding of pharmaceuticals is more efficient amorphization method than traditional ball-milling, as the material is completely frozen during that process. It was believed, for some time, that chemical degradation does not occur in this case, because the liquid nitrogen temperature should prevent from local temperature warm-up. However, cryogenic grinding has recently turned out to be very powerful and energizing method that can activate and accelerate not only structural changes, but also chemical decomposition of ground material [34]. Thus, in some cases cryogenic grinding device must be considered as a chemical reactor in which, under favorable conditions, chemical reactions are mechanically initiated.

In the case of mechanical milling, the nature of the 'end product' is strongly determined by the milling temperature, especially its relative position with respect to the glass transition temperature of examined material. This issue was firstly reported by Descamps and co-workers for pharmaceutical, fananserine [35]. The glass transition temperature of fananserine is 292 K. Mechanical milling of crystalline form III or IV performed at 298 K transforms fananserine into metastable crystalline form I. On the other hand, when milling is performed at 273 K, completely amorphous fananserine is obtained.

Interestingly, despite years of intensive studies the mechanism of solid state amorphization via mechanical milling is not clearly understood. The following theories have been proposed to explain this transformation:

(a) It has been suggested that during mechanical impact, a certain amount of mechanical energy is liberated. This can cause a local heating effect resulting in local melting of the sample followed by fast quenching. However, as demonstrated by Descamps et al. [36] in the amorphous state of carbohydrates undergoing mutarotation process obtained by ball-milling, there is only one pyranose anomer present, whereas in the glassy state obtained by melt quenching two anomers exist. It is worth mentioning that mutarotation is thermally activated

process and occurs only when carbohydrates are melted (or dissolved in aqueous solution). Thus, it is reasonable to believe that no significant increase of temperature upon milling occurs.

(b) The Lindemann criterion suggests that melting of a metastable crystal occurs when the sum of dynamic and static mean-square atomic displacements reaches a critical value identical to that for melting of the perfect crystal. It requires that the melting temperature of a defective crystal must decrease with increasing static atomic disorder and leads to a universal polymorphous melting curve for metastable crystals when the melting temperature is plotted as a function of mean-square static displacement. Within the framework of this more general melting concept, the crystalline-to-amorphous transformation is simply melting of a critically disordered crystal at temperatures where the supercooled liquid exists in a configurationally-frozen state i.e. the glassy state [37].

(c) The spontaneous production of lattice defects upon mechanical milling raises the energy of the system, thereby providing a thermodynamic driving force, which leads to amorphization [38].

(d) Amorphization occurs as a result of softening of the crystalline lattice vibrations, leading in a consequence to its collapse.

(e) 'Driven Material Concept' explains amorphization as competition between thermally independent disordering process induced by milling and diffusion effects which tend to revert the system to lower energy configurational states [39]. The physical state of the system upon milling at the real temperature T is that of the system in the absence of milling at an effective temperature [39]

$$T_{eff} = T\left(1+\frac{D_B}{D'}\right) \tag{1.1}$$

where D_B is ballistic jump frequency independent of the temperature, but depending on the milling intensity. D' is the rate of thermal jump which decreases with increasing temperature. At high temperature, thermal jumps restore the equilibrium so that $T \cong T_{eff}$ and milling has no practical influence on the physical state. At low temperature, thermal restoration become less efficient and T_{eff} increases. Consequently, amorphization will always occur at low milling temperature or alternatively high milling intensities, because only that time T_{eff} overcomes the value of the melting temperature.

1.2.2. Chemical methods of amorphization

8. Gelation – the sample in a sol is brought into a gel, and then removal of extra components forms corresponding amorphous state.

9. Precipitation by chemical reaction – some chemical reactions in solution produce amorphous precipitates.

10. Dehydration of hydrate crystals – removal of water from hydrated crystalline material at certain temperature results in disorder anhydrous sample that cannot keep anymore crystalline lattice. For example, Li and co-workers demonstrated that crystalline carbamazepine hydrate converts to an amorphous material (T_g=329 K) upon dehydration at 318 K [40]. Hydration of such anhydrous amorphous solids restores very easily the crystalline order.

In my studies, the amorphous systems of greatest pharmaceutical interest were obtained using following methods: melt quench, compression of liquid and cryogenic grinding.

1.2.3. Effect of preparation method and water content on physical stability of amorphous materials

Depending on the preparation method, the amorphous material might reveal differences in thermal behavior, water vapor sorption, surface energy, physical stability and so on. As an example one can mention indomethacin, known as a 'model amorphous drug'. The glassy state of indomethacin obtained by very slow cooling of liquid is stable against crystallization over two years, whereas the amorphous form obtained by cryogenic grinding recrystallizes to 90% after approximately 13–15 hours of storage at room temperature [41, 42]. It is generally claimed, that physical stability of amorphous materials prepared by grinding is reduced as compared to that obtained by quenching of liquid. Moreover, grinding produces large increase in specific surface area, which might result in considerable water uptake. It is established, that amorphous samples with higher particle size reach lower saturation level of crystallization (i.e. surface crystallization), when compared with samples having lower particle size. Moreover, scratched surface crystallizes rapidly indicating faster surface crystallization tendency [17].

The presence of water has also a significant influence on the stability of amorphous materials, because water acts as potential plasticizer and decreases the value of the glass transition temperature T_g. A typical profile of T_g against water uptake is presented in Figure 1.4.

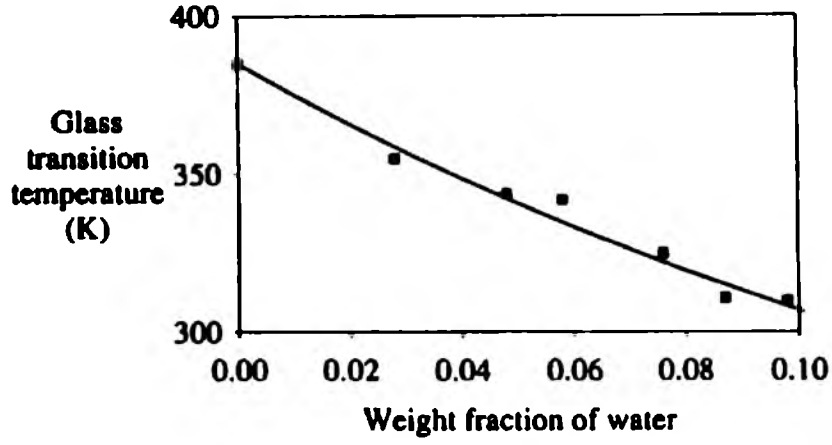

Figure 1.4. Variation of the glass transition temperature with water content for a freeze dried lactose. Reprinted from [43].

With increasing water concentration in amorphous solid the glass transition temperature T_g decreases accordingly to the Gordon–Taylor equation [44]

$$T_g^{mixt} = \frac{w_1 T_{g1} + k w_2 T_{g2}}{w_1 + k w_2} \tag{1.2}$$

where w_1 and w_2 are mass fractions of each component, T_{g1} and T_{g2} are the corresponding T_g values of each component. Thus, at particular temperature and humidity conditions the physical stability of amorphous system may change significantly, if it absorbs water. Surana and co-workers have studied the effect of water sorption on crystallization of trehalose prepared by quenching, spray-drying, lyophilization and dehydration [45]. They found out that vitrified material is the most resistant against crystallization, spray- and freeze- dried samples show similar crystallization abilities, whereas the least stable was dehydrated amorphous trehalose. Recently, Ediger and co-workers have shown that highly stable glasses can be formed by vapor deposition [46, 47, 48]. The physical stability of indomethacin glass produced in this way is comparable to that produced by aging an ordinary glass for 7 months. Moreover, highly stable vapor deposited glasses turned out to be nearly 2% denser and even 5 times more resistant to water uptake than glasses prepared by conventional cooling of the liquid.

As briefly described above, preparation method might have a significant impact on the physical stability of amorphous materials. This makes any comparative studies between properties of amorphous samples obtained using various techniques very challenging task.

CHAPTER 2

SUPERCOOLED LIQUIDS AND GLASSES

2.1. Phenomenology of the glass transition

When a liquid is cooled from high temperature two scenarios are possible. If slow cooling rate is applied crystallization takes place. This is the first-order transition accompanied by abrupt decrease of liquid's volume (or enthalpy), as illustrated in Figure 2.1. On the other hand, by cooling a liquid with sufficiently high cooling rate it is possible to avoid crystallization. Any liquid which does not crystallize at T_m enters into a metastable phase known as 'supercooled liquid', and is having higher free energy than crystal [49]. Upon cooling of supercooled liquid its viscosity increases and molecular motions slow down. However, molecules do not reach their equilibrium state immediately, but rather the liquid equilibrates to it with time. This process is known as structural relaxation (or α-relaxation), and it is associated with characteristic structural relaxation time τ_α. The alpha relaxation reflects cooperative rearrangements of molecules and is closely related to the viscosity i.e. as the viscosity increases with cooling, so does the time required for molecules to rearrange and reach equilibrium positions. At some temperature molecules will eventually move so slowly that cannot rearrange to their equilibrium positions before the temperature is lowered further. As a result, the liquid's volume falls out of equilibrium and such non-equilibrium system becomes a glass. This phenomenon is called 'glass transition', and the temperature associated with the glass transition is termed as 'glass transition temperature T_g' [49]. In practice, the glass transition temperature is usually defined as a temperature at which viscosity is 10^{13} Pa·s, and structural relaxation is of the order of 100 seconds. The structural relaxation changes from 100 s at T_g to thousands of years deep in the glassy state, so it is not possible to wait for the system to reach its thermodynamic equilibrium. As a consequence, it is impossible to directly follow the structural relaxation in the glassy state by any standard experimental setup. Thus, below T_g the liquid's structure is defined to be 'frozen' on the timescale of experimental observations.

As illustrated in Figure 2.1, formation of the glassy state is characterized by gradual break in slope of the T-V plot. The glass transition T_g can be estimated by extrapolation volume in

the glassy state back to the supercooled liquid line. The volume of the glass continues to decrease also below the glass transition temperature, although not as significant as in the liquid state. It is important to emphasize that the glass transition temperature depends upon cooling rate. Slow cooling rate produces 'Glass a', with the glass transition temperature T_{ga}, while fast cooling rate leads to 'Glass b' with the glass transition at temperature T_{gb}. However, the change of T_g as a result of different cooling rate usually does not exceed more than 3-5 K [49].

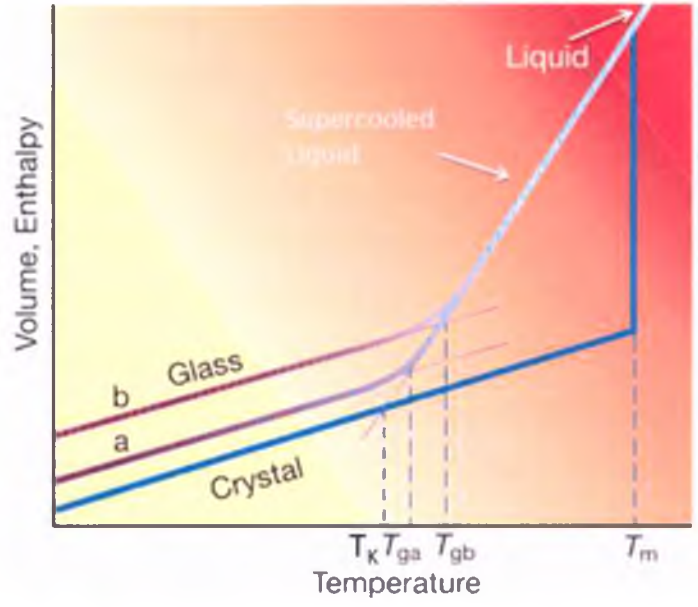

Figure 2.1. Temperature dependence of a liquid's volume (or enthalpy) from the region above the melting point to below the glass transition temperature. Original figure was taken from [50].

At the glass transition the heat capacity ($C_p = \partial H / \partial T$) and other thermodynamic derivatives such as thermal expansion ($\alpha_T = \partial \ln V / \partial T$) or compressibility ($\kappa_T = -(\partial \ln V / \partial p)_T$) reveal discontinuity. Figure 2.2 shows typical behavior of the heat capacity across glass transition region. Going from liquid to glassy state the specific heat capacity of supercooled liquid drops at T_g to lower value, close to the value of the crystalline state. On reheating and passing the glassy state, the enthalpy recovery peak shows up. This hysteresis results from the fact that below T_g the system slowly equilibrates with time (ages) and thermodynamic variables as well as their derivatives change. Moreover, the temperature at which the specific heat falls rapidly depends on the cooling rate of the liquid, i.e. upon slow cooling the curve shifts to lower temperature. Thus, thermodynamic properties of the glassy

state depend upon how the glass was formed. In case of pharmaceuticals as well as many non-pharmaceutical materials, it is established that the value of T_g is determined as the midpoint of the heat capacity increment measured during heating run.

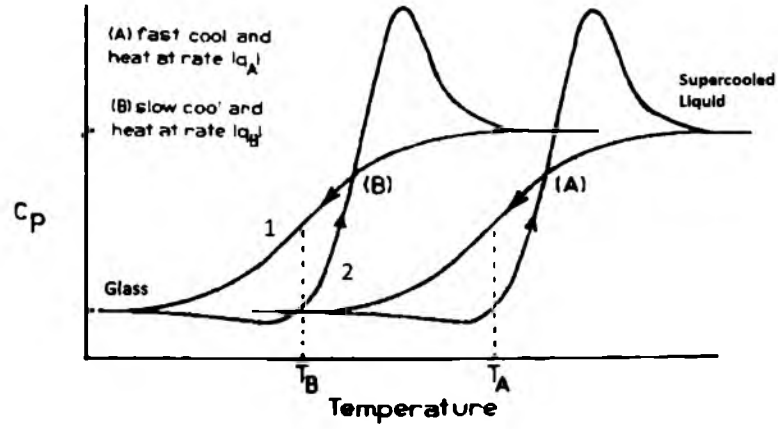

Figure 2.2. Temperature dependence of the specific heat recorded in vicinity of the glass transition region for different heating and cooling rates (Curves A and B). Line 1 refers to the data recorded upon cooling from supercooled melt to glassy state. Line 2 refers to glass reheating. Original figure was taken from [51].

Until now, one of the most hotly debated issues is whether the glass transition involves an underlying kinetic or thermodynamic phase transition [52]. The supporters of the former idea claims that the glass transition results from dynamic transition in the relaxation of the supercooled liquid which doesn't change thermodynamic properties of the liquid across the transition. This point of view was also confirmed by the Monte Carlo simulations [53]. From thermodynamic point of view, dynamical slowing down at the liquid-glass transition is manifestation of an underlying hidden thermodynamic transition. This explanation originates from the famous Kauzmann paradox. In the glassy state, below certain temperature T_K ($T_K \cong T_g - 50K$) the entropy of supercooled liquid would fall below that of the corresponding crystal causing 'entropy crisis'. Gibbs and Di Marzio [54] proposed the occurrence of a true thermodynamic phase transition at T_K, where the difference between the entropy of supercooled liquid and the entropy of corresponding crystalline material is supposed to vanish. Such thermodynamic transition at T_K would be characterized by discontinuity of the specific heat and viscosity divergence. Assuming that the vibrational entropy of the liquid is close to that of the crystal, the configurational entropy S_c (number of different configurational states that the system can visit), can be identified with the excess entropy ($S_{exces} = S_{liquid} - S_{crystal}$). Configurational entropy S_c should also vanish at T_K indicating

for possibility of existence 'ideal glass' (state with zero configurational entropy). However, the entropy crisis is in practice avoided by intervention of the glass transition and no matter how slowly the liquid is cooled, the glass transition should be always observed above T_K. In the glassy state, most of orientational degrees of freedom become frozen in. Thus, below T_g the entropy excess and consequently configurational entropy will no longer decrease with temperature, as it happens in the supercooled liquid (Figure 2.3). Unfortunately, the most significant difficulty associated with verification of the glass transition nature is that we cannot directly approach the structural relaxation time at temperature T_K.

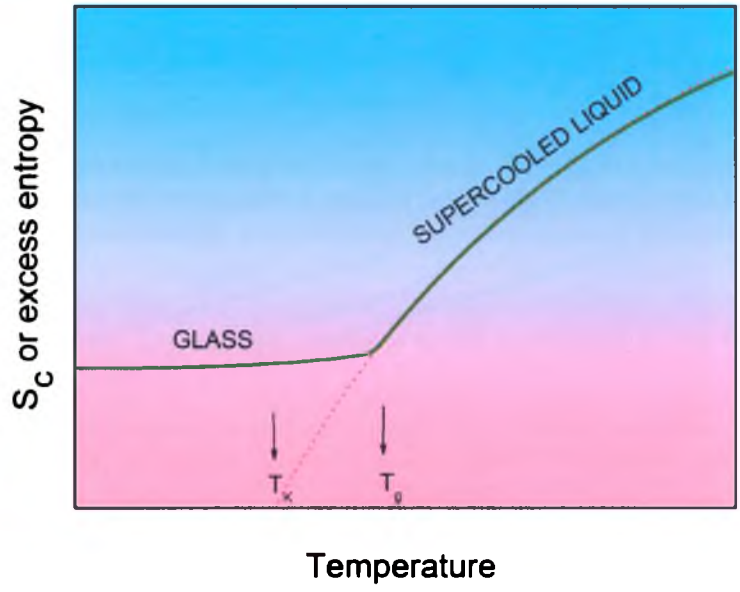

Figure 2.3. Schematic plot of the temperature behavior of configurational entropy (or excess entropy) in the vicinity of the glass transition. Dotted line corresponds to the extrapolation of supercooled behavior to lower temperature.

2.2. Models of the glass transition

Despite years of studies the glass transition phenomenon is still puzzling. In the past, several models were proposed to describe dynamical slowing down in vicinity of T_g. However, none of them describe successfully all aspects of the glass transition. By and large, two opposite approaches were proposed i.e. entropy based models, and alternative free-volume models. The former ones neglect the role of volume, while the latter ones thermal energy effects in governing dynamics of the supercooled liquid while approaching the glass transition. Selected models of the glass transition will be briefly described below.

2.2.1. Free-Volume models

Generally, free-volume models assume that molecules need vacant space in their surroundings to be able to rearrange [55]. As temperature decreases upon cooling, there is less free-volume available for molecules to rearrange. Decrease of free-volume while approaching the glass transition explains the slowing down of molecular motion on cooling. In view of this concept, the non-Arrhenius temperature dependence of viscosity (relaxation time) can be describe by Doolittle equation [56]

$$\tau = A\exp\left(B\frac{V-V_f}{V_f}\right) \tag{2.1}$$

where V_f is free space available per molecule.

Free-volume models have attracted a lot of criticism, because some of the thermodynamic aspects of the glass transition cannot be explained just as a function of volume. Recent studies have also demonstrated that α-relaxation times decrease faster than predicted by free-volume model. Within the framework of free-volume approach, one cannot also explain results from pressure experiments, as it is evident that V is not the dominant control variable [57].

2.2.2. Entropy models

The principle idea of entropic models is that slowing down of relaxation dynamics upon cooling is brought by dearth of the configurational entropy (i.e. the number of available configurations). One of the most popular entropy based model is the Adam – Gibbs approach [58]. This model assumes that with decreasing temperature of supercooled liquid the number of cooperative rearranging regions (CRR) increase and at certain temperature the size of this regions will be equal to the size of the sample. As the size of CRR increases, greater cooperativity is required and structural relaxation time increases. The relaxation time of the system depends on the configurational entropy S_c

$$\tau = \tau_o \exp\left(\frac{C}{TS_c(T)}\right) \tag{2.2}$$

where τ_o and C are constants.

The entropy based models relate dynamics of the supercooled liquid to its thermodynamics by assuming that the slowing down of structural relaxation reflects the existence of an underlying second-order phase transition to a state of zero configurational entropy.

Analogously as in the case of free-volume concept, some of the basic ideas of entropic models are very problematic. For example, it is claimed that cooperatively rearranging regions contain four up to eight molecules at the glass transition temperature, and even fewer at higher temperatures [59]. Certainly, this is not enough to explain the assumption that CRR act independently of their surroundings. Moreover, the entropy models' validation in experiments bases on the conjecture that $S_{excess} \cong S_c$. However, nowadays this assumption is believed to be incorrect, as the vibrational entropies of crystal and supercooled liquid cannot be in general state to be approximately the same [60].

2.2.3. Two Order Parameter Model (TOP)

The TOP model was proposed by Hajime Tanka to provide new description of the glass transition [61]. It is based on the assumption that in any liquid two competing ordering occurs: long-range density ordering leading to crystallization and short-range bond ordering toward formation of locally favored structures, not consistent with the crystallographic symmetry. The former tries to maximize local density, while the latter one to maximize the quality of bonds with neighboring molecules. The essential difference between TOP model and other models is that it regards crystallization as a key phenomenon that plays a crucial role in liquid-glass transition, whereas previous models regarded vitrification as a result of increasing density and cooperativity in molecular motions. Accordingly to TOP model, the liquid–glass transition is controlled by the competition between long-range density ordering and short-range bond ordering. Besides kinetic factor (viscosity), energetic frustration plays also an important key role in preventing the crystallization and control the nature of liquid–glass transition. The scale of this frustration is related to the bond order parameter S, given by the following equation

$$\bar{S} = S_0 \exp[\beta(\Delta E - P\Delta v)] \tag{2.3}$$

where $\bar{S}$ is average value of S, $\beta = 1/k_B T$, P is pressure, ΔE and Δv are the energy gain and the specific volume change upon the formation of a locally favored structure, respectively. TOP model predicts stronger frustration for 'stronger' liquids and weaker frustration for 'fragile' liquids ($S \to 0$). Therefore, greater stability of glass-former against crystallization can be reached when the degree of frustration increases.

CHAPTER 3

MOLECULAR DYNAMICS IN SUPERCOOLED AND GLASSY STATES

During cooling molecular motions of supercooled liquid decrease significantly. This slowing down of molecular dynamics spans from picoseconds (rotation times observed for 'normal' liquids) up to 100 seconds in the glass transition regime. Typically, for supercooled liquids close to the T_g there is more than one relaxation process observed. Structural relaxation is the slowest process that appears in supercooled liquid state, and is associated with molecular rearrangements. The two most characteristic features of the structural relaxation in practically all glass-forming materials are: (*i*) non-Arrhenius behavior of relaxation times while approaching the glass transition and (*ii*) non-Debye character of the relaxation process. Surprisingly, despite years of studies these two phenomena are still puzzling.

In the vicinity of the glass transition, except for the structural relaxation, local motions of much shorter time scale also occur. They are generally termed as secondary processes, and may have inter- or intra- molecular origin. One of the most characteristic features of secondary relaxations is that they persist in the glassy state and maintain the only source of information about motions below T_g.

Such a broad range of dynamics (covering more than 12 decades in relaxation times) and appearance of several relaxation processes create huge experimental challenges in studying of dynamical properties of glass-formers. In present days, dynamic response of supercooled liquids and glasses can be monitored using different experimental techniques such as dielectric spectroscopy, mechanical spectroscopy, depolarized light scattering or nuclear magnetic resonance spectroscopy. Mentioned above techniques probe different aspects of molecular mobility, as investigated material is subjected to different external perturbation fields which drive it out of equilibrium. For example, electric field as it happens in the case of dielectric spectroscopy, strain and stress – for mechanical spectroscopy (linear response of the material is of the key importance). This causes the macroscopic response of the system that originates from the microscopic relaxation of entities. Association of relaxation dynamics

with certain molecular movement is usually strongly coupled and can be used to probe slowing down of molecular motions in glass-formers. In present work, molecular dynamics of supercooled and glassy materials was monitored by dielectric spectroscopy. In short, dielectric spectroscopy probes polarization response *P(t)* of a dielectric material subjected to time-dependent electric filed.

3.1. Theoretical backgrounds of dielectric response in supercooled liquids

3.1.1. Dielectric Polarization in time-dependent electric field

The response of dielectric material is assumed to composed of two polarization parts: orientational polarization $\mathbf{P_{or}}$ due to orientation of permanent dipoles along the electric field and the induced polarization $\mathbf{P}_\infty$, caused by translation effects [62]. When external field is applied (or removed) to a dielectric, polarization of material reaches its equilibrium value. However, this doesn't happen instantaneously, but rather over a period of time. In that case [63]

$$\mathbf{P}(t) = \mathbf{P}_\infty + \varepsilon_0 \int_{-\infty}^{t} \varepsilon(t-t') \frac{d\mathbf{E}(t')}{dt'} dt' \tag{3.1}$$

where $\varepsilon(t)$ is the time dependent dielectric function, which can be measured directly as the time dependent response caused a step-like change of the external electric field. The relationship between the time dependence of the step-like change electric field, polarization and the time dependent relaxation function is presented in Figure 3.1.

If a stationary periodic electric field $\mathbf{E}(t)(\omega) = E_0 \exp(-i\omega t)$ is applied to the system, Eq. (3.1) transforms to

$$\mathbf{P}(t)(\omega) = \varepsilon_0(\varepsilon^*(\omega) - 1)\mathbf{E}(t)(\omega) \tag{3.2}$$

where $\varepsilon^*(\omega) = \varepsilon'(\omega) - i\varepsilon''(\omega)$ is the complex dielectric permittivity. The real part $\varepsilon'(\omega)$ is proportional to the energy stored reversibly in the system per period and the imaginary part $\varepsilon''(\omega)$ is proportional to the energy which is dissipated per period [63].

The relationship of $\varepsilon^*(\omega)$ to the time-dependent dielectric function $\varepsilon(t)$ is a one-side Fourier transformation

$$\varepsilon^*(\omega) = \varepsilon_\infty - \int_0^\infty \frac{d\varepsilon(t)}{dt}\exp(-i\omega t)dt \tag{3.3}$$

Like for all one-sided Fourier transformations, the real and imaginary part of complex dielectric permittivity are related to each other by the Kramers-Kroning relations [63]

$$\varepsilon'(\omega) = \varepsilon_\infty + \frac{2}{\pi}\int_0^\infty \frac{x\varepsilon''(x)}{x^2-\omega^2}dx \tag{3.4}$$

$$\varepsilon''(\omega) = -\frac{2}{\pi}\int_0^\infty \frac{\omega[\varepsilon'(x)-\varepsilon_\infty]}{x^2-\omega^2}dx \tag{3.5}$$

where x is a real variable. The fact that $\varepsilon'(\omega)$ and $\varepsilon''(\omega)$ dependent on each other and both carry the same information is very important from experimental point of view. For example, application of Kramers-Kroning relations might be very helpful in estimation of structural relaxation times from the real part of complex dielectric permittivity $\varepsilon'(\omega)$ in the case when dielectric spectra $\varepsilon''(\omega)$ are completely covered by large dc-contribution (e.g. [64]).

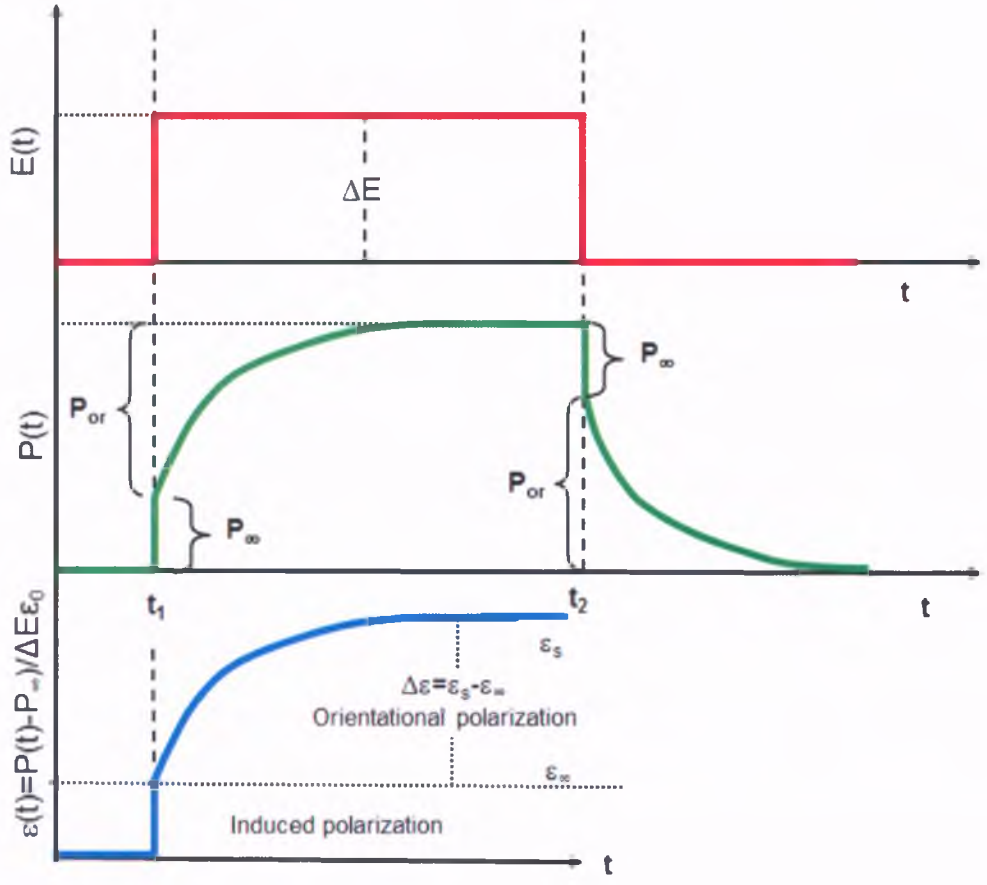

Figure 3.1. Relationship between the time dependence of external electric field, polarization and time dependent relaxation function $\varepsilon(t)$.

3.1.2. Debye and Non-Debye Relaxations

The simplest way to calculate the time dependence of dielectric behavior is to assume that polarization change is proportional to its actual value [63]

$$\frac{dP(t)}{dt} = -\frac{1}{\tau_D} P(t) \tag{3.6}$$

where τ_D is a characteristic relaxation time. This leads to an exponential decay for the correlation function $\Phi(\tau)$

$$\Phi(\tau) = \exp\left[-\frac{t}{\tau_D}\right] \tag{3.7}$$

Consequently, for complex dielectric permittivity $\varepsilon^*(\omega)$ one can obtain Debye formula [65]

$$\varepsilon^*(\omega) = \varepsilon_\infty + \frac{\Delta\varepsilon}{1 + i\omega\tau_D} \tag{3.8}$$

The real and imaginary parts of Debye function are given by

$$\varepsilon'(\omega) = \varepsilon_\infty + \frac{\varepsilon_s - \varepsilon_\infty}{1 + \omega^2 \tau_D^{\,2}} \tag{3.9}$$

$$\varepsilon''(\omega) = \frac{(\varepsilon_s - \varepsilon_\infty)\omega\tau_D}{1 + \omega^2 \tau_D^{\,2}} \tag{3.10}$$

where ε_s and ε_∞ are dielectric constants in the limits of low and high frequency, respectively. Real and imaginary parts of Debye function are both presented in Figure 3.2.

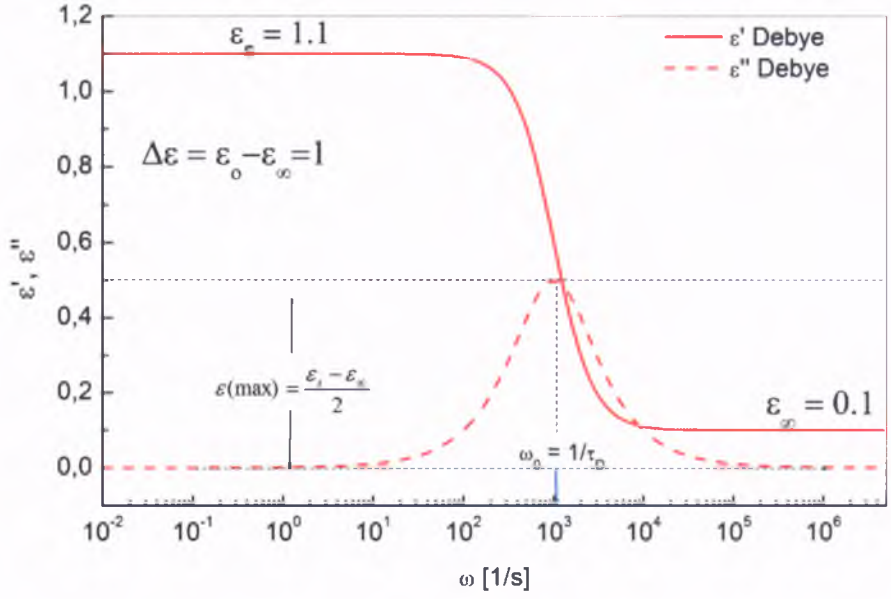

Figure 3.2. Frequency dependence of the real and imaginary parts of complex dielectric permittivity for Debye-type relaxation.

It is worth noticing that Equation (3.8) was originally derived by Debye to describe single relaxation of a system in which all dipoles are spherical and do not interact with each other. Debye formula turned out to successfully describe relaxation processes in gasses and some very simple liquids. Unfortunately, it fails to describe experimental results in majority of complex systems (including supercooled liquids) where cooperative movements occur. In case of glass-formers distribution of relaxation times are much broader than for classical Debye relaxation and experimental results are actually described better by non-exponential relaxation functions.

Thus, in frequency domain relaxation data are often described by the empirical Havriliak-Negami (HN) expression [66]

$$\varepsilon^*(\omega) = \varepsilon_\infty + \frac{(\varepsilon_s - \varepsilon_\infty)}{\{1 + (i\omega\tau_0)^\alpha\}^\beta} \tag{3.11}$$

where α and β are shape parameter describing symmetric and asymmetric broadening of the complex dielectric function ($0 < \alpha, \beta \leq 1$). Havriliak-Negami function is assumed to represent the superposition of many Debye relaxations with various relaxation times. The specific case is for $\alpha = 1$ and $\beta = 1$ when Eq. (3.11) transforms to Debye formula (3.8); $\beta = 1$ and $\alpha \neq 1$ corresponds to Cole-Cole (CC) equation, and the case of $\beta \neq 1$ and $\alpha = 1$ gives Cole-Davidson (CD) formula.

If dynamic properties of molecules are studied in time domain, the non-Debye relaxation of many glass-forming liquids and polymers can be described by the Kohlrauch-Williams-Watts (KWW) law [67, 68]

$$\phi(\tau) = \exp\left\{-\left(\frac{t}{\tau_{KWW}}\right)^{\beta_{KWW}}\right\} \tag{3.12}$$

where τ_{KWW} is a characteristic relaxation time and β_{KWW} is stretched exponent $0 < \beta_{KWW} < 1$. For $\beta_{KWW} = 1$ Eq. (3.12) corresponds to simple exponential power law. The stretching parameter β_{KWW} leads to an asymmetric broadening of relaxation function $\phi(\tau)$ at short times (high frequencies) compared with exponential decay ($\beta_{KWW} = 1$) [63].

To transform relaxation function from time to frequency domain the one-sided Fourier transformation should be applied

$$\frac{\varepsilon(\omega) - \varepsilon}{\varepsilon_0 - \varepsilon_\infty} = \int_0^\infty e^{-i\omega t}\left[-\frac{d\phi}{dt}\right]dt \tag{3.13}$$

As proven experimentally, molecular relaxation processes in glass-forming materials are mostly non-exponential. Consequently, full width at half maximum of the structural relaxation peak is much broader than for classical Debye response (1.14 decades). This is clearly illustrated in Figure 3.3 where structural relaxation for indomethacin recorded at 328K ($\beta_{KWW} = 0.59$ [69]) is presented along with simple Debye-type relaxation.

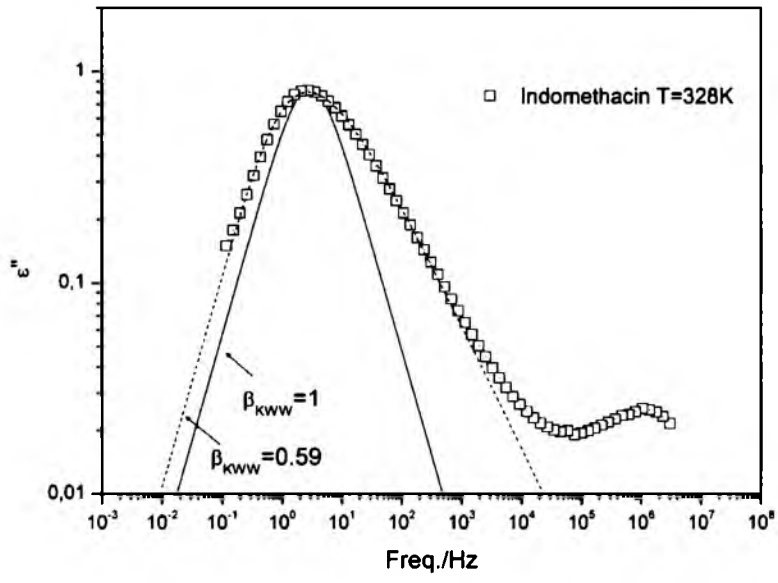

Figure 3.3. Dielectric loss spectra of indomethacin measured in supercooled liquid state at T=328 K. Solid and dotted lines represent KWW fits with $\beta_{KWW} = 1$ and $\beta_{KWW} = 0.59$, respectively. Data for indomethacin were taken from [69].

Generally, for all supercooled liquids structural relaxation process at very high temperatures ($\tau_\alpha \leq 10^{-9} s$) can be described by β_{KWW} close to unity. As temperature of supercooled liquid drops off so that $\tau_\alpha \leq 10^{-7} s$, the β_{KWW} gradually decreases and reaches almost constant value in the range of $\tau_\alpha \geq 1s$ [70, 71]. In that region the time-temperature superposition (TTS) appears to be applicable, which means that distribution of α-relaxation times is invariant to temperature change. In reference [72] authors showed that for systems with intermediate fragility TTS can hold even several decades above T_g.

Finally, the most striking question concerning non-Debye character of structural relaxation is whether it has homogeneous or heterogeneous origin. In homogenous scenario, each entity relaxes nearly identically in an intrinsically non-exponential way. In heterogeneous scenario every molecule relaxes nearly in exponential way, but the relaxation times vary significantly

between each other. Thus, non-Debye relaxation originates from the average relaxation time of molecules that relax exponentially, however, with different relaxation times [73]. Homo- and heterogeneous scenarios are hotly discussed in recent years, but the problem is still not resolved. For example, studies conducted by Richert on the heterogeneity of supercooled liquids suggest that liquid itself is structurally homogeneous, but its dynamics is heterogeneous, i.e. at given time different parts of the liquid move in different way [74]. On the other hand, Kawasaki and Tanaka revealed that supercooled liquid is not spatially homogeneous, but intrinsically has static structural heterogeneity (medium-range bond orientational order) [75].

3.1.3. Relaxation versus Retardation

The most common representation of dielectric data for typical glass-former is susceptibility representation. In this case, orientational polarization of a dielectric material results from reorientation of the permanent dipole moments and position of dielectric loss peak indicates the characteristic relaxation time of the orientational mobility. Unfortunately, susceptibility representation fails in case of ionic conductors, for instant ionic liquids. Therefore, dielectric data for these materials are commonly described in terms of electric modulus, which is defined as reciprocal of the complex dielectric permittivity [63]

$$M^*(\omega) = \frac{1}{\varepsilon^*(\omega)} \tag{3.14}$$

$$\text{with } M'(\omega) = \frac{\varepsilon'(\omega)}{\varepsilon'^2(\omega) + \varepsilon''^2(\omega)} \quad \text{and} \quad M''(\omega) = \frac{\varepsilon''(\omega)}{\varepsilon'^2(\omega) + \varepsilon''^2(\omega)} \tag{3.15}$$

Dielectric susceptibility and electric modulus formalisms reflect two alternative ways of description dielectric phenomenon. In the first one, time-dependent variation of dielectric displacement vector **D**, under constant electric field **E**, is recorded, while for the second one the constraint of a constant dielectric displacement **D** is applied and variation of the electric field **E** with time is recorded [65]. $\varepsilon^*(\omega)$ as well as $M^*(\omega)$ reflect the same dynamics of orientational polarization of permanent dipoles, but under different **E** and **D** conditions.

Presentation of dielectric data in $M''(\omega)$ plot instead of $\varepsilon''(\omega)$ effectively suppress large dc-contribution, because in modulus representation dc-conductivity translates into a pronounced Debye-type peak which can be assumed to be related to the translational ionic motions. Thus, interpreting relaxation data in the framework of modulus representation is

commonly employed method to obtain information about the charge-carriers dynamics in ionic conductors.

Relaxation is in general faster than retardation, i.e. the decay of the electric modulus response function $\varphi_M(t)$ takes less time than the time-dependent permittivity response function $\varphi_\varepsilon(t)$. For a simple Debye-type relaxation at fixed temperature the characteristic relaxation time τ_M is faster than the retardation time τ_ε in accordance with the following equation

$$\tau_M \cdot \left(\frac{\varepsilon_s}{\varepsilon_\infty}\right) = \tau_\varepsilon \tag{3.16}$$

Slowness of the build-up charge can be attributed to the renewal process of continuous reinvestment of potential made redundant by relaxation [76].

Finally, it is worth remembering that dielectric permittivity function actually describes not dielectric relaxation, but retardation of the build-up of the condenser charge after a step potential is applied, while the electric modulus function directly refers to the dielectric relaxation of the condenser potential after the application of a step charge [76,77].

3.2. Slow dynamics - Structural relaxation

3.2.1. Temperature dependence of the structural relaxation time above T_g

With decreasing temperature of supercooled liquid structural relaxation time increase. This reflects slowing down of molecular motions while approaching the glass transition. The Arrhenius activation model is the simplest one that can be applied to describe temperature dependence of relaxation time (or viscosity) in supercooled liquids. The Arrhenius temperature behavior of relaxation time is given by the following equation [78]

$$\tau = \tau_\infty \exp\left(\frac{E_A}{k_B T}\right) \tag{3.17}$$

where τ_∞ is the relaxation rate in the high frequency limit and E_A is temperature independent activation energy for concerned relaxation process.

In most cases the experimentally measured temperature dependence of molecular motions above T_g cannot be described satisfactory by simple Arrhenius equation, but the Vogel-Fulcher-Tamman equation (VFT) [79, 80, 81]

$$\tau = \tau_{\infty} \exp\left(\frac{B}{T - T_0}\right) \tag{3.18}$$

where τ_{∞}, B and T_0 are constants. The temperature T_0 is often called the Vogel temperature and refers to the temperature in the glassy state at which the molecular mobility associated with structural relaxation approaches zero. When $T_0 = 0$ K the VFT equation transforms to the Arrhenius expression and the constant $B = E_A / k_B$. For most of fragile systems the Vogel temperature was found to lie closely to the Kauzmann temperature T_K, i.e. 50- 70 K below T_g. It is believed that storage of amorphous APIs below this temperature guarantees long-term stability over typical shelf-life of pharmaceutical product.

The VFT function is certainly very useful to describe the temperature dependence of structural relaxation times. However, it is rarely found to give a good fit over the temperature range covering more than 10 decades of relaxation times. Thus, two sets of the VFT equations are usually required to portray the temperature dependence of structural relaxation time from the region just above T_g up to high temperatures. The first equation describes well $\tau_{\alpha}(T)$ dependence up to the temperature $T_B \cong 1.2T_g$, while for $T > T_B$ another VFT equation is needed [82, 83]. Typically, the dynamic crossover occurs at relaxation time of $10^{-7} s$ which is considered to be "magic", universal time-scale for any glass forming material [84]. It was suggested that crossover temperature is a direct result of strong increase of intermolecular cooperativity [85].

Extrapolation of the VTF fit to 100 seconds is a usual way of estimation the glass transition temperature from dielectric measurements. In a standard scheme for characterization of glass-forming liquids, except T_g, another very important parameter is usually calculated. This is 'fragility' which is a measure of non-Arrhenius character of the temperature dependence of α-relaxation times [86]. Viscous liquids with large departure from Arrhenius behavior while approaching the glass transition are called 'fragile'. When the temperature dependence of structural relaxation times in the supercooled liquid is Arrhenius - like, the material is 'strong' glass-former.

Fragility concept is usually demonstrated on so-called Angel plot [86], showing the logarithm of the structural relaxation time (or viscosity) for a number of viscous liquids as a function of inverse temperature normalized to unity at T_g (Figure 3.4).

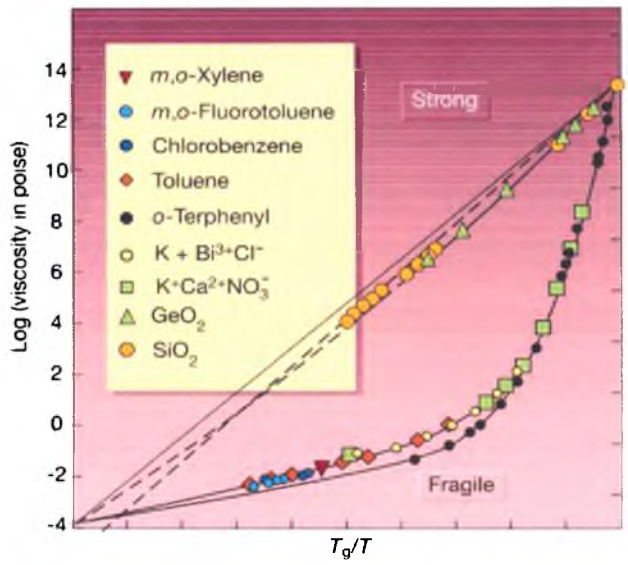

Figure 3.4. The logarithm of the viscosity as a function of the inverse temperature normalized to 1 at T_g. Strong liquids exhibit Arrhenius behavior, which yields to a straight line on Angel plot. Fragile liquids exhibit non-Arrhenius temperature dependence, which yields to a concave curve. Figure reprinted from [50].

The most common measure of fragility is 'steepness index' defined in the following way [86]

$$m = \left. \frac{d \log_{10} \tau}{d(T_g / T)} \right|_{T=T_g} \tag{3.19}$$

The minimal and maximal constraints of fragility are $m_{\min} = 17$ (strong liquids) and $m_{\max} = 200$ (fragile liquids). By analyzing the temperature behavior of structural relaxation times for more than 70 compounds Angel and co-workers [87] found that in the vast majority of cases, viscous liquids show faster than predicted from Arrhenius relation change in their relaxation times (viscosities) upon cooling toward the glass transition, with $m \sim 80$ being a typical value for fragile glass-formers.

Another possible measure of fragility is 'strength parameter', D, which can be calculated from the VFT equation by substituting $B = DT_0$. Small values of D ($D < 10$) are typical for fragile systems, whereas large ones for strong systems ($D > 10$).

At any time, it is also possible to calculated the steepness index from the VFT fits using the following equation

$$m = \frac{BT_g}{(T_g - T_0)^2} \tag{3.20}$$

Angel et al. have found that there is a correlation between fragility and non-Debye behavior of structural relaxation (quantified with the use of stretched exponent β_{KWW}) which can be expressed in the following way [87]

$$m = 250(\pm 30) - 320\beta_{KWW} \tag{3.21}$$

In accordance with this equation, fragile materials (having large values of m) should relax more non-exponentially (broad distribution of relaxation times, small values of β_{KWW}). On the other hand, strong glass-formers should exhibit more exponential-like behavior (narrow distribution of relaxation times, large values of β_{KWW}). However, the above equation isn't universal, because there is a large group of compounds which do not satisfied the correlation between β_{KWW} and m.

In recent years Wang and Angel [88] have proposed a new method of estimation fragility which is based on calorimetric measurements

$$m = 56\frac{\Delta C_p T_g}{\Delta H_m} \tag{3.22}$$

where ΔC_p is a difference between heat capacity of liquid and glass at T_g and ΔH_m is heat of fusion. As proven for more than 40 glass-formers, this simple expression is able to predict correct values of kinetic fragility [89]. A very similar equation was also proposed by Lubchenko and Wolynes [90]

$$m = 34.7\frac{\Delta C_p T_m}{\Delta H_m} \tag{3.23}$$

Estimation kinetic fragility of supercooled liquid from purely thermodynamic quantities has been hotly debated by scientists within the field, because the validity of Eq. (3.22) and (3.23) might suggest that the behavior of structural relaxation can be directly revealed from thermodynamic data. The opponents refer to some exceptions and the fact that there is no correlation between ΔC_p and kinetic fragility. Thus, many-body molecular dynamics is too complex to be solely described by thermodynamics [91, 92].

It is also worth to remind that dynamic fragility is entirely related to the structural relaxation, which governs the dynamics on approaching the glassy transition, whereas thermodynamic fragility is composed of contributions of the primary and secondary processes, and reflects the behavior displayed by the excess entropy i.e. the difference between the entropy of the liquid and the entropy of the underlying crystal.

Ongoing studies have shown that the increase of structural relaxation time as supercooled system is cooled towards the glass transition is brought about thermal and density (volume) effects [93,94]. The former one reflects decreasing of kinetic energy of molecules which don't have enough energy to jump over potential barrier, and the later one increasing of molecular crowding. Quantifying the relative importance of these two effects in governing the relaxation dynamics in the vicinity of the glass transition is usually done by means of the E_v / E_p ratio [95], i.e. the activation energy at constant volume E_v to the activation enthalpy at constant pressure E_p, defined by the following expressions

$$E_v = R\left[\frac{\partial \ln \tau_\alpha}{\partial T^{-1}}\right]_V \tag{3.24}$$

$$E_p = R\left[\frac{\partial \ln \tau_\alpha}{\partial T^{-1}}\right]_p \tag{3.25}$$

The magnitude of E_v / E_p varies from 0 to 1. If E_v / E_p tends to unity, thermal energy fully dominates molecular dynamics, whereas the volume effect can be neglected. This implies complete failure of the free-volume model. On the other hand, if E_v / E_p ratio approaches to zero, free volume plays a decisive role in controlling molecular dynamics.

The enthalpy ratios can be calculated in terms of the isobaric $\alpha_P = V^{-1}\left(\frac{\partial V}{\partial T}\right)_P$ and isochronic $\alpha_\tau = V^{-1}\left(\frac{\partial V}{\partial T}\right)_\tau$ thermal expansion coefficients [96]

$$\left.\frac{E_V}{E_P}\right|_{T_x} = \frac{1}{1+\alpha_p/|\alpha_\tau|} \tag{3.26}$$

Based on the value of the E_v / E_p ratio, the slow dynamics in glass-forming liquids can be divided into 3 categories:

(*i*) volume-dominated dynamics - found in case of some polymers and van der Waals liquids: 1,1'-di(4-methoxy-5-methylphenyl)cyclohexane (BMMPC) - $E_v / E_p = 0.39$ [97] or polyphenylene oxide (PPO) - $E_v / E_p = 0.25$ [98]).

(*ii*) temperature-dominated dynamics - typical for associated liquids such as glycerol - $E_v / E_p = 0.94$ or sorbitol - $E_v / E_p = 0.87$ [97].

(*iii*) molecular dynamics controlled by both temperature and volume in practically equal way - very common for van der Waals liquids, e.g. ortho-terphenyl (OTP) - $E_v / E_p \approx 0.49$, propylene carbonate (PC) - $E_v / E_p \approx 0.64$ [97].

3.2.2. Temperature dependence of the structural relaxation time below T_g

The glassy state is far from equilibrium and the time scale of structural relaxation below T_g is exceedingly long. Although the system slowly relax to equilibrium, it is impossible to wait and directly determine the structural α-relaxation time τ_α deep in the glassy state by any conventional experimental setup. Thus, τ_α is an unknown quantity at temperatures sufficiently lower than T_g. However, the knowledge of the time scale of the global mobility below T_g is crucial for selecting appropriate storage conditions of amorphous pharmaceuticals that will guard against crystallization and chemical instability during typical shelf life of pharmaceutical product (3-5 years). Hence, it is important to have some means to estimate τ_α deeply in the glassy state.

One of the earliest expressions allowing probing structural relaxation deep in the glassy state was the modified Adam–Gibbs equation proposed by Hodge, basing on the nonlinear Adam–Gibbs equation [99]

$$\tau_\alpha(T,T_f) = \tau_\infty \exp\left(\frac{DT_0}{T-(T/T_f)T_0}\right) \tag{3.27}$$

where τ_∞, B and T_0 are parameters from VFT equation used to fit $\tau_\alpha(T)$ dependence above T_g. T_f is the fictive temperature defined as the temperature at which the observed non-equilibrium excess property would be the equilibrium value. The fictive temperature depends on cooling rate. T_f can be calculated with the use of configurational heat capacity values ($C_p^{conf} = C_p^{liq} - C_p^{cryst}$) and the difference between heat capacity of liquid and glass ($C_p^{liq} - C_p^{glass}$), namely [100]

$$\frac{1}{T_f} = \frac{\gamma_{C_p}}{T_g} + \frac{1-\gamma_{C_p}}{T} \tag{3.28}$$

where

$$\gamma_{C_p} = \frac{C_p^{liq} - C_p^{glass}}{C_p^{liq} - C_p^{cryst}} \tag{3.29}$$

The values of heat capacities in above equation should be calculated at the glass transition temperature T_g. Parameter γ_{Cp} varies from 0 to 1, indicating type of the temperature dependence of structural relaxation times in the glassy state, i.e. γ_{Cp}=1 corresponds to Arrhenius behavior, while γ_{Cp}=0 implies purely VFT behavior below T_g. For most of glass-formers γ_{Cp} is usually intermediate (e.g. celecoxib γ_{Cp}=0.46 [101]).

Equation (3.27) was originally derived to describe non-equilibrium glassy dynamics. However, method for quantifying the temperature dependence of molecular mobility below T_g based on modified Adam-Gibbs equation is able to estimate structural relaxation times of only freshly prepared glass. With aging, structural relaxation times are expected to change approaching equilibrium values. Moreover, sufficiently below the glass transition temperature $\tau_\alpha(T)$ dependence for all glass-forming materials is believed to follow the Arrhenius pattern.

Very recently a new method to determine τ_α in the glassy state was proposed by Casalini and Roland (CR) [102]. This approach bases on the 'aging experiment', defined as the time-dependent variation of physical quantities when glassy sample approaches equilibrium after quenching it below T_g [103]. The method proposed by CR exploits the connection between the α-relaxation and the secondary β-relaxation of the Johari–Goldstein (JG) type. The structural relaxation times in the glassy state can be determined from isothermal time-dependent measurements of the imaginary part of the dielectric permittivity $\varepsilon''(\tilde{f})$ at fixed frequency f (lying in range of β-relaxation peak), which can be described by the following equation

$$\frac{\varepsilon''(\tilde{f},t_{ag})}{\varepsilon''(\tilde{f},t_{ag}=0)} = \left\{\Delta\varepsilon''(\tilde{f},t_{ag})\exp\left[-\frac{t_{ag}}{\tau_{ag}}\right]^{\beta_{ag}} + \varepsilon''_{eq}(\tilde{f})\right\} \Big/ \varepsilon''(\tilde{f},t_{ag}=0) \qquad (3.30)$$

where $\varepsilon''_{eq}(\tilde{f}) \equiv \varepsilon''(\tilde{f},t_{ag}\to\infty)$ is an equilibrium value, $\Delta\varepsilon''(\tilde{f},t_{ag}) = \varepsilon''(\tilde{f},t_{ag}=0) - \varepsilon''_{eq}$ is a change of ε'' during aging, β_{ag} is stretched exponent ($\beta_{ag}(T<T_g) = \beta_{KWW}(T_g)$), and τ_{ag} is the aging time constant which behavior is consistent with its identification as τ_α in the glassy state. Hence, by following the changes of the β-relaxation upon physical aging it is possible to probe structural relaxation dynamics unattainable experimentally.

The most striking feature of this method is that the deduced values of τ_{ag} turned out to be nearly the same as τ_α calculated from the Coupling Model (CM) [104, 105, 106] which was

originally used to show the correlation between structural relaxation and JG relaxation in the region above T_g

$$\tau_\alpha = [(t_c)^{\beta_{KWW}-1}\tau_0]^{1/\beta_{KWW}}, \quad \tau_\beta \approx \tau_0 \tag{3.31}$$

where t_c is about 2 ps for molecular and polymeric glass-formers and β_{KWW} is the stretch exponent of the Kohlrausch-Williams-Watts (KWW) function.

3.2.3. Dynamics of supercooled liquids at high pressure

The most natural and easiest way of obtaining glass is decreasing temperature of supercooled liquid. However, the glassy state can be also reached by increasing pressure under isothermal conditions. It is generally assumed that decreasing temperature and increasing pressure give similar effect, i.e. dramatic slowdown of the molecular dynamics. However, dynamical properties of glass-formers at elevated pressure might be completely different from that reported at ambient pressure. This is because temperature and pressure affect dynamics of investigated materials in completely different way. Temperature changes mainly rotational and vibrational excitation of molecules, while pressure influences intermolecular distances between molecules. Thus, high pressure experiments provide completely new information about molecular dynamics of glass-formers and broaden our understanding of the glassy nature [107]. It is also worth noticing that reaching the glassy state by compression of liquid has been much less exploited, which results mainly from experimental problems that are encountered when applying high pressure.

One of the first equations used to describe the pressure dependence of structural relaxation time was volume activated law, which is a simple pressure counterpart of the Arrhenius equation [108]

$$\tau = \tau_\infty \exp\left(\frac{P\Delta V}{RT}\right) \tag{3.32}$$

where R is the gas constant and ΔV is the activation volume. The activation volume is defined as the empty volume which has to be created to move relaxing molecules to another position (or accordingly with transition state theory - difference between the volumes occupied by a molecule in activated and non-activated states). According to Eq. (3.32) a linear dependence on pressure of $\log(\tau_\alpha)$ at constant temperature is expected. However, as proven experimentally the linear dependence holds only in a very narrow pressure range and for most of supercooled liquids while approaching the glass transition the $\tau_\alpha(P)$ dependence has a

non-linear character (e.g. [107, 109]). This indicates that the activation volume varies both with P and (inversely) with T.

The activation volume can be calculated from the following expression [108]

$$\Delta V = -RT\left(\frac{\partial \ln \tau}{\partial P}\right)_T \tag{3.33}$$

For different types of glass-forming liquids (van der Waals liquids, polymers, and hydrogen-bonded systems) the activation volume usually increases in nonlinear matter with increasing pressure, as illustrated in Figure 3.5 (right panels).

The activation volume provides a straightforward information about pressure sensitivity of investigated materials. For example, polymer poly(methyl-phenylsiloxane (PMPS) has considerably larger activation volume required to reorient than small molecules such as diisobutyl phthalate (DIBP) and xylitol [109]. It is also commonly believed the value of the activation volume is of the same order as that of the molar volume. The positive correlation between molar volume and the activation volume was found recently in a series of hydrogen-bonding materials, but this type of behavior cannot be treated as universal [110].

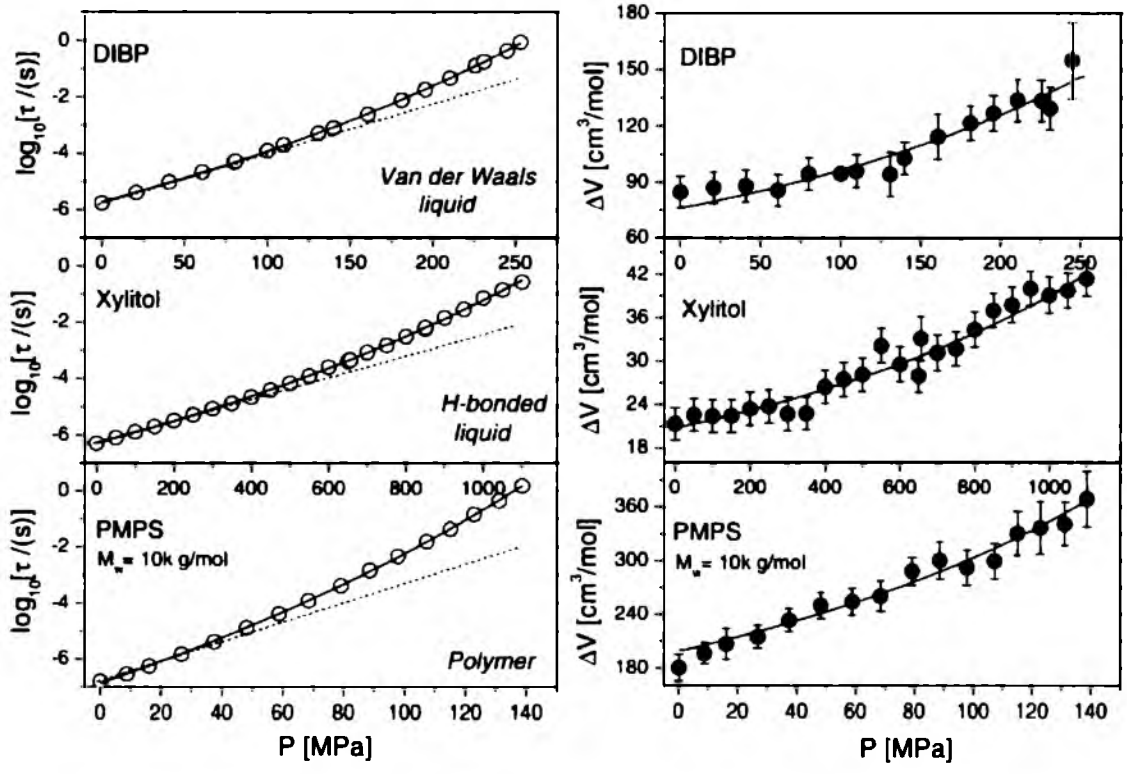

Figure 3.5. Left panels show the pressure dependences of α-relaxation times for three representative kinds of materilals: di-isobutylphthalate (DIBP) which is a typical van der Waals liquid, H-bonded xylitol and polymer polymethylphenylsiloxane (PMPS) of molecular weight of 10 000 g·mol^{-1}. Dotted lines demonstrate the linear behavior described by the Arrhenius law. Right panels present their pressure dependences of the activation volumes. Figure reprinted from [109].

The non-linear pressure dependence of structural relaxation time is usually described in terms of pressure counterpart of the VFT formula [111]

$$\tau = \tau_0 \exp\left(\frac{D_P P}{P_0 - P}\right) \tag{3.34}$$

where D_P, P_0 and τ_0 are constants. P_0 is the pressure for which τ_α would diverge and D_P is strength parameter. Only D_P and P_0 have to be extracted from fitting analysis, as preexponential factor τ_0 denotes the relaxation time at ambient pressure. The representative pressure dependences of structural relaxation times fitted by the Eq. (3.34) are presented in Figure 3.5 (left panels), where deviation from the pressure counterpart of the Arrhenius law is evident.

According to the general rule, with increasing pressure the value of the glass transition temperature also increases. This can be explained by the increase of molecular packing with compression. At low pressures, dependence $T_g(P)$ displays usually a linear character, but with further compression a weaker effect of pressure on T_g is observed. Satisfactory description of experimentally measured $T_g(P)$ dependence can be achieved using empirical relation proposed by Andersson and Andersson [112]

$$T_g(P) = T_g(0)\left(1 + \frac{b}{c}P\right)^{1/b} \tag{3.35}$$

where $T_g(0)$ is glass transition temperature at ambient pressure, b and c are material constants. By calculating the ratio $T_g(0)/c$ one can obtain the pressure coefficient of T_g, dT_g/dP, which can be used for characterizing the sensitivity of T_g on pressure for various materials.

Van der Waals liquids are generally pressure sensitive and calculated values of dT_g/dP are large (e.g. cresolphthalein-dimethylether (KDE) $dT_g/dp = 307K \cdot GPa^{-1}$). An opposite behavior is observed for hydrogen-bonded systems which are characterized by very weak effect of pressure on T_g resulting from strong intermolecular bonds (e.g. glycerol $dT_g/dp = 40K \cdot GPa^{-1}$, propylene glycol $dT_g/dp = 37K \cdot GPa^{-1}$ [97]).

3.3. Excess wing and Secondary relaxations

As temperature of supercooled liquid decreases and structural relaxation tremendously slows down other relaxation processes emerge in vicinity of the glass transition. They are generally termed as 'secondary relaxations' and reflect local motions of much shorter time scale. The most characteristic feature of secondary relaxations is that, unlike structural relaxation, they can be directly determined at temperatures way below the vitrification temperature. Consequently, they are being considered as the main source of movement in the glassy state. Secondary relaxations are denoted by the subsequent Greek letters (β, γ, δ...) in order of decreasing time scale. The slowest one is called Johari-Goldstein (JG) β-relaxation. This process is related to motion of entire molecule as a whole. From historical reasons, this type of relaxation is called JG β-relaxation, as in 1970s Johari and Goldstein were first who demonstrated existence of secondary relaxation in completely rigid molecules such as toluene and chlorobezene [113, 114]. Nowadays, the JG relaxation is believed to be an intrinsic feature of the glassy state and serves as the precursor of the primary α-relaxation [115]. Other secondary relaxations that might occur in the glassy state are generally faster than JG relaxation and originates from trivial motions of small isolated groups of the molecule. Secondary relaxations having intramolecular origin are called non-JG relaxations. It is worth mentioning that, both JG- and non-JG relaxations are less sensitive to temperature changes than α-relaxation, and below T_g their temperature dependences of relaxation times follow the Arrhenius pattern.

In the glassy state of a typical glass-former, there is always more than one secondary relaxation process, each relaxation is considered to have different molecular origin. In some cases, identification of the nature of secondary relaxations might be very complex. For example, it is possible that intramolecular secondary relaxation of much greater amplitude covers completely the JG relaxation. Moreover, as the amplitude of the JG relaxation is much weaker than α-relaxation, the secondary relaxation of intermolecular nature may not be visible in dielectric spectra as a distinctive relaxation peak. When that happens, instead of well pronounced β-relaxation peak an excess wing (also called 'high-frequency wing') shows up as a second power law at the high-frequency flank of the α-peak. In the past, this has led to the classification of glass-formers into two groups: A-type systems without β-process but showing an excess wing and B-type systems with well-separated β-process [116]. Schematic

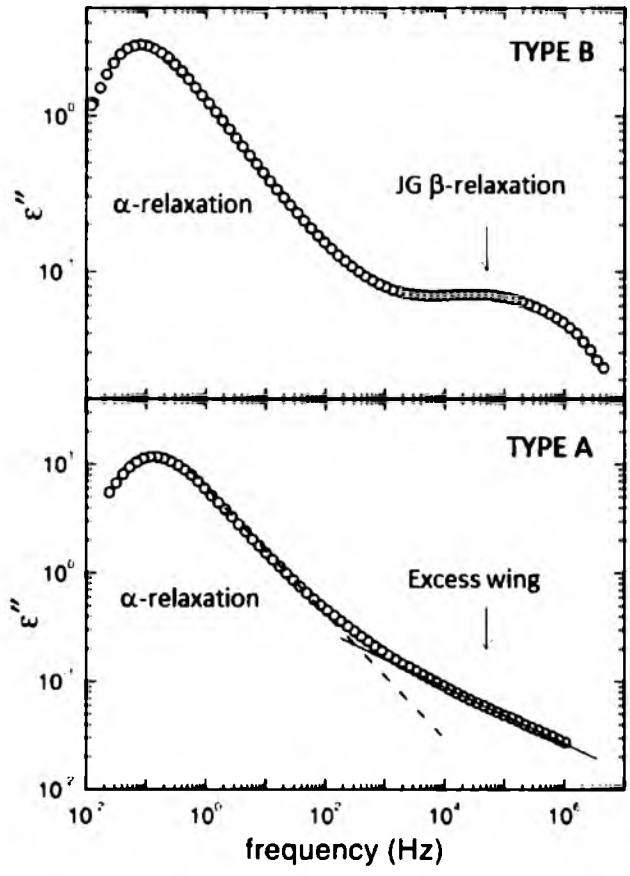

Figure 3.6. Dielectric spectra of Type B and Type A glass-forming liquids. The solid line in the lower graph shows the additional power law with a weaker slope than α-relaxation. The original figure was taken from [115].

view on loss spectra of type A and type B glass-formers can be found in Figure 3.6.

In the past, the excess wing was interpreted by some the scientists as an inseparable part of the α-relaxation [117]. Nowadays, the excess wing is believed to be an unresolved JG-relaxation, hidden under the intense α-peak. The first experimental proof was provided by aging experiments. During physical aging structural relaxation peak shift towards lower frequencies, while same time secondary β-relaxation causing excess wing is less affected. Thus, for some of glass-formers upon physical aging it is possible to develop excess wing into a well-separated β-peak (or shoulder) [118]. Unfortunately, there are also glass-formers for which both excess wing and β-process appear simultaneously. In this case, excess wing cannot be regarded as submerged β-relaxation, but rather as another relaxation phenomenon [119].

Chaos in the interpretation of the excess wing and secondary relaxations' nature can be resolved by performing dielectric measurements at elevated pressure (e.g. [97, 107, 120]).

This is because non-JG or pseudo-JG secondary relaxations (originating from motion of only a part of molecule) do not shift with pressure or reveal just a residual pressure sensitivity below T_g. One the other hand, some secondary relaxations are pressure sensitive, similar as α-relaxation. It means that they 'feel' changes in specific volume and entropy. Pressure sensitive secondary relaxation is termed as 'genuine JG' β-relaxation [115]. Similar as physical aging, experiments at high pressure can be very useful in identifying the nature of the excess wing. Due to different pressure sensitivities of JG and non-JG relaxations, excess wing can be transforms into distinct relaxation peak.

When it comes to identification of the secondary relaxations, pressure experiments are considered to be crucial. However, there are also theoretical tools that can be used for distinguishing secondary relaxations of intra- and intermolecular origin. One of the most valuable one is the Coupling Model (CM) [104, 105, 106]. The CM predicts connection between dynamically heterogeneous many body dynamics and the primitive motion of individual molecule. This is qualitatively expressed by the CM expression

$$\tau_0 = (t_c)^{1-\beta_{KWW}} \tau_\alpha^{\beta_{KWW}} \tag{3.36}$$

where τ_0 is primitive relaxation time of the CM, t_c is equal to about 2 ps for molecular and polymeric glass-formers and β_{KWW} is the stretch exponent of the KWW function. The primitive relaxation time τ_0 is of the same order of magnitude as JG β-relaxation time τ_{JG} ($\tau_{JG} \approx \tau_0$). Thus, by calculating the primitive relaxation and primitive frequency it is possible to predict relaxation frequency of the JG process.

By inspecting, for several glass-formers, the relationship between experimentally determined values of glass transition temperature T_g and activation energy of the β-relaxation (E_β), Kudlik et al. [121] have derived empirical expression

$$\frac{E_\beta}{RT_g} = 24. \tag{3.37}$$

The above equation implies universal behavior of the $\tau_\beta(T)$ dependence on the scale of T/T_g. However, Ngai and Capaccioli [122] have also shown that for some of JG β-relaxations the $E_\beta/(RT_g)$ ratio does not necessary equal to 24, and the following relation is more appropriate

$$\frac{E_\beta}{RT_g} = 2.303(2 - 13.7n - \log_{10}\tau_{\infty-\alpha}). \tag{3.38}$$

If the β-process is true JG secondary relaxation, left side of above equation should be equal to right side. Equations (3.37) and (3.38) can be applied to identify the JG relaxation, however, in some cases without high-pressure experiments prediction of the nature of secondary relaxations might be highly speculative.

Recent experiments at elevated pressure have also shown that JG β-relaxation 'senses' the structure of glass [123]. It was demonstrated that using specific thermodynamic pathways, it is possible to get an amorphous form with higher density. To produce glass by the compression of liquid two thermodynamic pathways can be used, as shown in Figure 3.7. In the first, the sample is isobarically cooled down to the final temperature T_f, and then we isothermally pressurized the liquid to the final pressure P_f (pathway A). In the second, the liquid is pressurized isothermally at high temperature to pressure P_f. Then, it is cooled at constant pressure down to the final temperature T_f (pathway B). As proven experimentally the glassy state reached by the compression of supercooled liquid at higher temperature and pressure (pathway B) is characterized by denser molecular packing. The greater density of compressed glass is usually manifested by the increase of relaxation times τ_β as well as the activation energy of the β-process [123].

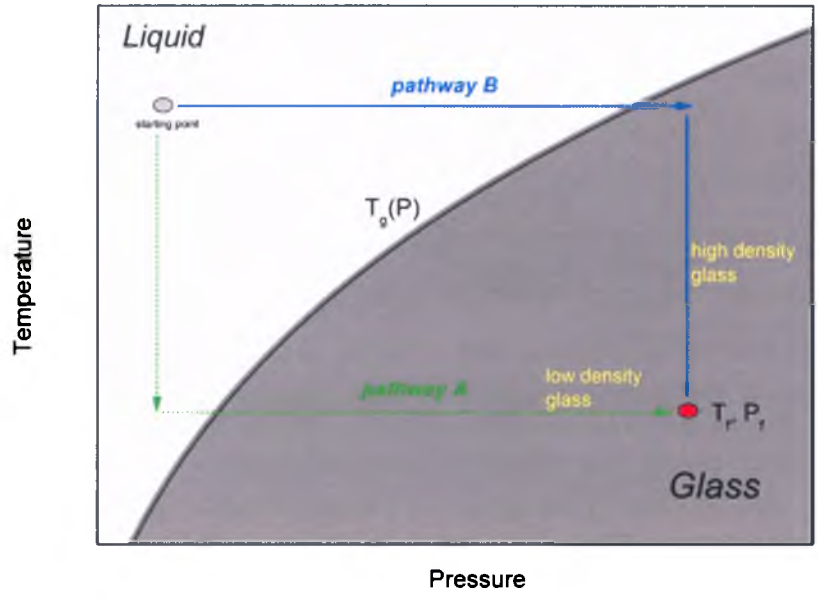

Figure 3.7. Schematic presentation of the thermodynamic pathways used to prepare glasses by compression of liquid.

CHAPTER 4

EXPERIMENTAL

4.1. Experimental Methods

4.1.1. Dielectric Spectroscopy (DS)

Dielectric Spectroscopy is one of the most powerful techniques that enables investigation of relaxation phenomenon in very broad range of characteristic relaxation times ($10^{4} \div 10^{-12}$ s), temperatures (93÷673 K) and even pressure (up to 5 GPa). This is the main reason why DS method occupies special place among other modern techniques used for characterization of dynamical properties of materials such as nuclear magnetic resonance, mechanical spectroscopy or depolarized light scattering. Since dielectric spectroscopy is sensitive to intermolecular interactions, cooperative processes in glass-forming liquids can be easily observed. The basic principle of dielectric (or impedance) measurements is illustrated in the following scheme (Figure 4.1.a).

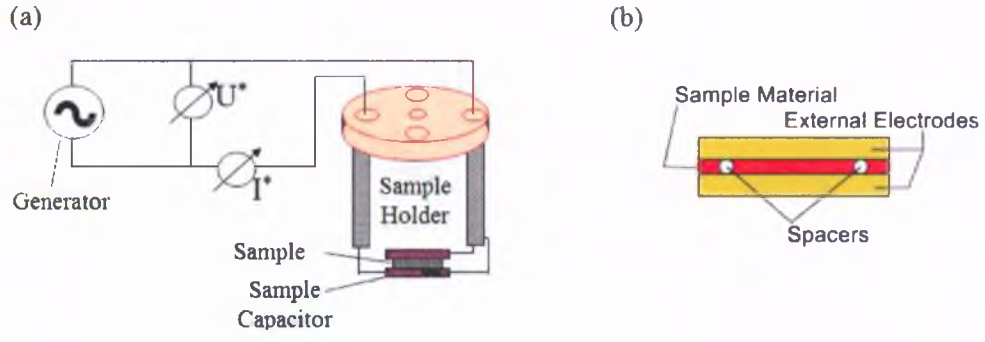

Figure 4.1. (a) Schematic presentation of the dielectric measurement principle (b) Sample mounted between external electrodes with spacers used to separate electrodes. Original figures were taken from [124].

Sample (viscous liquid or solid) is mounted between external electrodes (Figure 4.1.b) and connected to the appropriate analyzer (impedance or time domain analyzer) which measures capacitance and resistance of the sample. The distance between the electrodes is adjusted by spacers. It can be thin silica needles, small stripes of Teflon or Quartz ring. Sinusoidal voltage $U^*(\omega) = U_0 \exp(i\omega t)$ is applied to the capacitor filled with sample. As a results, $U^*(\omega)$ causes a current $I^*(\omega)$ at the same frequency in the sample. In addition, there will be a phase

shift between the current and voltage described by the phase angle ϕ. The measured impedance of the sample capacitor is given by

$$Z^*(\omega) = -\frac{i}{\omega C^*(\omega)} \tag{4.1}$$

where $C^*(\omega)$ denotes complex capacitance.

For capacitor filled with dielectric material, $\varepsilon^*(\omega)$ is defined as [63]

$$\varepsilon^*(\omega) = \varepsilon'(\omega) - i\varepsilon''(\omega) = \frac{C^*(\omega)}{C_0} = \frac{-\frac{i}{\omega Z^*(\omega)}}{C_0} = -\frac{i}{\omega Z^*(\omega) C_0} = \frac{1}{i\omega Z^*(\omega) C_0} \tag{4.2}$$

where C_0 is the vacuum capacitance. Thus, complex dielectric function can be derived by measuring the complex impedance $Z^*(\omega) = U^*(\omega)/I^*(\omega)$ of the sample.

Dielectric permittivity data displayed in this work were measured in the frequency domain using commercially available as well as home-made equipment. Isobaric dielectric measurements at ambient pressure were carried out using Novo-Control GMBH Concept 80 (NovoControl, Germany) dielectric spectrometer covering a frequency range from 10^{-2} to 10^7 Hz. Temperature was controlled using a nitrogen-gas cryostat with stability better than 0.1 K. Tested samples were placed in measurement capacitors made of stainless steel with Teflon or Quartz rings used to maintain a fixed distance between the plates. For measurements of dielectric data in the frequency range (10^6-10^9 Hz) Agilent 4291B impedance analyzer connected with Novo-Control GMBH system was used. Sample was placed between two gold-plated electrodes (diameter: 5 mm, gap: 0.05 mm). Dielectric measurements of examined pharmaceuticals were performed in a wide range of temperatures (typically 133 K to 473 K) which provide thorough picture of relaxation dynamics from the region deep in the glassy state up to the liquid state. Dielectric spectra were analyzed using WinFit software, which allowed advanced curve fitting for accurate and fast determination of material parameters.

Elevated pressure experiments were carried out using two dielectric setups: 500 MPa cell (with liquid pressure medium) and 1.8 GPa cell made from stainless still. In the former case, pressure was applied to the pressure chamber by press though a system of capliars. Pressure was measured by a Nova Swiss tensometric pressure meter, with resolution ± 0.1 MPa. A thermostat, which was connected to the pressure chamber, stabilized the temperature within accuracy ± 0.1 K. Temperature was measured by means of a platinum resistor (PT 100) placed in the jacket of the pressure chamber with an accuracy ± 0.1 K using Keithley 195A multimeter. A special homemade flat parallel capacitor was used. Thin Teflon spacers were

used to maintain fixed distance between the plates. The sample and two electrodes forming a capacitor were placed in sealed Teflon bellows and embedded in the pressure-transmitting liquid (silicone oil) located in the pressure chamber. The sample inside the capacitor was only in contact with stainless steel and Teflon. Measurements of the electric capacitance were carried using NovoControl Alpha dielectric spectrometer. Data were collected and stored on the computer.

For high pressure studies (up to 1.8 GPa) unique experimental setup constructed by Unipress (Institute of High Pressure Physics, Polish Academy of Science) was also used. Schematic illustration of the high pressure setup is shown in Figure 4.2.

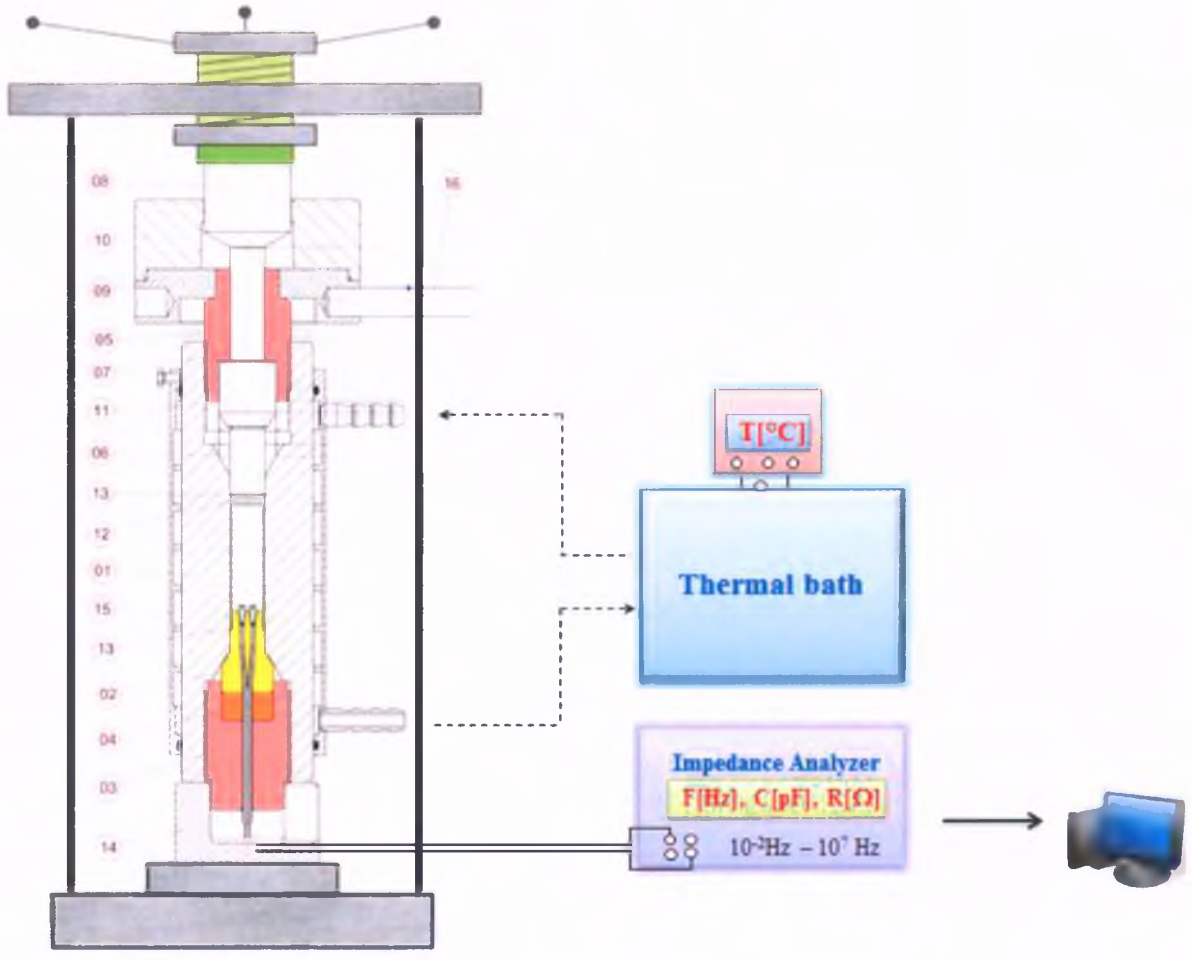

Figure 4.2. High-pressure dielectric cell for pressures up to 1.8 GPa, 01 - High-pressure chamber, 02 - Stainless steel stopper with two electric connections, 03 – Stopper screw, 04 – Stopper anvil, 05 – Piston screw, 06 – Piston, 07 - Flat-face follower, 08 - Anvil of the sheathing, 09 – Screw wheel, 10 – Wheel sheathing, 11 – Piston anvil, 12 - Teflon bellow, 13 - Anti-extrusion ring, 14 - Chamber base, 15 - Heating jacket, 16 - Peg for wheeling the screw.

Measurements were performed with the use of homemade flat parallel capacitor. The sample and two electrodes forming a capacitor were placed in Teflon bellows mounted in the high pressure chamber. Pressure was exerted via steel piston and hydraulic press. Pressure was measured by Nova Swiss tensometric pressure meter with an accuracy of ± 10 MPa. The temperature of high-pressure cell in the range from 383 K to 263 K was controlled to within 0.1 K by thermostatic bath and from 263 K to 218 K by Tenney Junior environmental chamber with the same accuracy.

4.1.2. Differential Scanning Calorimetry (DSC)

The basic principle underlying DSC technique is that it measures the difference in heat flow required to increase the temperature of a sample with respect to reference material. When thermal event occurs in the sample, DSC measures the enthalpy change at the reaction temperature. In general, the sample and reference are maintained at approximately the same temperature throughout the experiment. Whenever the sample undergoes thermal event (melting, crystallization, glass transition etc.) more or less heat will need to flow to it, compared to the reference, to maintain both sample and reference material at the same temperature [125]. The heat capacity C_p, is calculated as the sample heat flow rate (i.e. transmitted power measured in mW) divided by sample mass and heating rate. Depending upon whether more or less energy has to be supplied relative to the reference material, thermal events observed on DSC curve are either in endothermic or exothermic direction. In DSC, endothermic responses are usually presented as being positive, which corresponds to an increased transfer of heat to the sample compared to the reference [126].

There are two basic modes of DSC: power-compensation DSC and heat-flux DSC. The working principles of the two methods are illustrated in Figure 4.3. In the former, there are two furnaces used and the signal is related to the differential heat that is needed to keep the sample and the reference at the same temperature. In the latter, a single furnace is employed and the signal derives directly from the difference in temperature between the sample and the reference material [127].

Thermodynamic properties of examined materials were extracted from DSC measurements performed by means of Mettler-Toledo DSC apparatus equipped with a liquid nitrogen cooling accessory and a HSS8 ceramic sensor (heat flux sensor with 120 thermocouples). Temperature and enthalpy calibrations were carried out using indium and zinc standards while

heat capacity C_p calibration was performed using a sapphire disc. Amorphous sample for calorimetric studies was prepared in an open aluminum crucible (40μL) outside the DSC apparatus. First, the crystalline sample in the crucible was heated on the heating plate (CAT M 17.5) up to the melting point, and next immediately cooled to vitrify. Crucibles with such prepared glassy sample as well as with its crystalline counterpart were sealed with the top with one puncture. All samples were scanned at rate of 10 K/min over a temperature range of 298 K to well above the respective glass transition or melting points.

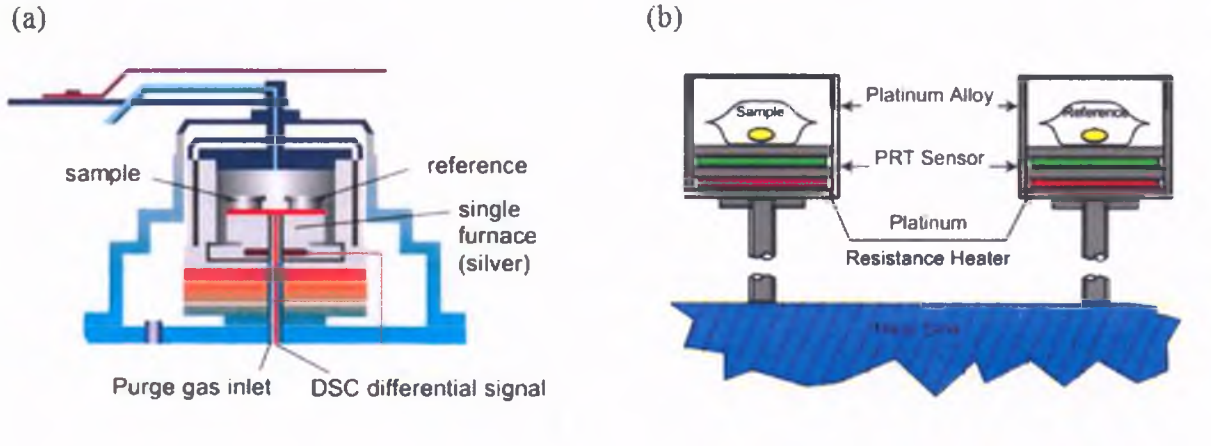

Figure 4.3. Schematic cross-section of two types of differential scanning calorimeter. (a) heat flux DSC and (b) power compensation DSC. Reprinted from [125].

4.1.3. The X-ray diffraction (XRD)

X-ray diffraction is a very powerful, non-destructive technique by which X-rays of a known wavelength are passed through a powder sample to fully characterized its crystalline structure. The X-ray diffraction can be used to provide information on the atomic arrangement in materials with long-range order, short-range order or not ordered at all. The wavelength of typical X-ray used in X-ray diffraction is in the vicinity of 1Å, which is comparable to the range of interatomic spacing in crystals. When a monochromatic X-ray beam hits a sample, in addition to absorption and other phenomena, elastic scattering takes place. The scattered X-rays are measured in diffraction experiment as they carry information about electrons distribution in the material. Depending on the atomic arrangement in the sample, the intensities and spatial distribution of the scattered X-ray form a specific and unique for each sample diffraction pattern [128].

The principle idea of observing X-ray diffraction peaks in crystalline materials is given in terms of the Bragg's law, which states that X-rays reflected from adjacent periodic atomic planes separated by a distance d of a crystal, interfere constructively when the path difference between them is an integer n multiple of the wavelength λ. The reflected rays make an angle of 2θ with the direction of the incident beam [129]. The condition for diffraction can be written as

$$n\lambda = 2d\sin\theta \tag{4.3}$$

The schematic illustration of diffraction according to Bragg's law is presented in Figure 4.4.

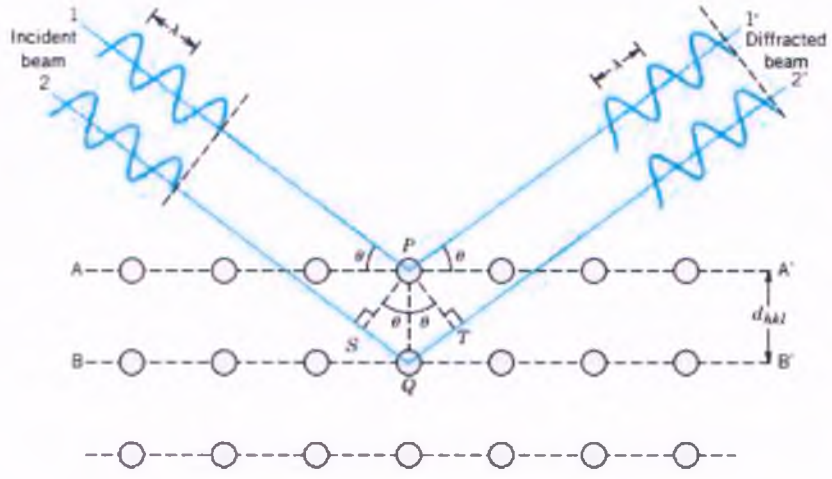

Figure 4.4. Diffraction of X-rays by planes of atoms. Reprinted from [130].

It is important to point out that Bragg's law holds true if atoms are replaced by molecules or groups of molecules, such as colloids, polymers or proteins. Diffraction patterns of crystalline solids reveal presence of sharp peaks corresponding to various crystal planes based on the Bragg's law. The peaks at low 2θ angles are from crystal planes of large d-spacing and vice-versa. Crystalline material in the powdery form contains a large number of small crystallites having random orientations. For any sets of planes with d-spacing there will be always few crystallites whose planes satisfy the Bragg reflection law. When 2D diffraction pattern is recorded, it shows Debye-Scherrer rings of scattering peaks corresponding to the various d-spacing the crystal lattice. As the amorphous solid do not have long-range order, there is no sharp Bragg's peaks but the scattered X-rays form typically one or to two smooth maxima with a very broad distribution in the 2θ range [128].

The X-ray diffraction measurements were performed at ambient temperature on Rigaku-Denki D/MAX RAPID II-R diffractometer (Rigaku Corporation, Tokyo, Japan) with a rotating anode AgK_α tube (λ=0.5608 Å), an incident beam (002) graphite monochromator and an image plate in the Debye-Scherrer geometry. The pixel size was 100 x 100 μm. All samples were placed inside Lindemann glass capillaries (2 mm in diameter) and measurements were performed for the sample filled and empty capillaries and the intensity for the empty capillary was then subtracted. The beam width at the sample was 0.1 mm. The two dimensional diffraction patterns were converted into the one dimensional intensity data using suitable software. The temperature measurements were performed by using the Oxford Cryostream Plus and Compact Cooler with resolution of 0.1 K.

4.2. Description of investigated materials and applied amorphization methods

Chemical compounds selected for present studies are mostly pharmaceutical important substances of van der Waals or hydrogen bonded interactions. Majority of investigated APIs were kindly gifted by Medical University of Gdansk (Poland). Other substances such as DNA and RNA nucleosides were supplied by Sigma Aldrich. Some materials were also deliberately synthesized for the purpose of this study. Tested samples were received as white, crystalline powders with declared purity > 98%, no further purification methods were applied. In order to prepare amorphous materials the following procedures were applied: melt quenching, compression of liquid and cryomilling. In case of some APIs, not all listed herein amorphization methods were possible to utilized.

To prepare qualitative analysis on the role of molecular dynamics in governing the physical stability of amorphous materials, only one amorphization method (i.e. vitrification) was mainly explored. Moreover, for detailed studies on the physical instability reasons very similar in chemical structure systems were selected (e.g. nucleosides and glucose derivatives). The choice of chemically similar compounds, but with completely different crystallization abilities turned out to be the most appropriate way to deal with instability issue of supercooled liquids and glasses.

Glassy samples were prepared in the following way. Crystalline material was placed on a polished stainless steel electrode and heated with the use of hotplate unit, until complete

melting was achieved. During this procedure temperature and color of samples were carefully controlled. In the next step, the electrode with melted sample was covered by another electrode (quartz or Teflon rings were used as spacers) and quenched with the use of cooled brass plate until its vitrification. In case of some materials with low glass transition temperature (e.g. Ibuprofen) or significant crystallization tendencies in the supercooled liquid state (e.g. Adenosine, Clarithromycin), crystalline samples were mounted in cryostat and heated up to their melting points with the use of NovoControl Quatro system (heated nitrogen gas stream). Then, they were cooled with the rate ca. 20 K/min to form the glassy state.

Before high-pressure studies on Ibuprofen were performed, investigated material was annealed at melting temperature (for up to 1 hour) to ensure that there was no crystallinity.

Grinding was performed using a cryogenic impact mill (6750 freezer/mill SPEX CertiPrep, Inc, USA) consisting of a stainless steel vessel immersed in liquid nitrogen, within which a stainless steel rod is vibrated by means of magnetic coil. Before grinding, 10 min of precool time was programmed. Then, the mill was planned to an impact frequency of 15 cycles per second for 6 min grinding periods separated by 3 min cool-down. The mass of each sample was 1 g. Total milling time was 1.5 hour. After milling, the grinding vial was immediately transferred to vacuum oven and allowed to warm to room temperature. Freshly prepared cryomilled samples are typically white powders. Before further investigation, water content was always determined by the Karl Fischer method (CRISON TitroMaticKF).

Prior to dielectric measurements, the amorphous nature of freshly made quenched and cryomilled materials were systematically verified by X-ray powder diffraction method. However, the usage of amorphous substances in pharmaceutical industry requires also successful passing many rigorous criterions, such as highest purity standards. Because of that reason, the chemical purity of outcome materials was validated as well, to make sure that amorphization process itself does not cause degradation of investigated APIs. This issue is particularly important in the case of substances which crystalline forms are thermally unstable or undergoing decomposition at melting temperature (e.g. Carbomazepine, Ziprasidone hydrochloride), so vitrification is simply not possible. Throughout my studies, I have encountered compounds that degrade as a result of extended mechanical milling at liquid nitrogen temperature [34]. Some of the amorphous substances, that I have dealt with, were also found to have an increase chemical reactivity and were prone to degradation process. Consequently, before any molecular dynamics studies were performed, the chemical purity of examined samples was always carefully verified. In order to test if examined compounds

undergo thermal degradation at melting point thermogravimetric measurements were carried out. Moreover, using Ultra Performance Liquid Chromatography (UPLC) additional information about purity of crystalline and amorphous samples were provided. This task was accomplished together with Preformulation Department of Pharmaceutical Works Polpharma SA (Poland). Our studies have revealed that upon amorphization of investigated in this work substances typically less than 1% of impurities is generated.

All materials selected for current studies can be supercooled. However, generally fast cooling rate is necessary to avoid crystallization. Upon heating from the glassy state cold-crystallization occurs in most cases. As a consequence, molecular dynamics cannot be measured over very broad range of characteristic relaxation times. Investigated samples represent intermediate and fragile glass-formers. Moreover, their glass transition temperatures span in a very wide range of temperatures, from 225 K (Ibuprofen) even up to 400 K (Telmisartan). As a result, some of them can be glasses even at room temperature, while the others not. A brief description of the most important properties of tested compounds are given below.

Compound's name	Features
Active Pharmaceutical Ingredients (APIs)	
Ibuprofen	**Chemical Formula**: $C_{13}H_{18}O_2$ **Molecular mass**: 206.28 g/mol **Melting Point**: 348 K **Glass transition temperature**: 225 K (from DS) **Fragility**: 87 **Additional information**: painkiller, supplied as racemic mixture by Medical University of Gdansk (original producer Hubei Biocause Pharmaceutical Co. Ltd) 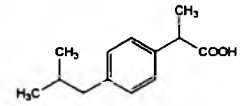
Telmisartan	**Chemical Formula**: $C_{33}H_{30}N_4O_2$ **Molecular mass**: 514.63 g/mol **Melting Point**: 540 K **Glass transition temperature**: 400 K (from DS) **Fragility**: 87 **Additional information**: prescribed for patients with high blood pressure, cardiac insufficiency and myocardial ischemia. Supplied by Medical University of Gdansk (original producer Dr. Reddy's Laboratories Ltd) as white crystalline powder 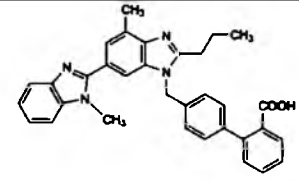
Antibiotics	
Azithromycin	**Chemical Formula:** $C_{38}H_{72}N_2O_{12}$ **Molecular mass:** 748.98 g/mol **Melting Point:** not determined **Glass transition temperature:** 375 K (from DS) **Fragility:** 117 **Additional information**: monohydrate, supplied as white crystalline powder by Pol-Nil (Warsaw, Poland). Amorphization via removal of hydrated water. 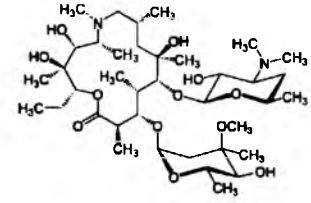
Clarithromycin	**Chemical Formula**: $C_{38}H_{69}NO_{13}$ Molecular mass: 747.95 g/mol **Melting Point:** 499 K **Glass transition temperature:** 382 K (from DS) **Fragility:** 118 **Additional information:** supplied as white crystalline powder by Pol-Nil (Warsaw, Poland). 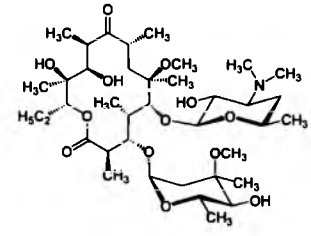
Roxithromycin	**Chemical Formula:** $C_{41}H_{76}N_2O_{15}$ **Molecular mass:** 837.04 g/mol **Melting Point:** not determined **Glass transition temperature:** 355 K (from DS) **Fragility:** 121 **Additional information:** supplied as white crystalline powder by Pol-Nil (Warsaw, Poland). Amorphization via removal of hydrated water. 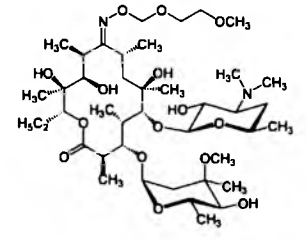

DNA and RNA Nucleosides	
β-Adenosine	**Chemical Formula:** $C_{10}H_{13}N_5O_4$ **Molecular mass:** 267.24 g/mol **Melting Point:** 508 K **Glass transition temperature:** 370 K (from DSC) **Fragility:** 90 **Additional information:** supplied by Sigma –Aldrich as white crystalline powder. Adenosine is neurotransmitter and anti-inflammatory agent. It also plays an important role in energy transfer and signal transduction. 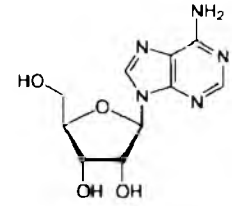
β-Uridine	**Chemical Formula:** $C_9H_{12}N_2O_6$ **Molecular mass:** 244.20 K **Melting Point:** 439 K **Glass transition temperature:** 336 K (from DSC) **Fragility:** 89 **Additional information:** supplied by Sigma –Aldrich as white crystalline powder. Uridine is one of the four basic components of ribonucleic acid (RNA). It plays an important role in the glycolysis pathway of galactose. 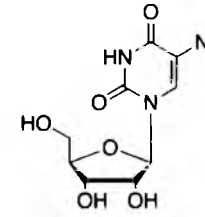
β-Thymdine	**Chemical Formula:** $C_{10}H_{14}N_2O_5$ **Molecular mass:** 242.23 g/mol **Melting Point:** 461 K **Glass transition temperature:** 328 K (from DSC) **Fragility:** 83 **Additional information:** supplied by Sigma –Aldrich as white crystalline powder. Thymidine is the DNA nucleoside T, which pairs with deoxyadenosine (A) in double-stranded DNA. 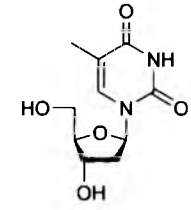
Saccharide derivatives	
Alpha-D-Glucose pentaacetate	**Chemical Formula:** $C_{16}H_{22}O_{11}$ **Molecular mass:** 390.34 g/mol **Melting Point:** 384-386 K **Glass transition temperature:** 289 K (from DS) **Fragility:** 88 **Additional information:** Synthesized by Division of Organic, Chemistry, Silesian University of Technology (purity 99%). Full name - 1,2,3,4,6-penta-O-acetyL-α-D-glucose. Used mainly in biochemical reactions and as medicine intermediate. 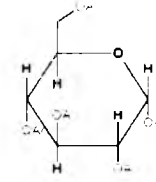
Beta-D-Glucose pentaacetate	**Chemical Formula:** $C_{16}H_{22}O_{11}$ **Molecular mass:** 390.34 g/mol **Melting Point:** 405 K **Glass transition temperature:** 288 K (from DS) **Fragility:** 88 **Additional information:** Synthesized by Division of Organic, Chemistry, Silesian University of Technology (purity 99%). Full name - 1,2,3,4,6-penta-O-acetyL-β-D-glucose. Used mainly in biochemical reactions and as medicine intermediate. 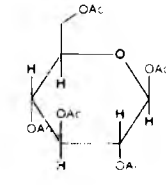

CHAPTER 5

ANALYSIS AND PRESENTATION OF EXPERIMENTAL RESUTS OBTAINED AT ATMOSPHERIC PRESSURE

5.1. Do dynamical properties of amorphous materials depends on the preparation method?

The question addressed in the above title is one of the most fundamental one concerning physics of amorphous materials. Subconsciously, we may believe that dynamical properties of amorphous materials do not depend on preparation way, as relaxation processes observed in dielectric spectra correspond to certain motions of molecules of either intra- or intermolecular origin. On the other hand, it is well documented in the literature that the characteristic properties of amorphous state, such as physical stability or thermal history, depend strongly on the treatment undergone by the material. So, why dynamical properties should be the same?

Very recently Carpentier and Descamps [131, 132] have claimed that mobility of trehalose below T_g depend on the way how the amorphous state was prepared. Based on experimental results, they have concluded that glasses may exist in many possible relaxation states with different kinetic properties. Unfortunately, this statement hasn't been confirmed for a broader group of substances. Thus, to verify if dynamical properties of amorphous materials depend on the amorphization method, selected substances were prepared in the amorphous state using two completely different routes available in our laboratory: vitrification and cryogenic grinding. In this section the appropriate results will be presented.

5.1.1. Telmisartan

First, relaxation dynamics of amorphous Telmisartan obtained by quenching of the melt will be presented. Figure 5.1. illustrates dielectric loss spectra of Telmisartan, measured at atmospheric pressure in supercooled liquid (panel a) and glassy state (b). The glass transition temperature T_g was defined as the temperature at which structural relaxation time τ_α is equal to 100 seconds, and its value for Telmisartan equals to 400 K. As illustrated, above glass

transition temperature α-peak moves towards lower frequencies with decreasing temperature, which indicates increasing time scale of global motions. The secondary β-relaxation is barely visible in the ε'' spectra at temperatures just above T_g, while in the glassy state it appears as a well pronounced β-peak. Very deep in the glassy state another, more faster secondary process (denoted as γ) appears. Unfortunately, it cannot be characterized as it did not show up completely within the experimental window.

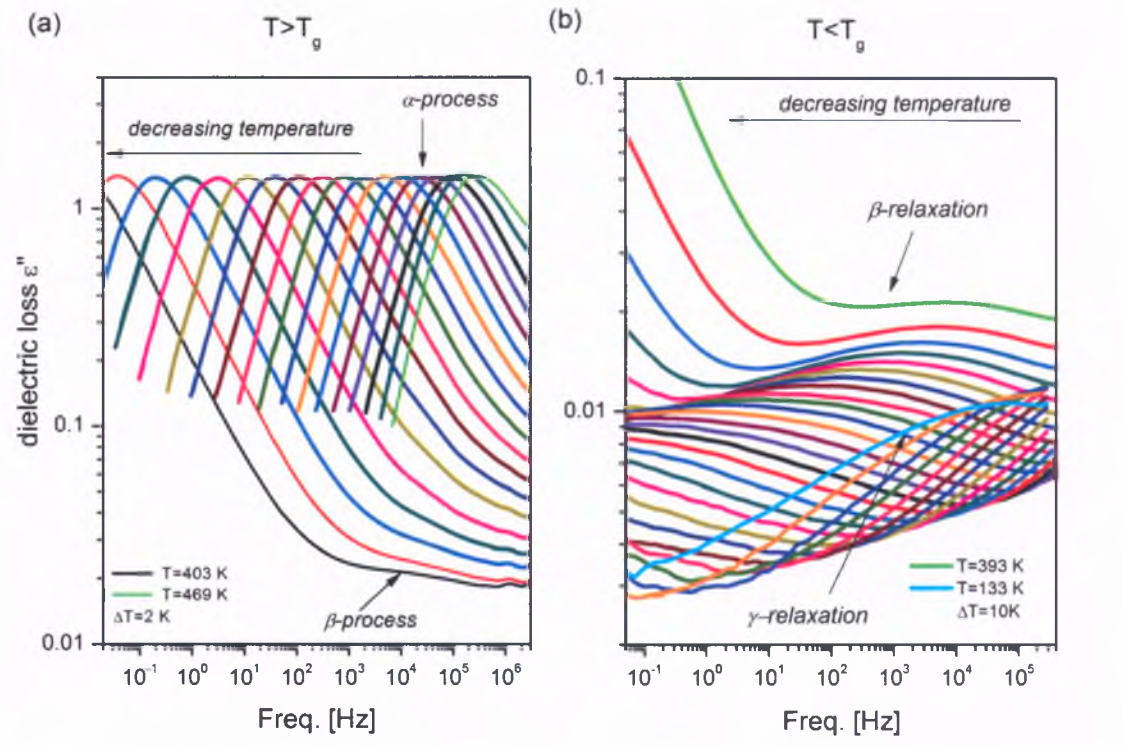

Figure 5.1. Dielectric loss spectra of Telmisartan obtained on cooling at ambient pressure. Panel (a) presents loss spectra collected above glass transition temperature, whereas panel (b) presents relaxation data collected in the glassy state of Telmisartan.

The temperature dependence of structural relaxation time τ_α measured over 10 decades in the supercooled liquid state was found to be satisfactory described by means of two VFT equations (Eq. 3.18), with the crossover temperature T_B=476 K. The temperature dependence of τ_β in the glassy state exhibit a linear dependence and can be well-described by the Arrhenius equation (Eq. 3.17). The activation energy E_β=81.8±1.2 kJ/mol is relatively high, which suggests intermolecular origin of this process. The $\tau_\alpha(T)$ and $\tau_\beta(T)$ dependences are shown in relaxation map of Telmisartan (Figure 5.2.(a)).

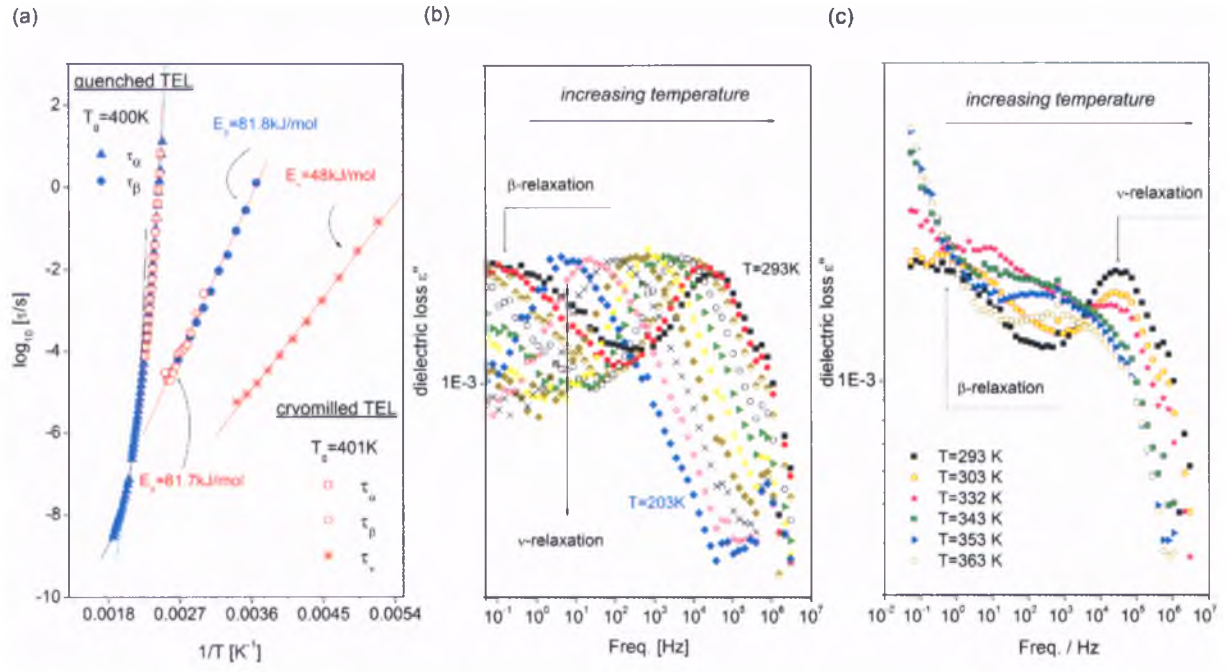

Figure 5.2. (a) Relaxation map of quenched and cryomilled Telmisartan. Blue filled triangles and circles denote structural and β-relaxation times of quenched sample. Open squares, circles and stars denotes τ_α, τ_β and τ_ν of cryomilled sample, respectively. Solid lines are VFT and Arrhenius fits to the temperature dependences of the structural and secondary relaxation times, respectively. Panels (b) and (c) present dielectric loss spectra in the amorphous state of cryomilled Telmisartan measured from 203 K to 293 K and 293 K to 383 K, respectively.

In the next step relaxation dynamics of cryomilled Telmisartan will be analyzed. Dielectric loss spectra were measured below and above glass transition temperature of cryomilled sample, which was found to be equal to 401 K. This value of T_g agrees very well with that reported for quench material (400 K). Representative spectra collected upon heating the amorphous sample obtained by cryogenic grinding are shown in Figure 5.2.(b) and (c). Similarly as for ordinary glass obtained by quenching of the melt, well-defined β-peak appears in the amorphous state of cryomilled material. However, in contrast to quenched sample, below glass transition temperature of cryomilled Telmisartan additional, faster relaxation mode appears (denoted as ν–relaxation). With further heating its amplitude decreases and the β-relaxation becomes more prominent (Figure 5.2. (c)).

Dielectric loss spectra of cryomilled Telmisartan collected above glass transition temperature are presented in Figure 5.3 (a). Subsequent heating of examined sample leads to a cold crystallization process, visible in dielectric loss spectra as the decrease of intensity of structural relaxation process at temperatures greater than 433 K. Because of that reason, it was impossible to follow α-relaxation dynamics in such wide range of temperatures as it happens

in the case of quenched sample. Herein, it is worth to note that the ease of recrystallization upon heating of cryomilled sample confirms that ground materials are in general physically less stable than quenched ones.

Figure 5.3 (b) presents comparison of dielectric loss spectra for cryomilled and quenched Telmisartan recorded in the liquid state at 411 K. As can be seen, the position of structural relaxation peaks as well as distribution of relaxation times were found to be practically the same. This finding indicates that irrespectively of the preparation method, once the material enters the supercooled liquid state differences in dynamical properties should be erased. In fact, studies that I have conducted for Telmisartan as well as many other compounds, have confirmed that this statement is essentially valid, but with one exception – substances which undergo tautomerization process. However, this issue won't be discussed herein as it is beyond the scope of this work.

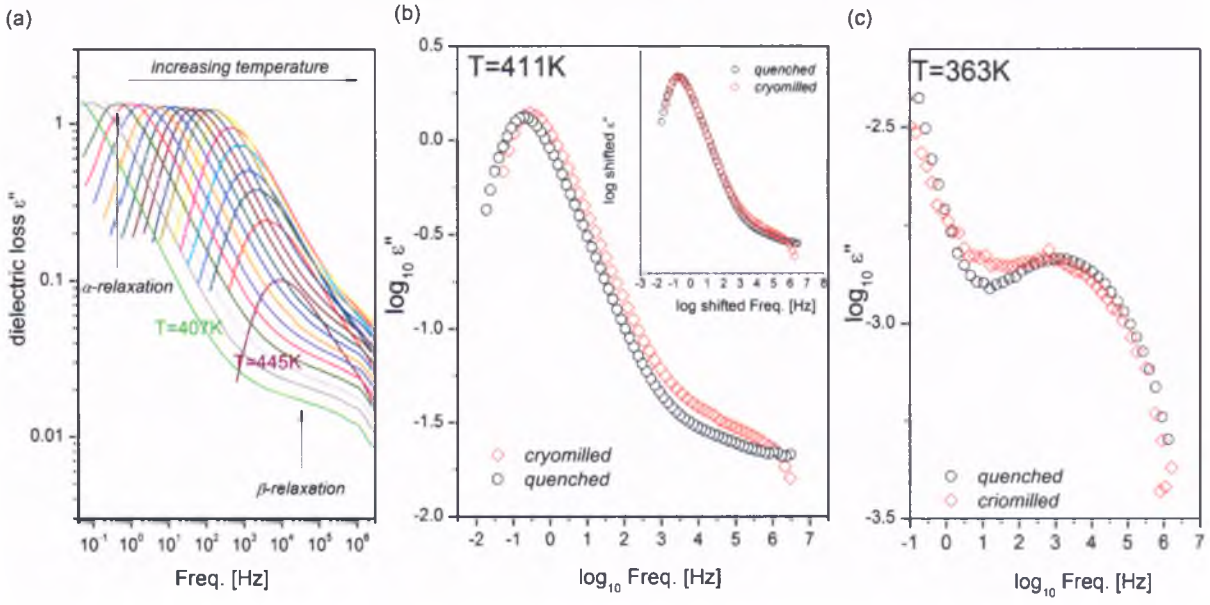

Figure 5.3. Dielectric loss spectra for cryomilled Telmisartan collected above T_g in steps of 2 K. (b) Comparison of dielectric loss spectra for quenched and cryomilled Telmisartan at 411 K. The inset presents the same data in double logarithmic scale horizontally shifted to superimpose. (c) Comparison of dielectric spectra for cryomilled and quenched Telmisartan collected at the same temperature located below T_g.

Figure 5.3 (c) presents comparison of dielectric loss spectra for cryomilled and quenched Telmisartan recorded below T_g, at 363 K. As can be seen, the position as well as the shape of β-peaks are essentially the same. For cryomilled sample, α-, β- and ν- relaxation times related to loss maximum ($1/2\pi f_{max}$) were calculated and added to the relaxation map of Telmisartan (Figure 5.2 (a)). The temperature dependences of β- and ν- relaxation times exhibit linear

pattern and can be described by Arrhenius power law with activation energies E_β=81.7±4.0 kJ/mol for β-relaxation and E_ν=48±1 kJ/mol for ν-relaxation. The same value of the activation barrier for β-relaxation in quenched and cryomilled Telmisartan indicates that irrespective of the amorphization method this mode exhibits the same behavior.

It is noteworthy that ν-process detected in cryomilled sample has the same temperature sensitivity as that reported for confined water [133]. This suggests that newly observed relaxation mode in the amorphous state of Telmisartan might be related to the relaxation of confined water molecules. Having this in mind, the Karl Fisher method was applied to identify the amount of water content in investigated samples. For cryomilled Telmisartan 4 % of water fraction was reported, while freshly made vitrified sample turned out to be practically anhydrous (less than 0.5 % of water). More so, when cryomilled sample was heated above T_g, annealed at temperature 433 K for about 1 hour and then quenched in order to its re-amorphization, the presence of the ν-relaxation was not detected. This suggest that all confined water has been removed during evaporation.

The opposite experiment was also performed for glassy sample (prepared by vitrification of liquid), which was stored at 80% RH and 298 K for 2 days. Dielectric measurements on hydrated glassy Telmisartan revealed presence of an additional ν-relaxation. Thus, it can be concluded that the presence of water in amorphous material significantly changes its relaxation dynamics and causes the appearance of a new mode associated with dynamics of confined water.

Results presented in this subsection indicate that, indeed, different routes of amorphization lead to amorphous materials with diverse molecular dynamics (presence of additional secondary relaxation). However, differences in dynamical properties below T_g for cryomilled and quenched Telmisartan arise only from the fact that during manufacturing processes (which are completely different in their nature) they uptake different amount of water from the surroundings. It is worth to stress that the temperature behavior of τ_β was found not change with the variation of water content in amorphous Telmisartan. Nonetheless, in some cases the temperature dependences of secondary relaxations are strongly related to water content. Typically, secondary relaxations are faster with increasing hydration. However, depending on the inter- or intermolecular origin of secondary relaxations, water might influences their dynamics in slightly different way [134].

5.1.2. Antibiotics

In the context of aroused question, I would like to present now results from dielectric studies performed for amorphous (quenched and cryomilled) antibiotics: Azithromycin, Roxithromycin and Clarithromycin. In Figure 5.4 panels (a-f), dielectric loss spectra collected during heating glassy antibiotics are shown. Freshly prepared vitrified antibiotics were found to be practically anhydrous (less than 0.7 % of water). For the sake of clarity, dielectric loss spectra of each antibiotic were divided into two panels presenting relaxation dynamics from the region above and below T_g. The glass transition temperature was defined as the temperature at which structural relaxation time τ_α is equal to 100 seconds. They are as follows 375 K, 382 K and 355 K for Azithromycin, Clarithromycin and Roxithromycin, respectively.

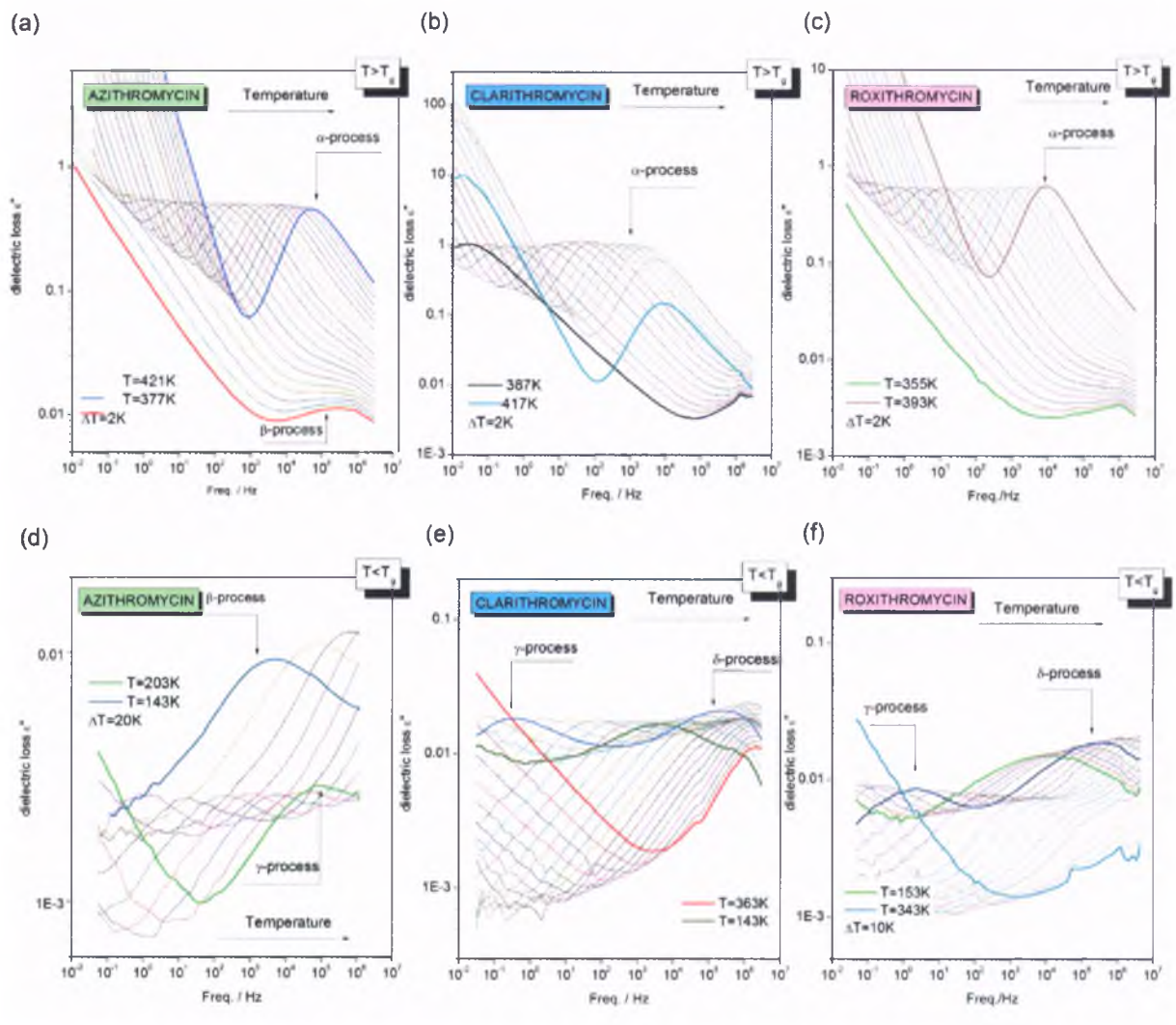

Figure 5.4. Dielectric loss spectra of anitbiotics: Azithromycin. Clarithromycin and Roxithromycin measured above (panels a, b and c) and below (panels d, e and f) their glass transition temperatures.

It is worth to mention that antibiotics possess completely different resistance against crystallization in the supercooled region i.e. during heating from the glassy state only Clarithromycin began to crystallize at temperature ~T_g+31.5 K, whereas two other antibiotics did not reveal no signs of crystallization abilities. The next essential difference between examined antibiotic agents is that only for Azithromycin in the vicinity of the glass transition the β-relaxation is clearly visible as a well-separated peak, while for Clarithromycin and Roxithromycin an excess wing appears on the high frequency flank of their α-loss peaks.

In panels (d), (e) and (f) of Figure 5.4 dielectric response in the glassy state of antibiotics is presented. For Clarithromycin and Roxithromycin two secondary processes were observed. The slowest one, denoted as γ–relaxation and the faster one, labeled as δ–relaxation. Interestingly, in the glassy state of Azithromycin β- and δ– relaxations were only detected, whereas γ-relaxation was absent. This is quite surprising, especially when similarities in the chemical structure of all three materials are taken into account. From the resolved β-, γ- and δ- relaxation peaks the corresponding relaxation times, related to loss maximums ($1/2\pi f_{max}$), have been determined and then, activation barriers were calculated. They are all listed in Table 5.1.

Table 5.1. Activation energies of secondary relaxations detected in the glassy state of antibiotics obtained using vitrification method.

Material	Activation energy β-relaxation [kJ/mol]	Activation energy γ-relaxation [kJ/mol]	Activation energy δ-relaxation [kJ/mol]
Azithromycin	61.3 ±0.5	51 ±1 (cryomilled sample)	24.8 ±0.5
Clarithromycin	- Excess wing	56.4 ±1.2	23.8 ±0.8
Roxithromycin	- Excess wing	54.8 ±1.2	27.5 ±0.2

It is interesting to point out that activation energies for γ- and δ- relaxations are practically the same, which suggest same molecular motions involved in. This is also clearly visible when γ- and δ- relaxation peaks recorded at the same temperature are plotted on the same

graph, as presented in Figure 5.5. For Clarithromycin and Roxithromycin the position of loss maximums related to γ- relaxation as well as peak shapes were found to be identical (Figure 5.5 (a)). Analogical situation happens also in the case of δ-relaxation (Figure 5.5.(b)), which for considered antibiotics has most probably the same molecular origin.

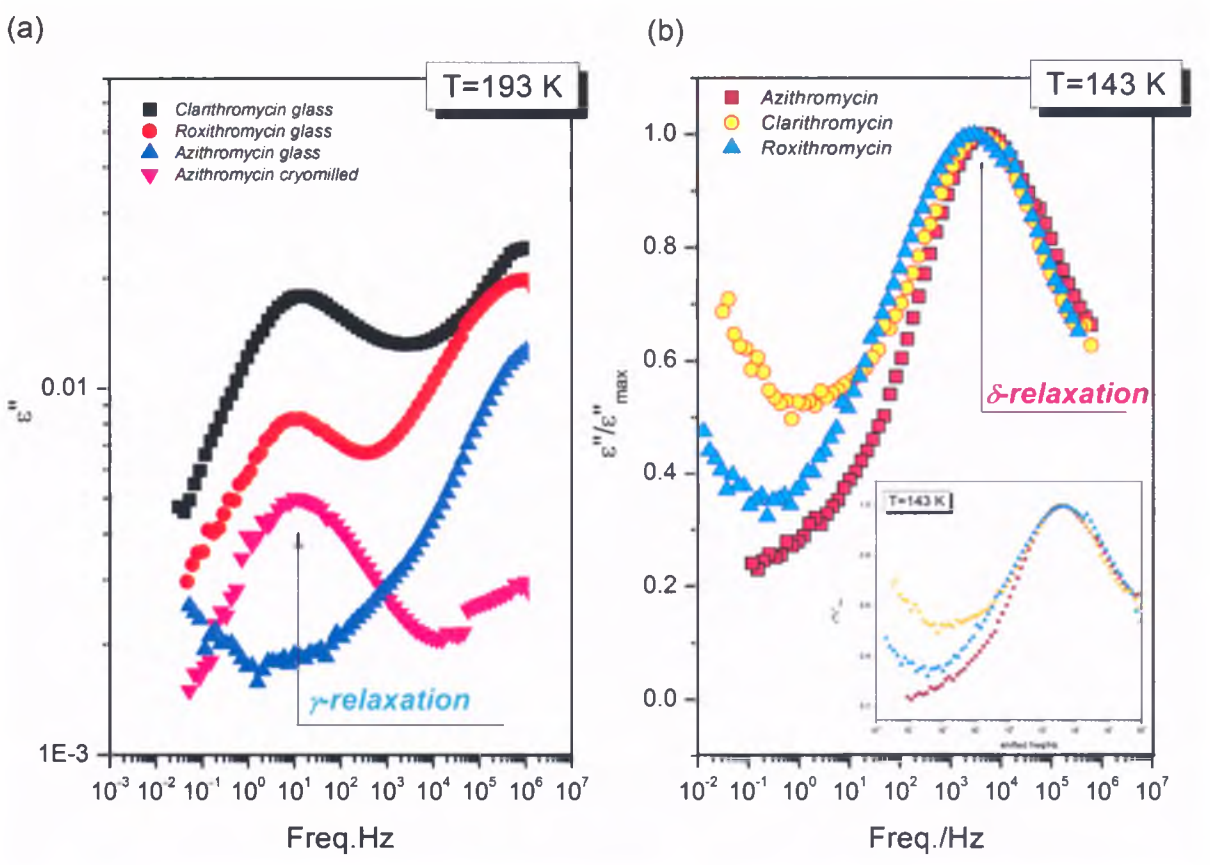

Figure 5 5. Comparison of (a) γ- relaxations in the glassy state of antibiotics at T=193 K. (b) δ-relaxations in the glassy state of antibiotics at T=143 K. The inset presents same, superimposed dielectric loss spectra.

Selected antibiotics, Azithromycin and Roxithromycin were also subjected to mechanical treatment in cryogenic mill in order to induce their amorphization. This enabled me to verify again if dynamical properties of amorphous substances depend on preparation method. It is worth to mention that the analysis with the use of Karl Fischer method revealed 4 %, 1.5 % and 2 % of water content in the initial crystalline antibiotics Azithromycin, Clarithromycin and Roxithromycin, respectively. Freshly prepared cryomilled Azithromycin and Roxithromycin contain 3.5 % and 2 % of water.

Let's consider first relaxation dynamics of cryomilled Roxithromycin. In Figure 5.6 dielectric loss spectra of cryomilled and quenched Roxithromycin recorded at 173 K and 383

K are presented together on the same graph to demonstrate that they molecular dynamics is essentially the same. The only difference in dynamical properties of cryomilled and glassy Roxithromycin concerns the amplitude of δ-relaxation, which is significantly lower in the former case. Upon heating of cryomilled Roxithromycin no crystallization event was observed in the supercooled liquid state.

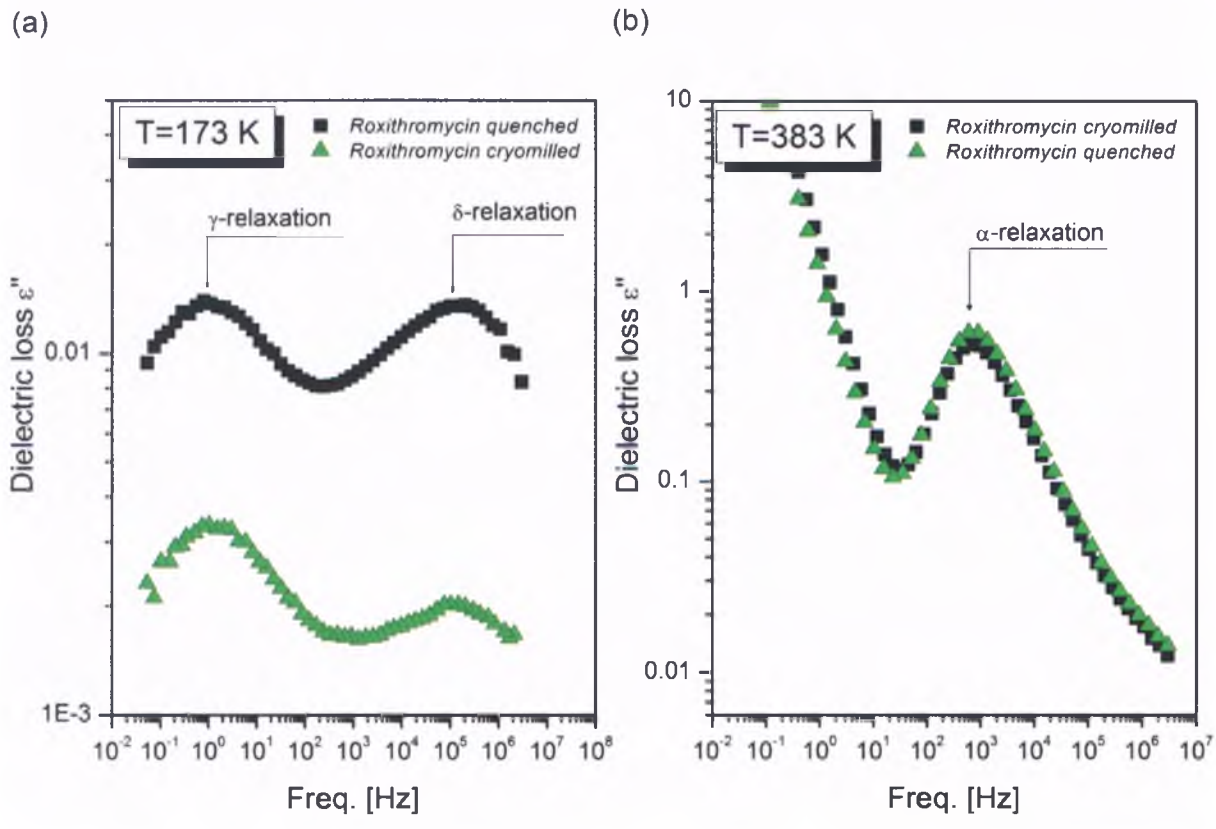

Figure 5.6. Comparison of dielectric loss spectra of quenched and cryomilled Roxithromycin recorded (a) in the amorphous state at temperature T=173 K and (b) in supercooled liquid state at temperature T=383 K.

In Figure 5.7 similar comparison is made for quenched and cryomilled Azithromycin. However, in this case the results are quite surprising. In dielectric loss spectra of cryomilled Azithromycin additional relaxation appears (Figure 5.7.(a)). This process was labeled as γ-relaxation, because it can be identified with γ-relaxation in the glassy state of Clarithromycin and Roxithromycin. The fact that in the supercooled liquid state structural relaxation times and α-peak shapes of vitrified and cryomilled Azithromycin are the same, is another conformation that once the material passes the glass transition temperature towards the liquid state, all differences in dynamical properties disappear.

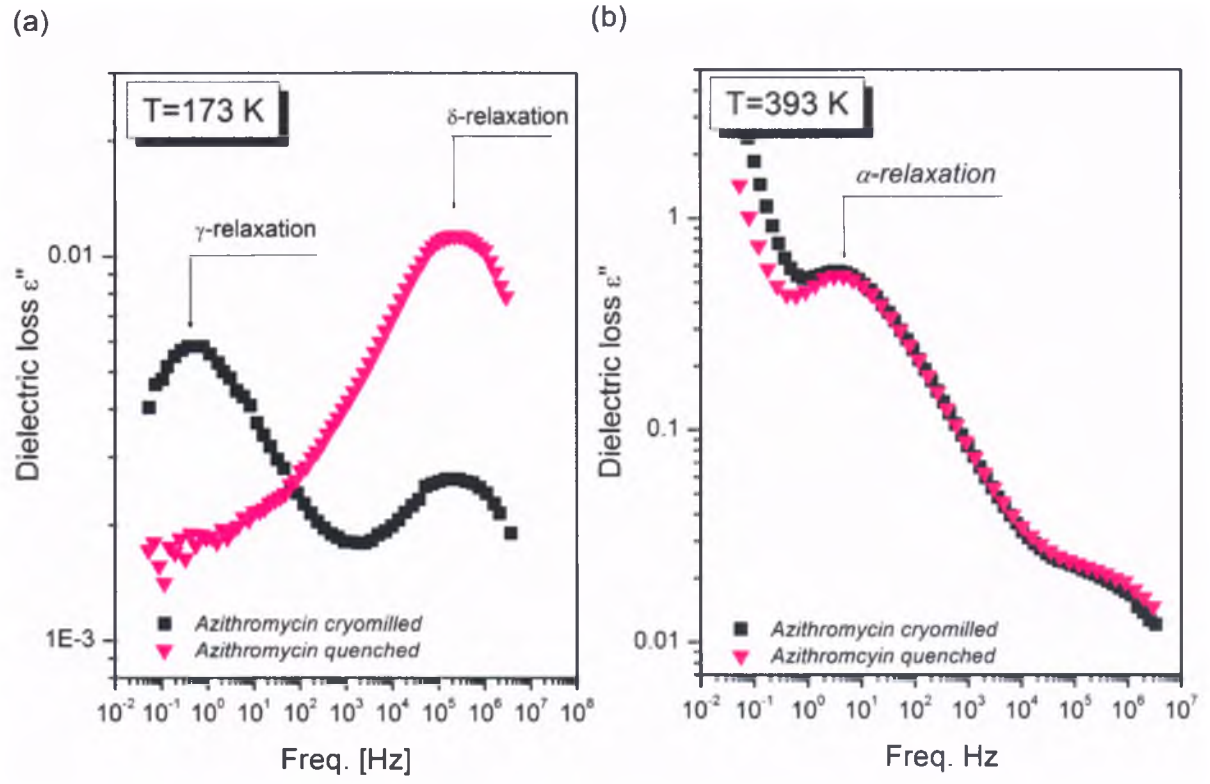

Figure 5.7. Comparison of dielectric loss spectra of quenched and cryomilled Azithromycin recorded (a) in the amorphous state at temperature T=173 K and (b) in supercooled liquid state at temperature T=393 K.

At this place it is worth to note that upon heating of cryomilled Azithromycin no crystallization event was observed. What is more, amorphous Azithromycin and Roxithromycin obtained by cryogenic grinding were found to be physically stable for more than 6 months of storage at ambient conditions. This is in contradiction to the common believe that cryomilled materials are prone to recrystallization.

Once the γ-relaxation visible in the amorphous state of cryomilled Azithromycin is plotted together with data presented earlier for vitrified Clarithromycin and Roxithromycin at 193 K, it becomes obvious that they molecular origin is most probably the same (Figure 5.5.(a)). The activation energy of the γ-relaxation in cryomilled amorphous Azithromycin was found to be equal to 51±1 kJ/mol (Table 5.1). The appearance of γ-relaxation was also observed for vitrified Azithromycin which was subjected to 80% RH at 298 K for 5 days.

Interestingly, heating of cryomilled as well as hydrated glassy Azithromycin to the temperature region well above T_g, and then cooling it back to the glassy state results in relaxation dynamics of vitrified anhydrous sample. This might lead to a straightforward conclusion that γ-relaxation is somehow related to the dynamics of water confined. However,

the presence of γ-mode was confirmed in dielectric loss spectra of anhydrous glassy Clarithromycin and Roxithromycin, and this relaxation doesn't vanish no matter how long both samples are annealed at high temperatures. Because of that reason, it was conjectured that γ-relaxation in the amorphous state of antibiotics must reflect some local motion that is inactive in anhydrous glassy Azithromycin, but activates in cryomilled sample due to the presence of water. Nevertheless, more detailed studies on that issue are essential in the future.

Summarizing, dynamical properties of amorphous substances prepared using two different amorphization routes, i.e. cryomilling and vitrification, were found to differ. However, discrepancies in molecular dynamics result mainly from the fact that during manufacturing they uptake different amount of water from the surroundings and this absorbed water has a significant influence on their properties. It is also worth to note that, typically cryomilled samples are considered to be physically less stable than quenched ones. However, there are always some exceptions such as described above antibiotics, or Telmisartan which amorphous state obtained by cryogrinding was found to be physically stable even after 1 year of storage at room temperature [135].

5.2. How to predict the time scale of structural relaxation below T_g ?

Structural relaxation gives us information about global molecular mobility of the system, which is one of the most important parameters determining physical stability of amorphous materials. The knowledge of the time scale of molecular motions in the glassy state is important for future applications in pharmaceutical industry, as it provides crucial information about storage conditions that will ensure their long-term stability. Unfortunately, due to an exceedingly long time scale, direct measurements of structural relaxation times below the glass transition temperature are fairly impossible. Thus, the temperature dependence of α-relaxation time below T_g, especially its VFT or Arrhenius-like character, is unidentified. However, there are still some means allowing estimation of the time scale of global molecular mobility in the glassy state. Here, I have made an attempt to examine them carefully in the context of pharmaceutical, Telmisartan. Finally, it should be noted that predicted using various methods structural relaxation times in the glassy state were never confronted with each other, so it is completely unknown whether they give back same time scale of global

motions below T_g. For simplicity, in this work the amorphous state obtained by vitrification of liquid was only considered.

5.2.1. Telmisartan

The first method that I have applied to predict the time scale of molecular motion is glassy state of Telmisartan was that proposed by Casalini and Roland (CR). It is worth to remind that the most important criterion of its successful utilization is JG nature of the β-relaxation. Thus, before any prediction of τ_α in the glassy state of Telmisartan was made, it was necessary to

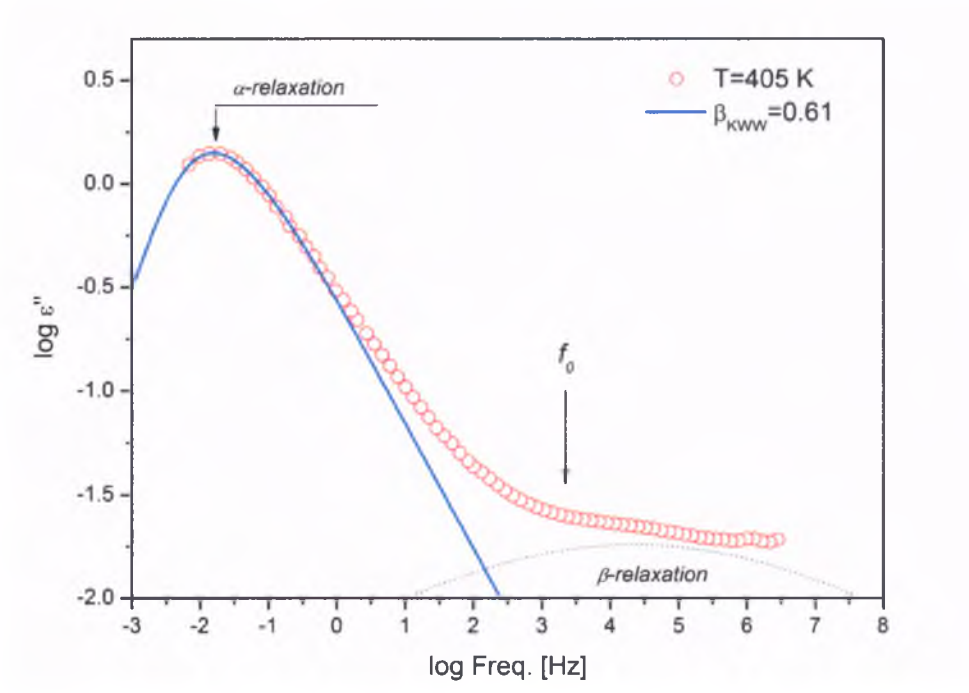

Figure 5.8. Dielectric loss spectrum of Telmisartan recorded at 405 K under atmospheric pressure. The arrow indicates the location of the calculated frequency f_0 of the primitive process.

verify its intermolecular origin. To do that, the Coupling Model was first applied. Figure 5.8 presents dielectric data recorded just above T_g at 405 K where β-peak is visible as broad shoulder. For Telmisartan, the value of stretching parameter β_{KWW}=0.61 was used to calculate the primitive relaxation time τ_0 from Eq. (3.36). The position of the primitive frequency f_0 lies within the range of broad shoulder, and hence support identification of the β-process as JG-relaxation. Furthermore-, Eq. (3.37) and (3.38) were used as another tests of the JG nature of the β-relaxation. In case of Telmisartan T_g=400 K, E_β=81.8 kJ/mol and

$\log_{10}[\tau_{\infty-\alpha}(s)]=-15.9$, so the left side of Eq. (3.38) is equal to 24.6, whereas the right side gives 28.9. Comparable values obtained for the left and right sides serve as further evidence that β-process visible in dielectric loss spectra of Telmisartan is JG type. Moreover, the ratio E_β/RT_g=24.6 is in good agreement with the value of 24 (Eq. 3.37) found by Kudlik for JG β-relaxation in several glass-formers.

Having the nature of the β-relaxation validated, aging experiments were performed at four temperatures: 393 K, 373 K, 353 K and 333 K. Figure 5.9 (a) shows representative dielectric spectra of Telmisartan recorded as a function of time at constant temperature T= 353 K. As usual, with physical aging separation between α- and β- relaxations increases and both, intensity and dielectric strength of the β-relaxation decrease.

Interestingly, the underlying mechanism responsible for decrease of dielectric strength of the JG relaxation with aging is still not clear. Two possible scenarios were proposed. The first one bases on the idea of 'islands of mobility' proposed by Johari and Goldstein [113]. In view

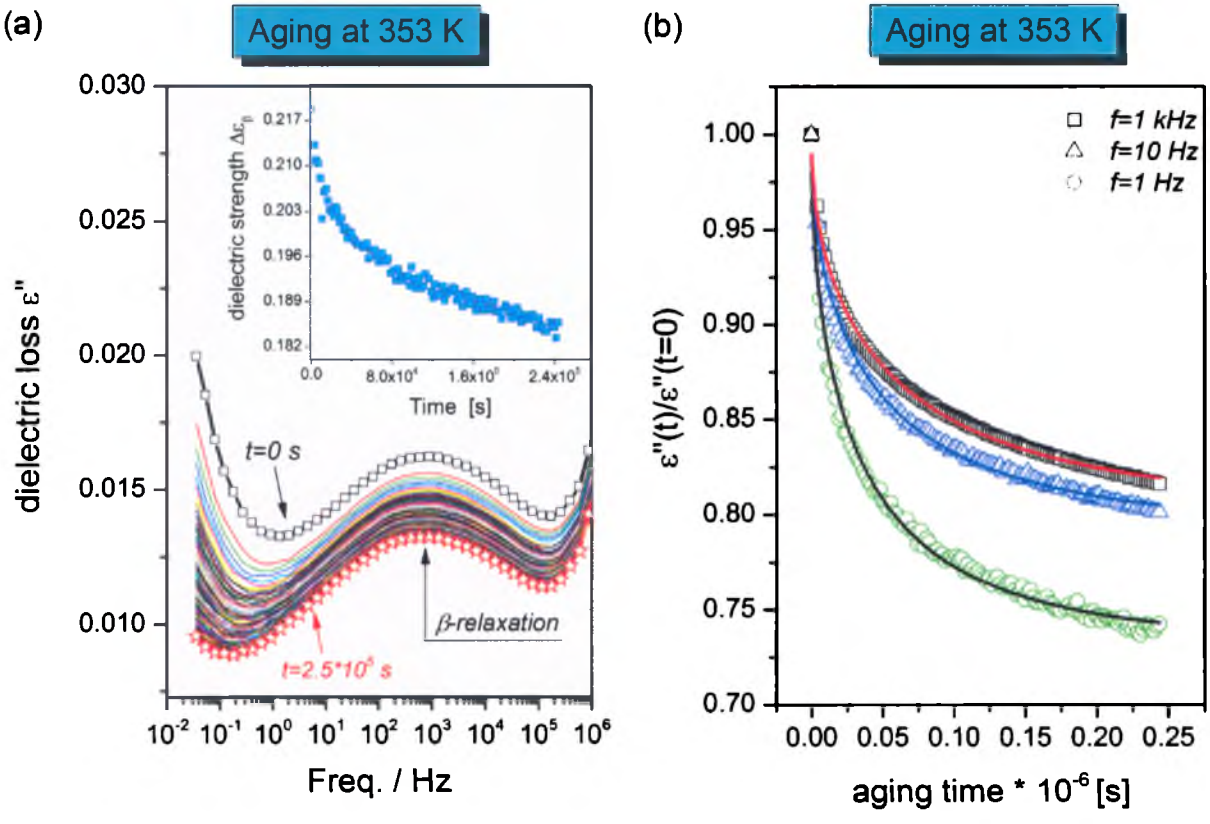

Figure 5.9. Panel (a) Dielectric loss spectra at T=353 K during physical aging. The inset presents time evolution of dielectric strength of the JG relaxation upon aging ; Panel (b) Normalized dielectric loss plotted versus aging time for three fixed frequencies. All curves were fitted to Eq. (3.30). Irrespectively of the chosen frequency, similar time constant $\tau_{\alpha g}$ was obtained.

of this concept, as the structure of glass becomes kinetically frozen the size of loose packing regions ("islands of mobility") and their population decreases. This results in a decrease of dielectric strength of the JG relaxation. The other scenario is based on the NMR results [136], which suggest that all molecules will contribute to the JG relaxation by undergoing a small-angle rotational diffusion, after which the larger angle diffusion corresponding to the structural relaxation would occur. The NMR measurements revealed that rotational angle is independent of temperature. Thus, if all molecules were contribute to JG relaxation, on increasing density upon aging its dielectric strength would increase with time due to increasing number density of dipoles N ($\Delta\varepsilon \propto N/T$). In recent days the most credible explanation assumes that with physical aging the population of relaxing dipoles decreases and this brings about the number of events that acts as precursor of the α-relaxation also to decrease.

Figure 5.9 (b) presents $\varepsilon''(f,t_{ag})$ dependences normalized by the factor $\varepsilon''(f,t_{ag}=0)$, which were described by means of Eq. (3.30). The best fits are displayed as solid lines. CR approach assumes that distribution of structural relaxation times does not change below the glass transition temperature so, $\beta_{ag}(T<T_g)=\beta_{KWW}(T_g)$. Hence, to fit the experimental data fixed value of stretching parameter β_{KWW}=0.61 was used. It is worth pointing out that the fitting function with fixed β_{ag}=0.61 describe experimental points quite well, but not perfectly. To ensure that τ_{ag} does not significantly change during aging experiment, the normalized dielectric permittivity curves were divided into few intervals (covering, overlapping and exceeding the whole range of the experiment) and then simultaneously fitted to Eq. (3.30), while τ_{ag} was allowed to vary independently. As it turned out, the value of aging time constant τ_{ag} does not change appreciably for different time intervals. Casalini and Roland stated that the estimated, by Eq. (3.30), τ_{ag} do not necessarily represent equilibrated τ_{α}, but they are isostructural values whose time scale depends on the structural relaxation [102].

Similar analysis as that presented above was also performed for three other temperatures, and same changes in the dielectric permittivity were observed. However, for the sake of clarity the corresponding data won't be presented in this work. The calculated values of τ_{ag} plotted versus inverse of temperature are shown in relaxation map of Telmisartan. As illustrated in Figure 5.10 (red stars), the time scale of τ_{ag} is considerably larger than τ_{α}

measured above T_g. More so, its temperature dependence in the glassy state is rather Arrhenius-like.

To extract information about structural relaxation time in the glassy state of Telmisartan more simple and certainly less precise method was also applied. This approach bases on the construction of master curve i.e. selected α-relaxation peak which is located near but above T_g was shifted horizontally to the temperatures below T_g so that its high frequency side superimposes with the low frequency side of the spectrum collected below T_g. It should be noted that before each spectrum below T_g was collected, the sample was reheated above T_g

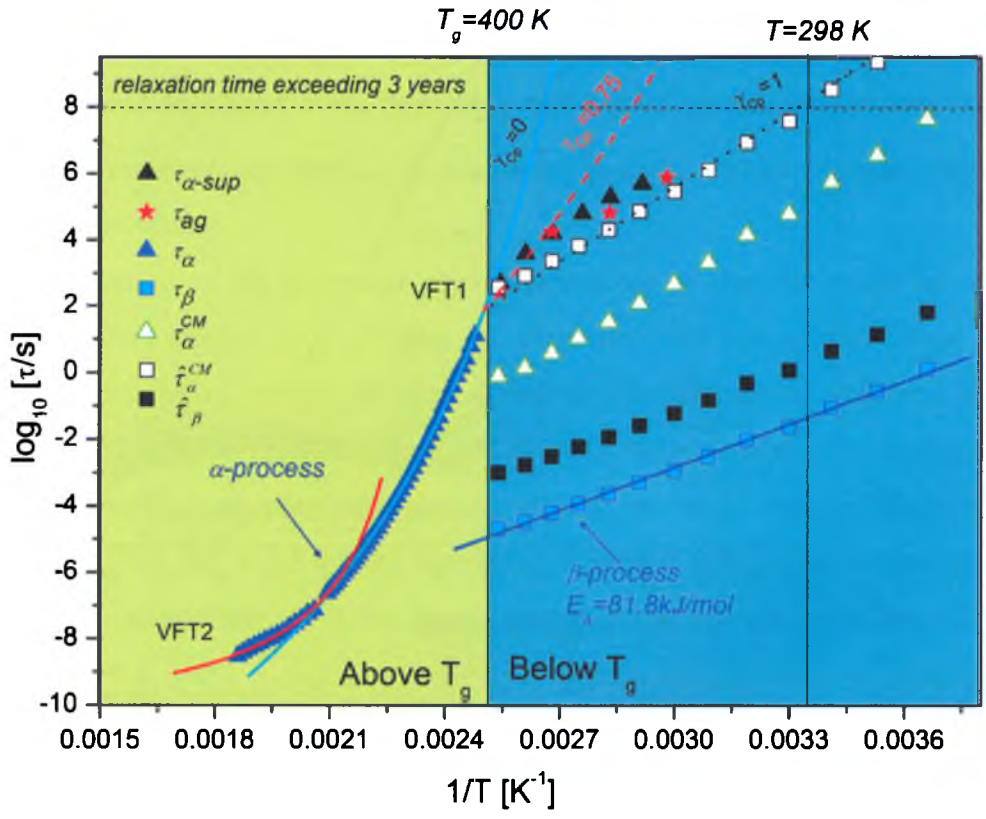

Figure 5.10. Relaxation map of Telmisartan. Temperature dependence of τ_α above T_g was described by two VFT equations. Structural relaxation times in the glassy state were estimated in different ways: by horizontal shift of the α-peak from the region above T_g to the temperatures below T_g ($\tau_{\alpha\text{-}sup}$), basing on aging induced changes in JG relaxation in accordance with Casalini and Roland approach (τ_{ag}) and from the Coupling Model. The structural relaxation times τ_α^{CM}, shown as green open up triangles, were calculated using Eq. (3.31) with β_{KWW}=0.61 and $\tau_\beta \equiv 1/(2\pi f_p)$ represented by closed blue squares. The temperature dependence of $\tau_\beta(T)$ follows Arrhenius behavior below T_g. The structural relaxation times $\hat{\tau}_\alpha^{CM}$ shown by black open squares were calculated using CM with β_{KWW}=0.61 and $\hat{\tau}_\beta \equiv 1/(2\pi \hat{f}_p)$ represented by closed black squares, where $\hat{f}_p$ is 1.7 decade lower than f_p. Red dashed line represent structural relaxation behavior predicted using modified Adam-Gibbs equation (Eq. 3.27) with γ_{C_p}=0.75 extracted from calorimetric measurements. The upper and lower extremes of γ_{C_p} are shown as cyan solid and black dotted lines, respectively.

and allowed to relax. Then, it was cooled down again to the glassy state. This procedure ensures that estimated structural relaxation times were indeed isostructural. The schematic illustration of master curve approach is present in Figure 5.11. The basic assumption of this method is that the time-temperature superposition (TTS) for the α-relaxation is valid above as well as below T_g. Relaxation times, $\tau_{\alpha\text{-}sup}$, determined in this way are shown in Figure 5.10 as black filled triangles. Surprisingly, they are more or less the same as that estimated from CR approach.

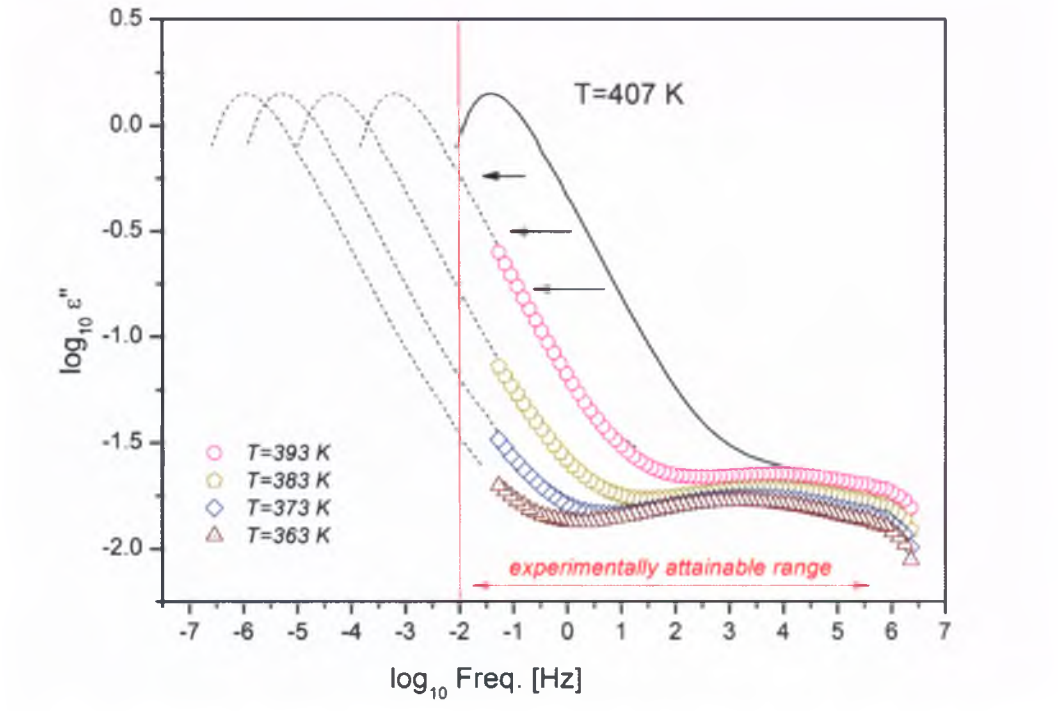

Figure 5.11. Master curves of Telmisartan formed by horizontal shift of structural relaxaion peak recorded at 407 K to overlap with spectra measured at temperautres below T_g.

Structural relaxation times in the glassy state of Telmisartan were also calculated basing on Coupling Model relation (Eq. 3.31) and by assuming again that frequency dispersion of α-relaxation, described in terms of stretching parameter β_{KWW}=0.61, does not change below T_g. These results (τ_α^{CM}) are presented in relaxation map of Telmisartan (Figure 5.10) as green open triangles. At first glance, one can note serious inconsistency between calculated values of τ_α^{CM} and $\tau_{\alpha g}$, or even $\tau_{\alpha\text{-}sup}$. This might suggest that correlation between JG relaxation and structural relaxation given in terms of the CM, originally derived to show the correlation between structural relaxation and JG relaxation in the region above T_g, does not hold any

more below T_g. However, one can explained this glaring disagreement by the width of the β-loss peak in Telmisartan which is unusually broad, when compared with other glass-formers. This brings large uncertainty in identifying the characteristic β-relaxation time determined from its very broad maximum as $1/2\pi f_p$, where f_p is the frequency of peak maximum.

Let's consider now the following situation. When $\hat{f}_p$ is taken to be 1.7 decades lower than f_p, one can estimate from the flat β-loss peak that $\varepsilon''(\hat{f}_p)$ is only about 10% less than $\varepsilon''(f_p)$. Thus, this choice of $\hat{f}_p$ is as valid as f_p to stand for the characteristic β-relaxation frequency f_β, and $\hat{\tau}_\beta \equiv 1/(2\pi \hat{f}_p)$ for the corresponding characteristic β-relaxation time. Now, $\tau_0 = \hat{\tau}_\beta$ (Fig. 5.10, black filled squares) together with $\beta_{KWW}=0.61$ were taken to calculate $\hat{\tau}_\alpha^{CM}$ from Eq. (3.31). As illustrated in Figure 5.10, there is a quite good agreement between $\hat{\tau}_\alpha^{CM}$ (open squares) and τ_{ag}, however, the method of estimation 'correct' values of β-relaxation times might be highly speculatve.

The key assumption of all presented above approaches is that the shape of structural relaxation peak won't change upon crossing the glass transition temperature (fixed value of stretching parameter β_{KWW}). In such situation Arrhenius-like behavior of structural relaxation time below T_g was obtained. However, the same shape of the structural relaxation peak above and below glass transition temperature is not as certain as one might suppose. In the literature it was speculated that the width of the structural relaxation will increase with separation between α- and β- relaxations [137]. As cogent argument one can also give that τ_{ag} shifts to longer times on aging, while τ_β not, so the consistency with the CM requires increase of $n \equiv 1-\beta_{KWW}$.

Now, it is of interest to estimate the temperature dependence of structural relaxation time in the glassy state of Telmisartan on the basis of its thermodynamic properties. For that reason, the modified Adam-Gibbs approach was applied and then, consistency with previously determined structural relaxation times was tested. Firstly, γ_{Cp} was calculated from Eq. (3.29) using following values of experimentally measured for Telmisartan heat capacities data at T_g: C_p^{liq}=1.92 J/(K·g), C_p^{cryst}=1.4 J/(K·g) and C_p^{glass}=1.53 (J/K·g). For a freshly formed glassy Telmisartan, γ_{Cp} was found to be 0.75±0.07, which suggest more VFT-like behavior of structural relaxation times in the glassy state. This value together with VFT1 fitting parameters from the region just above T_g ($\log_{10}[\tau_\alpha(s)]=-15.9$, D=4.6 and T_0=318 K) were

used to generate curve that describes structural relaxation behavior in the glassy state (Eq. (3.27)). Predicted dependence $\tau_\alpha(T)$ in non-equilibrated glassy state of Telmisartan is presented in Figure 5.10, as red dashed line. Simultaneous curves were also generated for two opposite extremes of γ_{Cp}, i.e. γ_{Cp}=0 (extended VFT1 fit) and γ_{Cp}=1 (Arrhenius temperature dependence). As illustrated in Figure 5.10, relaxation times τ_{ag} and even $\tau_{\alpha\text{-}sup}$ follow the dependance prediced by the modifed AG equation only in the vinicity of glass transition. Deep in the glassy state their undergo smaller changes with temperature than evaluated from the modified AG equation. When we assume that the correlation between α-relaxation and JG process persists in the glassy state, we may expect then typical strong behavior of structural relaxation time represented by $\hat{\tau}_\alpha^{CM}$.

Substantial discrepancy between relaxation times estimated previously and those predicted based on modified Adam-Gibbs method is evident. However, it should be also pointed out that significant limitation of modified Adam-Gibbs method is that it is appropriate for predicting dynamics of only freshly formed glass. This makes descriptive comparison between degree of molecular mobility predicted from modified AG equation and other approaches very difficult.

As can be seen in Figure 5.10, for a system which structural relaxation time below T_g follows Arrhenius-like dependence the typical shelf-life time is reached at vastly lower temperature, far from glass transition temperature. However, even if we assume that structural relaxation time below T_g of Telmisartan follows $\hat{\tau}_\alpha^{CM}$ dependence, the time scale of global motions at room temperature (and even human body temperature) would exceed 3-years. Indeed, it was confirmed experimentally by XRD examination that the glassy state of that drug is still physically stable after 2.5 years of storage at ambient conditions. Because of that reason, amorphous Telmisartan prepared by vitrification of liquid is very promising candidate for further pharmaceutical investigations.

5.3. What Governs the Physical Stability of Amorphous Pharmaceuticals? Global Mobility, Local Mobility or Maybe Something Else?

This section deals with critical factors that are responsible for recrystallization from the glassy state, with special interests to molecular mobility. The physical stability of selected glass-formers will be discussed in the context of global as well as local mobility. Generally, it is accepted that when amorphous material is stored at or below Kauzmann temperature T_K it will exhibit maximal stability. However, from practical standpoint storage at temperature $T<T_K$ is not possible in many cases. Thus, it is important to understand which factors and in which way can be responsible for instability issue.

In recent years a lot of attempts have been made to correlate crystallization tendencies of completely different chemical compounds with their molecular mobility. This is usually done by analyzing the impact of only one selected parameter related to their relaxation dynamics, for example fragility or the width of α-relaxation process. However, neglecting same time other factors such as thermodynamics, preparation method or even chemical structure and molecular architecture makes such analysis rather unfair. Thus, for my studies I have chosen chemically quite similar compounds, prepared them using same amorphization technique and investigated different crystallization abilities of examined materials based not only on differences in molecular mobility, but also thermodynamic properties and even molecular conformations. This approach should provide a more substantial advance in understanding of the fundamentals of the physical instability reasons of glass-forming materials.

5.3.1. DNA and RNA nucleosides

In this section results from molecular dynamics and calorimetric studies of three biologically important DNA (β-thymidine) and RNA (β-adenosine and β–uridine) nucleosides will be presented. Adenosine and uridine are nucleosides composed of simple monosaccharide D-ribose joined via beta-glycosidic linkage respectively to adenine (purine base) and uracil (pyrimidine base). Thymidine consists of pyrimidine base - thymine attached to 2-Deoxy-D-ribose via beta-glycosidic linkage. Due to similarities in chemical structure, but different crystallization abilities above and below T_g, nucleosides are ideal materials to study

which factors (kinetic or thermodynamic) and in which way relate to their diverse stability behavior.

Physical stability studies along with dielectric and calorimetric measurements were performed in the liquid and glassy states of nucleosides. In the first step, molecular dynamics of nucleosides will be characterized. Figure 5.12 (panels a- f) presents dielectric loss spectra of nucleosides collected above and below their glass transition temperatures. Panels (a), (b) and (c) of Figure 5.12 refer to relaxation dynamics in the supercooled liquid state of β-adenosine, β-thymidine and β-uridine, respectively. The prominent loss peak visible in the region above T_g comes from the structural α-relaxation. For the sake of clarity the dc-conductivity contribution was subtracted from dielectric loss spectra of β-adenosine and β -uridine.

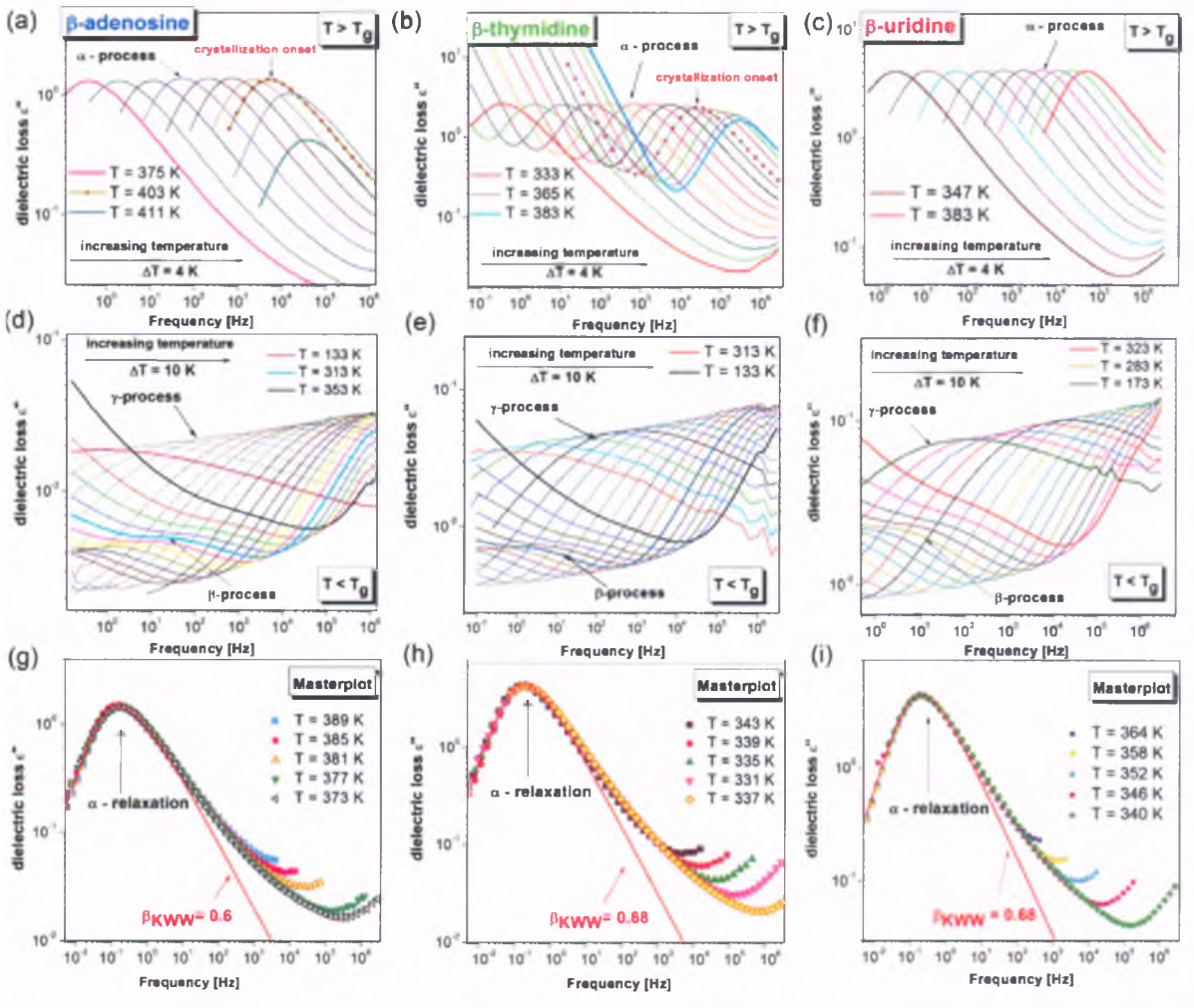

Figure 5.12. Dielectric loss spectra of nucleosides: β-adenosine, β-thymidine and β-uridine measured above (panels a, b and c) and below (panels d, e and f) their glass transition temperatures.

Upon slow heating from the glassy state β-adenosine and β-thymidine begin to crystallize at temperatures respectively (T_g + 34.5 K) and (T_g + 32.5 K), which is visible as decrease in signal intensity. β-uridine was found not to cold-crystalized during standard heating run. In the temperature region above T_g apart from the structural relaxation an excess wing appears on the high frequency flank of α-loss peak, indicating presence of the JG β-relaxation hidden under the prominent structural process. In the glassy state the excess wing transforms into well-separated β-relaxation, as illustrated in panels (d, e, f) of Fig. 5.12. Except for the β-relaxation, very deep in the glassy state of nucleosides another more faster secondary relaxation appears, labeled as γ–process.

As presented in Figure 5.12 panels (g, h, i), the shape of the structural relaxation in nucleosides is essentially invariant to temperature change. Consequently, time-temperature superposition symmetry of liquid dynamics is fulfilled. In order to compare the breadth of the structural relaxation in nucleosides stretching exponents β_{KWW} were determined by fitting experimental data to the Fourier transform of the Kohlrausch-Williams-Watts function. A representative fits are shown in Figure 5.12 panels (g, h, i) as red sold lines with β_{KWW} =0.6 for β-adenosine and β_{KWW} =0.68 for β-thymidine and β-uridine. Obtained values of β_{KWW} stretching parameter imply asymmetric and much broader than that for classical Debye response distribution of relaxation times.

Shamblin et al [138] have postulated that there is a correlation between width of the distribution of relaxation times and physical stability. Precisely, resistance against crystallization and chemical degradation of amorphous materials stored at different temperatures (but similar relaxation times τ_α) decreases in the order as β_{KWW} decreases. Based on this statement, β-adenosine with the broadest distribution of structural relaxation times should be the least stable against crystallization among examined nucleosides, while two other nucleosides should reveal similar crystallization tendencies. However, as can be seen in Figure 5.12. the ease of crystallization for supercooled β-thymidine and β-uridine is completely different. As will be also presented in the further part of this section, β-thymidine and β-uridine reveal completely different physical stabilities in the glassy state, so correlation between the width of the structural relaxation peak and crystallization abilities has also failed in this case.

In Figure 5.13 temperature dependencies of primary and secondary relaxation times for nucleosides are presented. The corresponding parameters from the VFT and Arrhenius

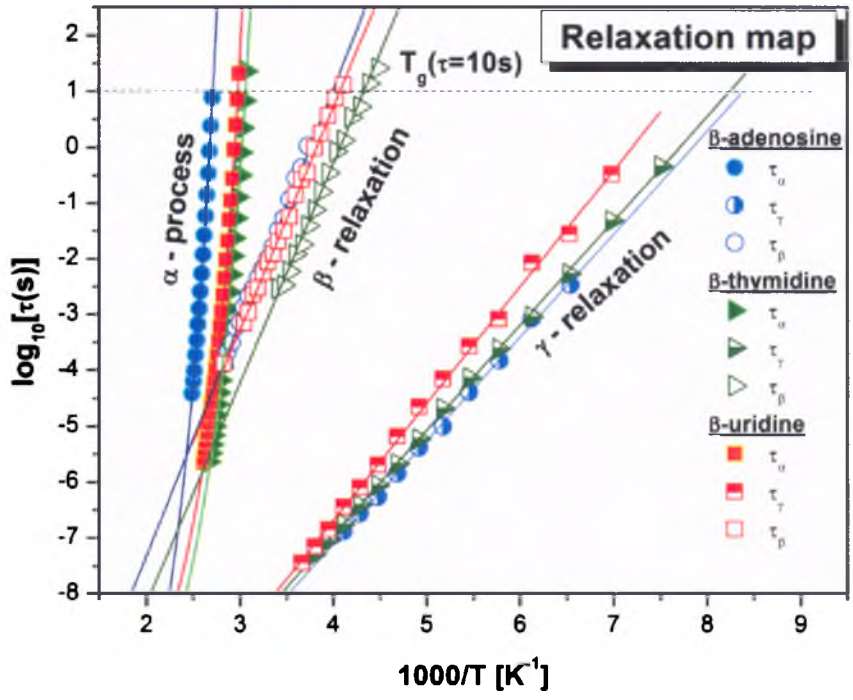

Figure 5.13. Relaxation map of nucleosides. Temperature dependences of structural relaxation times were fitted to the VFT equation, while the temperature dependences of secondary relaxations were described by the Arrhenius equation. These fits are denoted as solids lines.

Table 5.2. Glass transition temperatures, fragilities, fitting parameters from the VFT equation and activation energies of the secondary relaxations calculated for nucleosides on the basis of dielectric measurements.

Material	$\log_{10}$ [τ_∞(s)]	D	T_0 [K]	T_g [K] (τ_α=10s)	Fragility m	Activation energy β-relaxation [kJ/mol]	Activation energy γ-relaxation [kJ/mol]
β-adenosine	-16.4 ±0.4	4.2 ±0.3	296.9 ± 2.5	368.6 ±1.0	90 ±5	80.2 ±1.2	35.5 ±0.4
β-thymidine	-14.3 ±0.1	3.5 ±0.1	266.0 ±1	326.5 ±0.5	83 ±3	75.5 ±1.2	35.8 ±0.2
β-uridine	-13.2 ±0.1	2.7 ±0.1	282.0 ±1	335.6 ±0.5	89 ±3	76.8 ±0.7	40 ±0.4

equations are collected in Table 5.2. In order to avoid data extrapolation, kinetic glass transition temperature was calculated as the temperature at which structural relaxation time τ_α is equal to 10 s. This procedure leads to the following values of T_g: 368.6 K, 326.5 K and

335.6 K for β-adenosine, β-thymidine and β-uridine, respectively. Using Eq. (3.19) fragility parameters were also calculated. Comparable values of fragilities were obtained, i.e. m= 90 for β- adenosine, m=83 for β-thymidine and m=89 for β-uridine, indicating that nucleosides are rather fragile glass-formers. It is worth to note that activation barriers evaluated for secondary relaxations in the glassy state of DNA and RNA nucleosides are comparable and lie within the range $E_\beta \cong$ 75-80 kJ/mol for β-relaxation and $E_\gamma \cong$ 35-40 kJ/mol for γ-relaxation (Table 5.2).

In order to examine the impact of global mobility on physical stability of supercooled nucleosides, crystallization kinetics studies were performed at temperatures T=405 K for β-adenosine, 363 K for β-thymidine and 375 K for β–uridine, where approximately the same structural relaxation time was attained, i.e. $\tau_\alpha \approx 1{,}6 \times 10^{-5}$ s. Spectra of the real part of complex dielectric permittivity upon crystallization are shown in Figure 5.14 panels (a-c). After awaiting certain time t_0 at which changes in $\varepsilon'(t)$ spectra (collected from low frequency region) were not observed, the response has dramatically altered, as shown in panels (d-f).

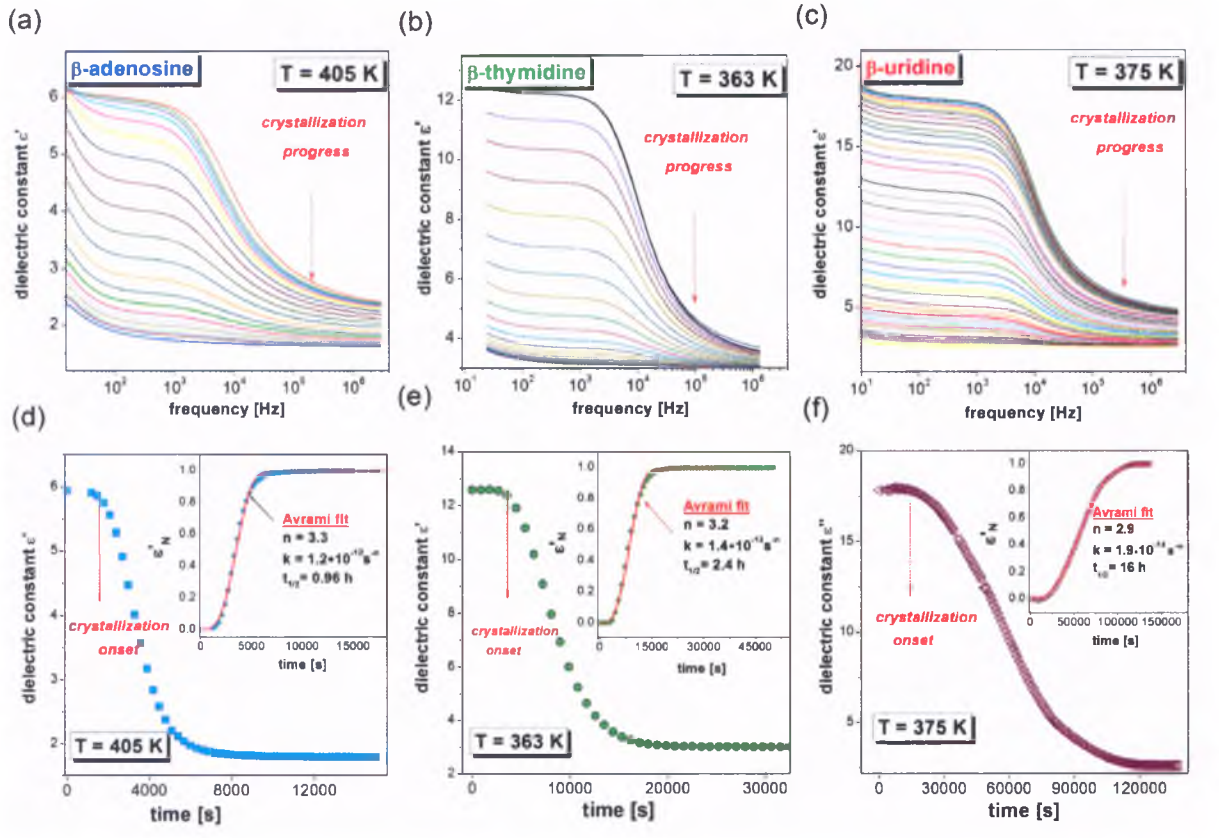

Figure 5.14. Dispersion spectra in the frequency domain measured for (a) β-adenosine, (b) β- thymidine and (c) β-uridine at indicated temperatures during crystallization. Panels (d), (e) and (f) present time evolution of dielectric constant of α-relaxation for β-adenosine, β- thymidine and β-uridine, respectively. Insets present evolution of normalized dielectric constant during crystallization progress for respective nucleosides. Red solid lines are best fits of experimental data to the Avrami equation, Eq. (5.2).

Decrease of static permittivity increment is due to reduction of the number of reorientating dipoles as crystallization proceeds.

It is worth to remind that crystallization experiments were carried out at temperatures at which all nucleosides have approximately the same structural relaxation time (viscosity). Consequently, if global mobility is the key parameter controlling crystallization, one should expect very similar onsets of crystallization, t_0, for individual nucleosides. Surprisingly, they are not the same. The induction times were found to be as follows 0.4 h, 0.75 h and 4 h for respectively β-adenosine, β-thymidine and β-uridine.

Crystallization progress was analyzed by means of normalized real permittivity

$$\varepsilon'_N(t) = \frac{\varepsilon'(0) - \varepsilon'(t)}{\varepsilon'(0) - \varepsilon'(\infty)} \tag{5.1}$$

where $\varepsilon'(0)$ is dielectric constant at the beginning of crystallization, $\varepsilon'(\infty)$ is the long time limiting value of dielectric constant, and $\varepsilon'(t)$ is the value at time t. Normalized curves plotted versus time are shown in the insets of Figure 5.14 (d), (e) and (f). In the next step, isothermal crystallization data were fitted using Avrami law [139]

$$\varepsilon'_N(t) = 1 - \exp[-kt^n] \tag{5.2}$$

where k is rate constant and n is Avrami parameter, which is often related to the nucleation geometry [140]. Solid red lines presented in the insets of Figure 5.14 (d), (e) and (f) are best fits of the experimental data to the Avrami equation, and they turned out to describe experimental data in satisfactory way. Fitting parameters can be found in Table 5.3. Values of Avrami parameters close to 3 indicate that in all three cases crystallization mechanism might involve spherical growth in three dimensions.

Tables 5.3. Crystallization kinetics parameters for nucleosides.

Material	Induction time t_0[h]	Avrami parameter n	Rate constant k [s^{-n}]	Half time $t_{1/2}$ [h]	Rate constant $k^{1/n}$ [s^{-1}]
β-adenosine	0.40 ±0.08	3.3 ±0.1	1.2×10^{-12} $_{\pm0.4\times10^{-12}}$	0.96 ±0.08	2.4×10^{-4} $_{\pm0.2\times10^{-4}}$
β-thymidine	1 ±0.1	3.2 ±0.1	1.4×10^{-13} $_{\pm0.3\times10^{-13}}$	2.4 ±0.1	9.6×10^{-5} $_{\pm0.6\times10^{-5}}$
β-uridine	4 ±0.25	2.9 ±0.1	1.9×10^{-14} $_{\pm0.5\times10^{-14}}$	16 ±0.25	1.8×10^{-5} $_{\pm0.2\times10^{-5}}$

The crystallization half-time, $t_{1/2}$ i.e. time at which the degree of crystallinity reaches 50% of the maximal crystallinity, was determined for each sample as well. The following values were obtained: $t_{1/2}$= 0.96 h for β-adenosine, $t_{1/2}$= 2.4 h for β-thymidine and $t_{1/2}$= 16 h for β-uridine. Based on crystallization kinetic data, which are summarized in Table 5.3, it can be concluded that the induction time as well as the overall crystallization time increase in order: β-adenosine < β-thymidine < β-uridine. Consequently, for the same molecular mobility related to α-process, the former compound was found to be the least stable against crystallization above T_g, while the latter one the most stable.

In order to provide some basic information about the time scale of global motions below T_g and its potential impact on stability, structural relaxation times in the glassy state of nucleosides were estimated. As described in Section 5.2, there are a few methods allowing estimation τ_α in the glassy state. For the purpose of current studies, the simple master curve approach was applied. Structural relaxation times below T_g determined in this way are presented along with α-relaxation times from the region above T_g in Fig. 5.15. As it turned

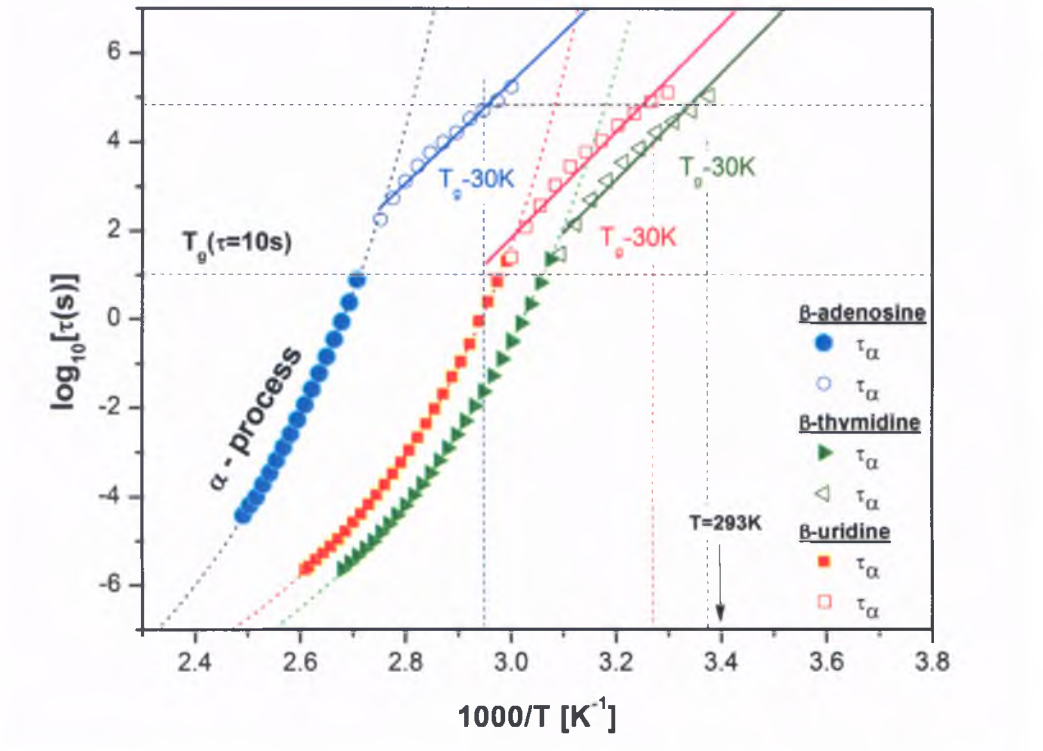

Figure 5.15. Temperature dependences of τ_α above and below glass transition temperatures of respective nucleosides. Filled symbols refer to structural relaxation times in the supercooled liquid state, while open symbols to relaxation dynamics below T_g. Alpha-relaxation times in the glassy state were estimated by horizontal shift of α-peak from the region above T_g to the temperatures below T_g.

out, investigated nucleosides have approximately the same structural relaxation time (same time scale of global mobility) at temperatures T_g–30 K, i.e., ~27 h, which is quite reasonable result if we take into account values of fragility parameters.

Having the time scale of global mobility below T_g estimated, physical stability in the glassy state of nucleosides was examined. Unfortunately, recrystallization event below T_g is practically impossible to be observed upon dielectric measurements, because changes in dielectric strength of the secondary relaxation due to crystallization can be very easily mixed up with the effect of physical aging on secondary relaxation. Thus, to avoid this problem the X-ray diffraction measurements were performed. In Figure 5.16. results from time dependent isothermal XRD studies at temperatures ~T_g–30 K are presented. Examined temperatures were as follows 340 K, 298 K and 307 K for β-adenosine, β-thymidine and β-uridine, respectively. As can be seen, within the first 8 h of measurements all three investigated nucleosides were completely amorphous. After 26 h β-thymidine has started to recrystallize, while two other nucleosides were completely amorphous. Interestingly, even after 47 h of

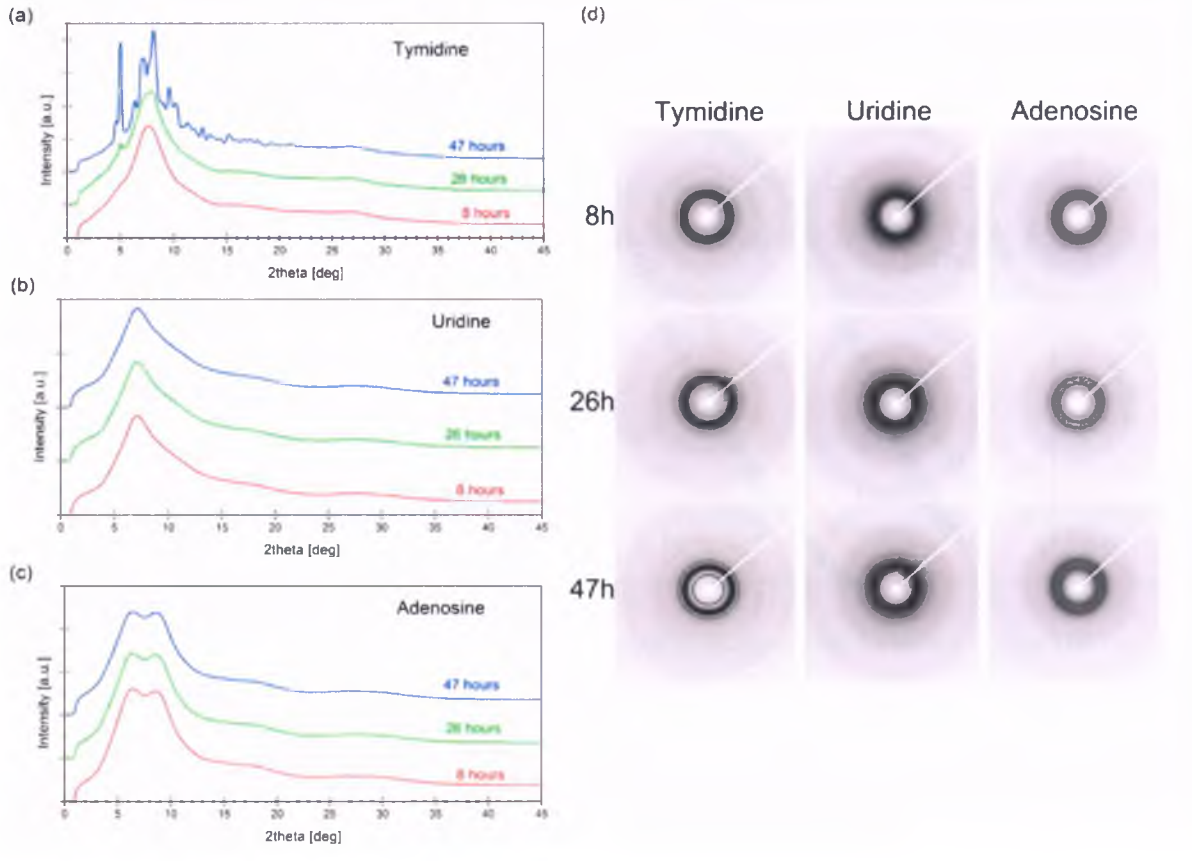

Figure 5.16. Representative X-ray diffraction patterns and their snapshots for glassy nucleosides (β-thymidine, β-uridine and β-adenosine) at temperatures T_g-30 K taken after different times.

measurements in the glassy state of β-uridine and β-adenosine no trace of crystallinity was found, whereas recrystallization of amorphous β-thymidine has proceeded further. From that experiment it can be concluded that global mobility is not the only factor responsible for physical instability and there must be some something else of much greater importance.

Until now, global (alpha mobility) was discussed as potential source of recrystallization. However, in the glassy state of nucleosides except for very slow structural relaxation there are also local motions of much faster amplitude. What is more, they can be still detectable below T_g, even very deep in the glassy state. As in some cases structural relaxation was found to be too slow to control the crystallization along the glass transition, it was speculated that there must be a relationship between instability of glass-formers and JG β-relaxation [141, 142, 143]. Having this in mind, degree of non-cooperative β mobility was taken into consideration as possible source of crystal growth below T_g.

In the glassy state of nucleosides, at temperatures T_g-30 K β-relaxations are still detectable, as demonstrated in Figure 5.17. However, due to small dielectric strength they are barely visible in dielectric loss spectra. Thus, to make β-peak more outstanding the contribution of the α-relaxation was subtracted. At temperatures T_g-30 K local motions associated with

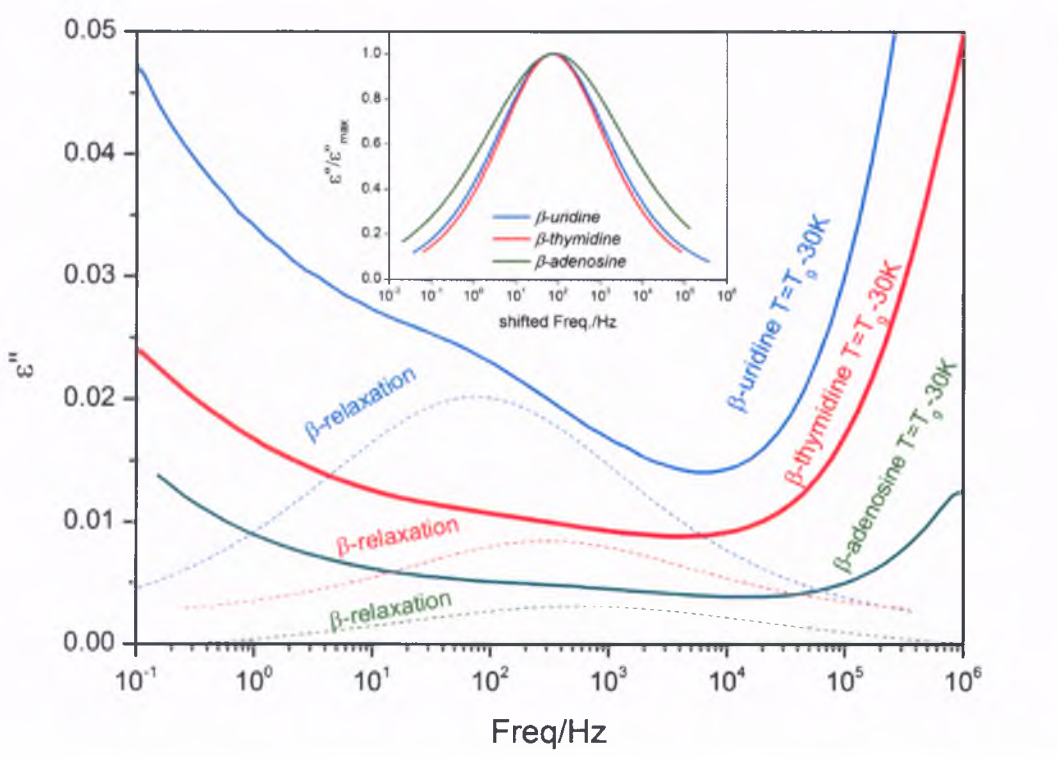

Figure 5.17. Dielectric loss spectra for nucleosides at temperatures T_g-30 K. Dashed lines depict same spectra but after subtraction the contribution from α-relaxation. The inset present superimposed β-peaks.

β-relaxation are significantly faster than global mobility, i.e. τ_β= 3.25×10^{-4} s (β-adenosine), τ_β=1.57×10^{-3} s (β-thymidine) and τ_β=3.62×10^{-3} s (β-uridine). However, if the relationship between local mobility and ease of crystallization exists, all three nucleosides should recrystallize within the same rate, as the time scale of their local motions below T_g are more or less comparable. The is also no correlation between distribution of β-relaxation times and instability issue, because β-relaxation peaks of thymidine and uridine are practically the same (Figure 5.17 inset), whereas only the former one crystallizes in the glassy state.

The fact that crystallization does not correlate with τ_β was also suggested for other systems such as OTP [144]. Even after β-peak disappears upon glass relaxation, recrystallization from the glassy state of OTP is still observed. It should be also remained that existence of well-separated secondary relaxation peak is not he necessary condition for observing crystal growth below T_g, which was demonstrated for ROY [145].

As presented just above differences in crystallization tendencies of nucleosides during time-dependent XRD measurements at temperatures T_g-30 K cannot be explained satisfactorily by the kinetic factor (i.e. molecular mobility). So, in order to fully understand physical instability reasons of supercooled liquids and glasses it was necessary to search for something else, potentially more important. This leads straightforwardly to thermodynamic factor.

Let's start with basic thermodynamic properties of nucleosides. In Figure 5.18 (a) DSC thermograms recorded during heating (10K/min) of the crystalline nucleosides are presented. A single sharp peak visible for each sample indicates melting isotherm. No other thermal effects were observed during these runs. On the other hand, during heating of the glassy materials (Figure 5.18(b)) few thermal effects were recorded: the glass transition temperature T_g (determined as the midpoint of the glass transition step), cold-crystallization T_c and melting endotherm T_m (determined as the onset of the endothermic peak). The values of the T_m, T_g and T_c for respective nucleosides were collected in Table 5.4. The glass transition temperatures estimated from calorimetric measurements were found to agree quite well with dielectric data.

Based on DSC data, the degree of crystallinity for each sample during non-isothermal crystallization was calculated. Full recrystallization was recorded only for β-adenosine, whereas β-thymidine and β-uridine recrystallized respectively to 38 % and 0.4 %. These results confirm that above glass transition temperatures of nucleosides stability against crystallization increase in order: β-adenosine < β-thymidine < β-uridine.

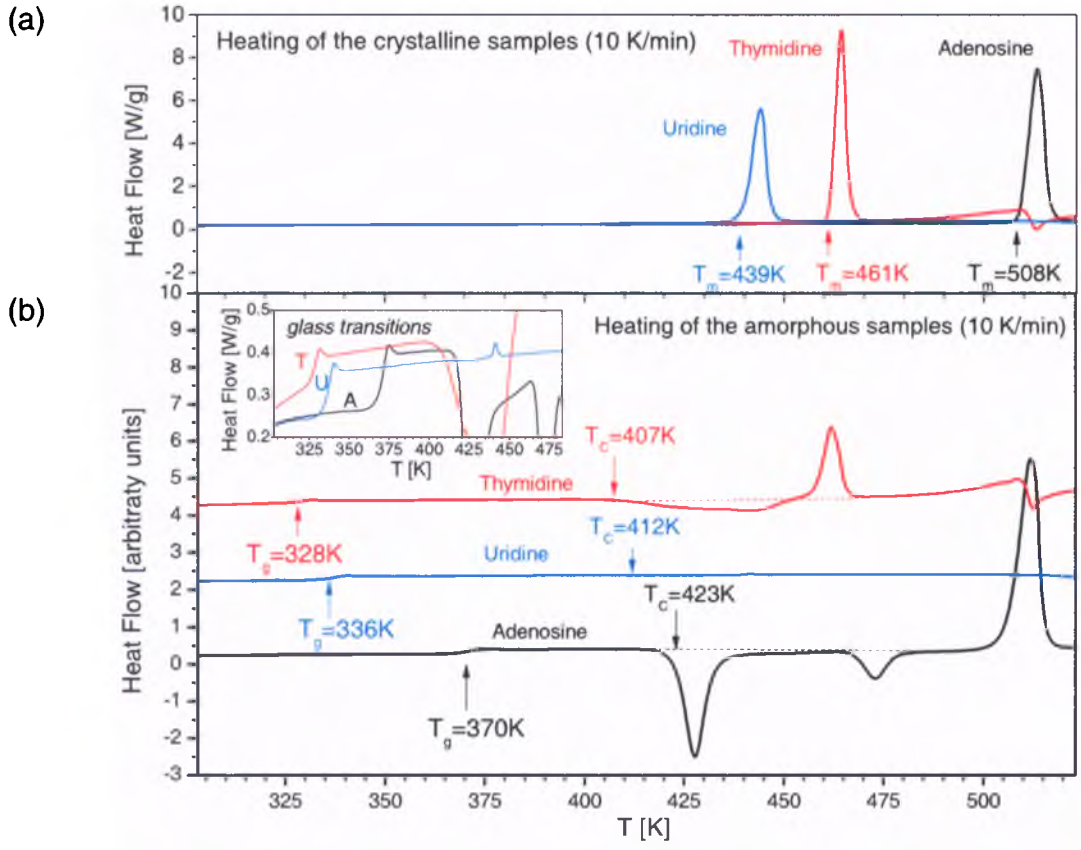

Figure 5.18. DSC thermograms for nucleosides performed on heating of the (a) crystalline and (b) amorphous forms.

As speculated in the literature, thermodynamic driving force for crystallization, defined in accordance with Hoffman relation [146], is greater for system having high values of heat of fusion [147]

$$\Delta G = \frac{\Delta H_m (T_m - T)T}{T_m^2} \tag{5.3}$$

In order to check this supposition, the effect of heat of fusion, ΔH_m, on the ease of crystallization was evaluated. Obtained values of ΔH_m for nucleosides are summarized in Table 5.4. As can be seen, the highest value of ΔH_m was recorded for β-adenosine (194 J/g) while the lowest one for β-uridine (145 J/g). Taking into account experimentally proven differences in crystallization abilities of nucleosides above and below their glass transition temperatures, it might be concluded that the relationship between crystallization of a system and ΔH_m surely works, but rather above T_g not below it. It is worth to remind that stability

against crystallization of nucleosides above T_g increases in order β-adenosine < β-thymidine < β-uridine, which corresponds to the lowering their heat of fusion values in analogical order.

From calorimetric data, the basic thermodynamic parameters characterizing glassy state of nucleosides were evaluated and collected in Table 5.4. Herein, the configurational quantities are of great interest as they express thermodynamic properties of the glassy state with respect to crystalline counterpart. It is also believed that differences in the thermodynamic quantities of the amorphous and crystalline states would dictate the account for crystallization tendencies [148].

Table 5.4. Thermodynamic properties of nucleosides.

Material	T_g [K]	ΔC_p (at T_g) [J·g^{-1}·K^{-1}]	$C_{p\text{-conf}}$ (at T_g) [J·g^{-1}·K^{-1}]	T_m [K]	ΔH_m [J/g] (initial crystal)	ΔH_m [J/g] (after recryt.)	$T_{recryst}$ [K]	D_c (degree of recryst. at T>T_g)	ΔS_m [J·g^{-1}·K^{-1}]	S_{conf} (T_g) [J·g^{-1}·K^{-1}]
Adenosine	370	0.78	0.66	508	194	194	423	100%	0.38	0.2
Thymidyne	328	0.35	0.87	461	172	66	407	38%	0.37	0.07
Uridine	336	0.63	0.39	439	145	0.53	412	0.4%	0.55	0.4

In recent years Zhou et al. [149] have postulated that $\Delta C_p(T_g)$ provides relative measure of number of accessible molecular conformations at T_g and therefore might be very helpful in predicting crystallization abilities of amorphous materials. The value of heat capacity change at T_g informs also how much does the degree of molecular mobility decrease while crossing the glass transition temperature (from liquid to glassy state). As claimed, large values of ΔC_p at T_g results in more stable glass (with lower molecular mobility). Taking this supposition into consideration, it turned out that β-thymidine with the lowest value of ΔC_p has actually the greatest drive towards crystallization below T_g. One the other hand, β-uridine and β-adenosine with significantly higher values of heat capacity steps at T_g revealed no signs of crystallization during isothermal time-dependent XRD studies.

The configurational heat capacity $C_{p\text{-}conf}$ at T_g, i.e. the difference between heat capacities of glass and crystal, is determined by the temperature dependence of configurational entropy, and thus can be used as a measure of the temperature dependence of non-vibrational

molecular mobility [148]. The close look at heat capacity data in vicinity of the glass transition is given in Figure 5.19.

Interestingly, values of $C_{p\text{-}conf}$ at T_g for nucleosides do not follow the same trend as ΔC_p at T_g. It is noteworthy, that now the highest value of $C_{p\text{-}conf}$ was found for β-thymidine which is the least stable in the glassy state. Basing on these results, one can hypothesized that β-thymidine has the greatest drive towards crystallization due to greater degree of non-vibrational mobility in the glassy state. On the other hand, the lowest non-vibrational mobility in the glassy state of β-uridine suggests the greatest resistance against crystallization. Herein one thing should be make more precise, the non-vibrational mobility of glass formers probe upon dielectric and calorimetric measurements are not essentially the same, because DSC probe all active in the liquid state motions, whereas dielectric spectroscopy only those which are related to the reorientation of the permanent dipole moment.

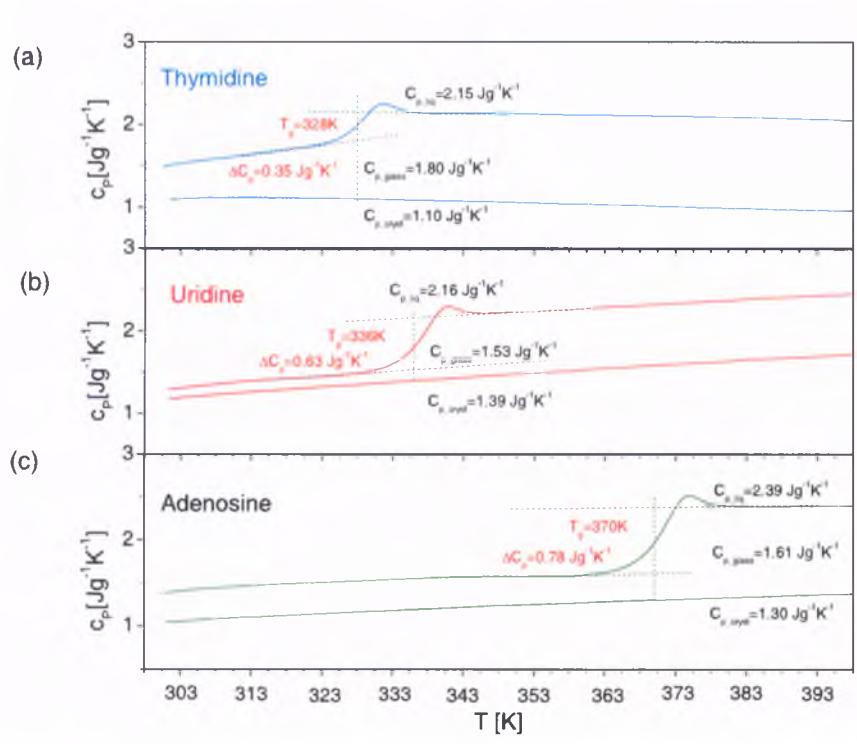

Figure 5.19. Heat capacity versus temperature for crystalline and glassy nucleosides (solid lines). The dashed line have been drawn to guide the measurement of heat capacities of liquid, glass and crystal.

In the next step, configurational entropies S_{conf} of nucleosides at respective glass transition temperatures will be estimated. The main motivation for this study is the fact that some of the authors have pointed out the importance of S_{conf} in predicting crystallization abilities of

amorphous materials. As believed, compounds with lower configurational entropies S_{conf} in the amorphous state are more susceptible to recrystallization, because their molecules require less configurations to sample before 'finding' the optimum one and begin to crystallize [149]. In order to verify if this may account for different crystallization abilities of examined herein nucleosides their configurational entropies were calculated based on the following expression

$$S_{conf}(T_g) = \Delta S_m - \int_{T_k}^{T_m} \frac{C_{p\_conf}(T)}{T} dT \tag{5.4}$$

where $\Delta S_m = \Delta H_m / T_m$ is entropy of fusion. A close look at the values of $S_{conf}(T_g)$, which are collected in Table 5.4, indicates that the least stable in the glassy state β-thymidine has, in fact, much lower value of configurational entropy at T_g when compared with two other nucleosides. This suggests that physical stability of glass-former below glass transition temperature might be, indeed, closely related to its configurational entropy in the glassy state.

In recent years a lot of effort has been made to correlate instability issue of glass-forming liquids with their fragility. Basing on Tanaka's Two Order Parameter (TOP) model it can be concluded that fragile glass-forming liquids should be less stable against crystallization than stronger ones, since their frustration against crystallization are weaker (bond order parameter $S \rightarrow 0$). In my studies I have systemically verified this assumption. As will be shown later on the TOP model prediction works quite well under elevated pressure for Ibuprofen. However, in the case of nucleosides from the values of fragility index one cannot extract any important information considering their crystallization tendencies. For example, β-adenosine and β-uridine revealed almost identical steepness indexes, but completely different stability against crystallization above their glass transition temperatures. More so, β-thymidine with the lowest value of fragility index (so potentially the most stable in the glassy state) was found to have the greatest drive towards crystallization when stored below T_g.

As a final point, the correlation between dynamic and thermodynamic fragilities of nucleosides will be examined. The values of thermodynamic fragilities were calculated using Eq. (3.22) and Eq. (3.23). Moreover, as relative measure of fragility parameter γ_{Cp} was used (Eq. (3.29)). Obtained values are listed in Table 5.5 together with fragility values estimated on the basis of dielectric measurements. As it turned out, values of thermodynamic fragilities for β-adenosine and β-uridine are only slightly lower than that calculated from dielectric data, whereas thermodynamic fragilities calculated for β-thymidine on the basis of Eq. (3.22) and Eq. (3.23) do not correspond to dielectric data at all.

Table 5.5. Kinetic and thermodynamic fragilities for examined nucleosides.

Material	γ_{Cp}	m_p from Wang and Angell	m_p from Lubchenko and Wolynes	m_p from dielectric (τ_α=10s)
Adenosine	0.71	83	71	90
Thymidyne	0.33	37	33	83
Uridine	0.82	82	66	89

Taking into account values of parameter γ_{Cp}, significant deviation is again visible for β-thymidine indicating its strong behavior. The value of 0.33 for β-thymidine is of course in serious contradiction with its VFT-predicted fragile behavior. As suggested by Cangialosi et al [150] the reason for a failure between dynamic and thermodynamic fragility might be associated with the residual excess entropy at T_0. At this temperature, accordingly to Adam-Gibbs equation, no α-relaxation-related excess entropy is expected. However, as it turned out, many materials have non-zero excess entropy at T_0, which represents all motion not related to the structural relaxation (i.e. secondary relaxations) and arised from internal degrees of freedom. Consequently, thermodynamic fragility is composed by contributions of the primary and secondary processes, but only the former is relevant to the dynamic fragility and must be extracted for a credible comparison of the thermodynamic and dynamic fragilities [151]. Consequently, the fact that thermodynamic fragility suffers from the effect of secondary relaxations might be a direct reason why correlation between thermodynamic and dynamic fragilities doesn't work well for nucleosides.

Summarizing, in this section comprehensive analysis of the physical stability in supercooled and glassy states of nucleosides was given, the weaknesses of the 'universal' relationships between dynamics and crystallization tendencies of glass-formers was also revealed. Since selected compounds were similar from chemical point of view and prepared using identical amorphization technique it was possible to evaluate the role of molecular mobility in governing their physical stabilities. As it turned out, global molecular mobility (associated with structural relaxation) is certainly an important parameter, as it can facilitate crystallization (above T_g crystallization proceeds faster than below T_g), however, it cannot 'cause' crystallization on its own. Thus, there must be other factor of much greater authority. Different resistance against crystallization of nucleosides upon time dependent crystallization experiments performed for the same structural relaxation time seems to confirm this

supposition very well. Moreover, there is no link between the width of the structural relaxation and crystallization tendencies of glass-formers. No essential information concerning stability of nucleosides can be also extracted from the values of their fragilities. Thus, crystallization abilities of glass-forming materials are much more complicated to be just 'successfully predicted' from any analysis, which bases on one or two simple parameters typically used to characterized their relaxation dynamics. Experimental results collected for nucleosides have also shown that there is no evident relationship between degree of local mobility and physical stability at temperature T_g-30 K. As nucleosides reveal significant differences in thermodynamic properties, it might be concluded that thermodynamic factor suits better as possible source of instability in this case.

5.3.2. Glucose derivatives

In search of physical instability reasons of glass-forming materials a very interesting results were obtained for carbohydrates: D-glucose, α-pentaacetylglucose and β-pentaacetylglucose. The essential difference between pentaacetyl derivatives of glucose and non-modified glucose is that in the former case all hydrogen atoms are substituted by acetyl groups. This exchange has a significant influence on intermolecular interactions, because supercooled glucose is strongly associating liquids that even forms clusters [152], whereas acetylic systems are typical van der Waals liquids. Pentaacetyl derivatives are rich in oxygens (from carboxyl groups) which are good acceptors for hydrogen bonds, but they do not have proton donors. Consequently, acetyl derivatives cannot create hydrogen bonds on their own.

The change of intermolecular interactions from strongly hydrogen bonding to classical van der Waals has considerable effect on molecular dynamics as well as physical stability. Let's first start with non-modified carbohydrate. It is well-documented in literature that D-glucose is very stable in the glassy state and in the absence of water it should not reveal crystallization tendencies for more than 2 years [153]. D-glucose is also physically stable in the supercooled liquid state, as demonstrated during time-dependent dielectric measurements performed at 353 K. As can be seen in Figure 5.20 static permittivity increment (panel a) and the intensity of α-relaxation peak (panel b) do not decrease with time, even after 20 hours of measurements. This suggests that indeed D-glucose is physically stable in the supercooled liquid state.

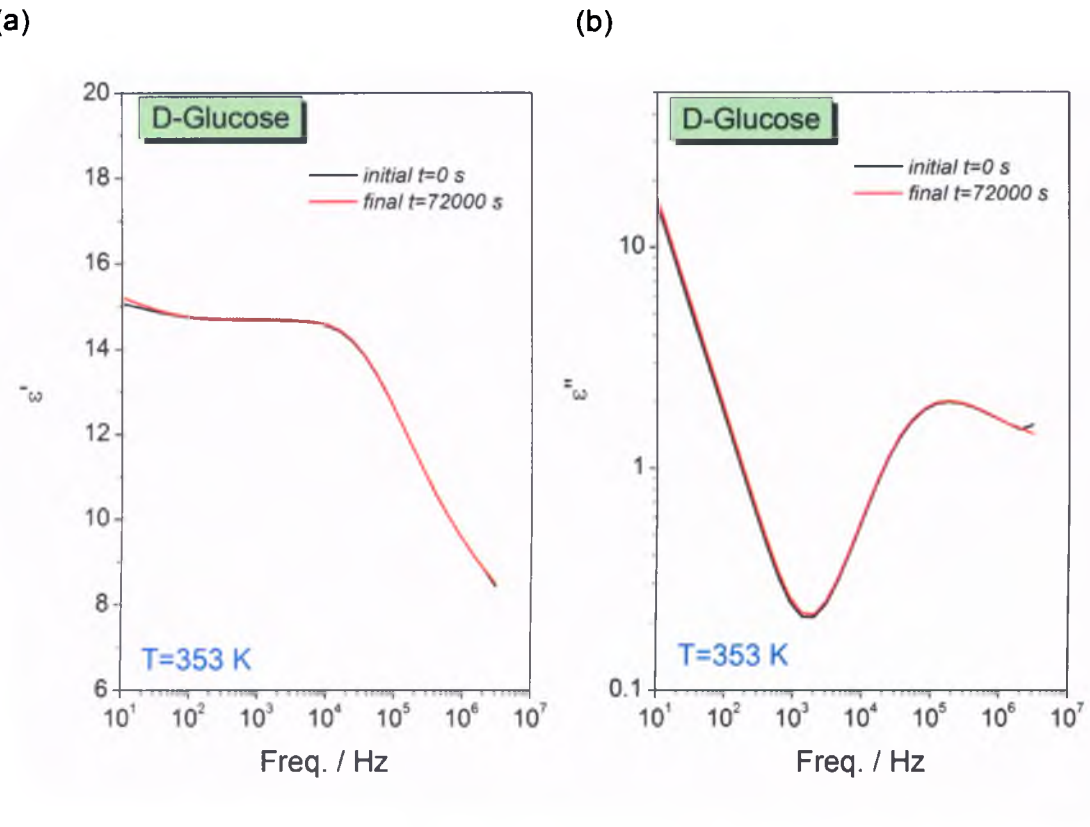

Figure 5. 20. The real ε' (panel a) and imaginary ε'' (pane b) parts of complex dielectric permittivity collected for D-glucose during time-dependent measurements at 353 K.

However, situation is severely different for acetyl derivatives of glucose. From the inspection of dispersion and loss spectra collected during time-dependent measurements at approximately the same temperatures (Figure 5.21), it becomes evident that supercooled α- and β-pentaacetylglucoses reveal crystallization tendencies. However, their resistance against crystallization is not the same, as α-anomer was found to be more stable than β- one. In the temperature region where β-pentaacetylglucose easily crystallizes, the induction time as well as the over crystallization time for α-pentaacetylglucose were significantly elongated. This is quite shocking finding if we take into account similarities in the chemical structure and molecular architecture.

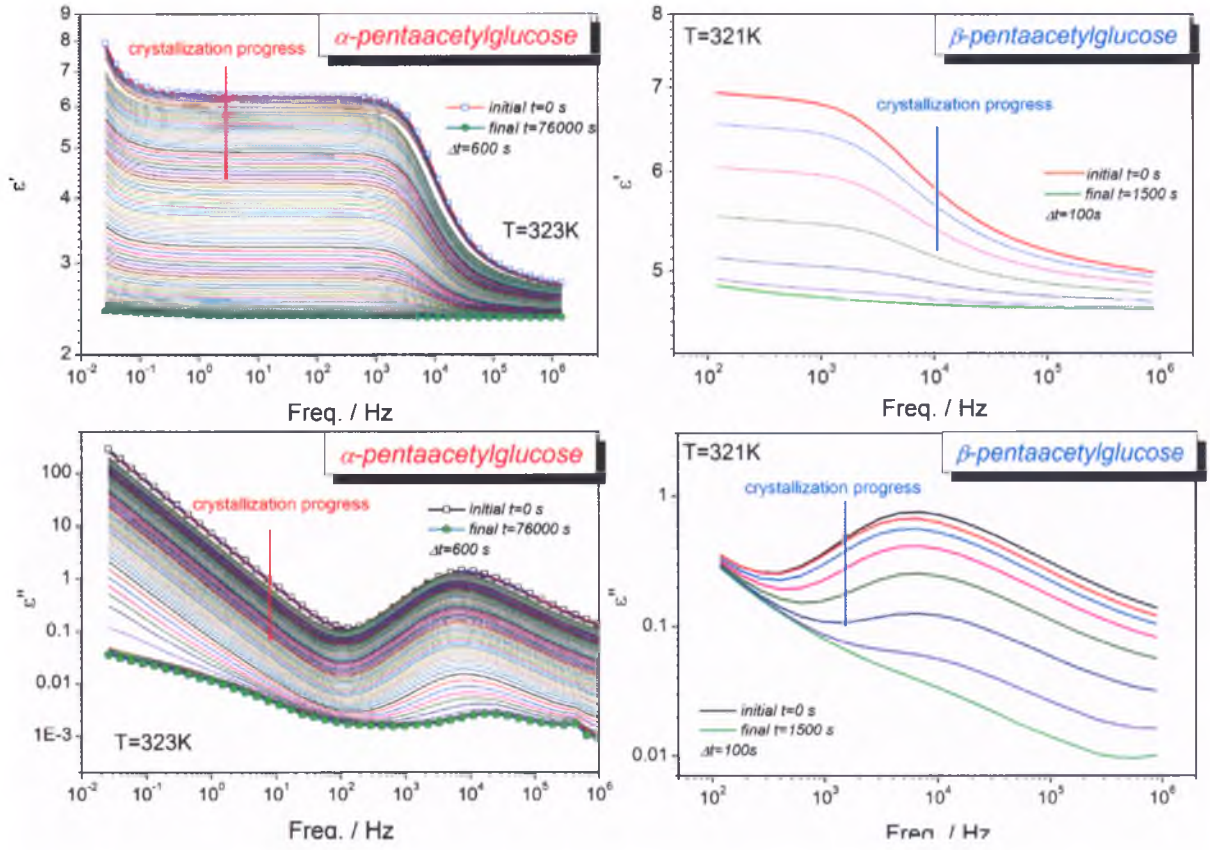

Figure 5.21. Spectra of the real (ε') and imaginary (ε'') part of complex dielectric permittivity in the frequency domain during crystallization of supercooled α- and β-pentaacetylglucoses.

In order to highlight differences in the crystallization rate of supercooled α- and β-pentaacetylglucoses in Figure 5.22 the variation of normalized dielectric constant ε'_N versus crystallization time is presented at similar temperatures (at which molecular mobility associated with the structural relaxation of pentaacetylglucoses is practically the same). To analyze isothermal crystallization data the Avrami equation, Eq. (5.2), was used. The accuracy of Avrami fits to the experimental data is satisfying and the fitting parameters for acetyl derivatives were found to be as follows: $k=4.35\times10^{-5} \pm 0.1\times10^{-6}$ s^{-1}, $n=1.9\pm0.1$ for α–pentaacetylglucose and $k=1.5\times10^{-3} \pm 0.1\times10^{-4}$ s^{-1}, $n=5.6\pm0.1$ for β-pentaacetylglucose.

By the projection on time-axis (in logarithmic units) the straight line for which $\ln(-\ln(1-\varepsilon'_N))=0$, it was possible to calculate crystallization times, τ_{cr} [154]. This is illustrated in Figure 5.22 (insets). The following values of τ_{cr} were estimated 20 417±600 s and 676±30 s for α- and β- pentaacetylglucoses, respectively. The characteristic crystallization time for β-pentaacetylglucose, is much shorter which unquestionably prove that for the same time scale of global mobility the β-isomer less stable than α-one.

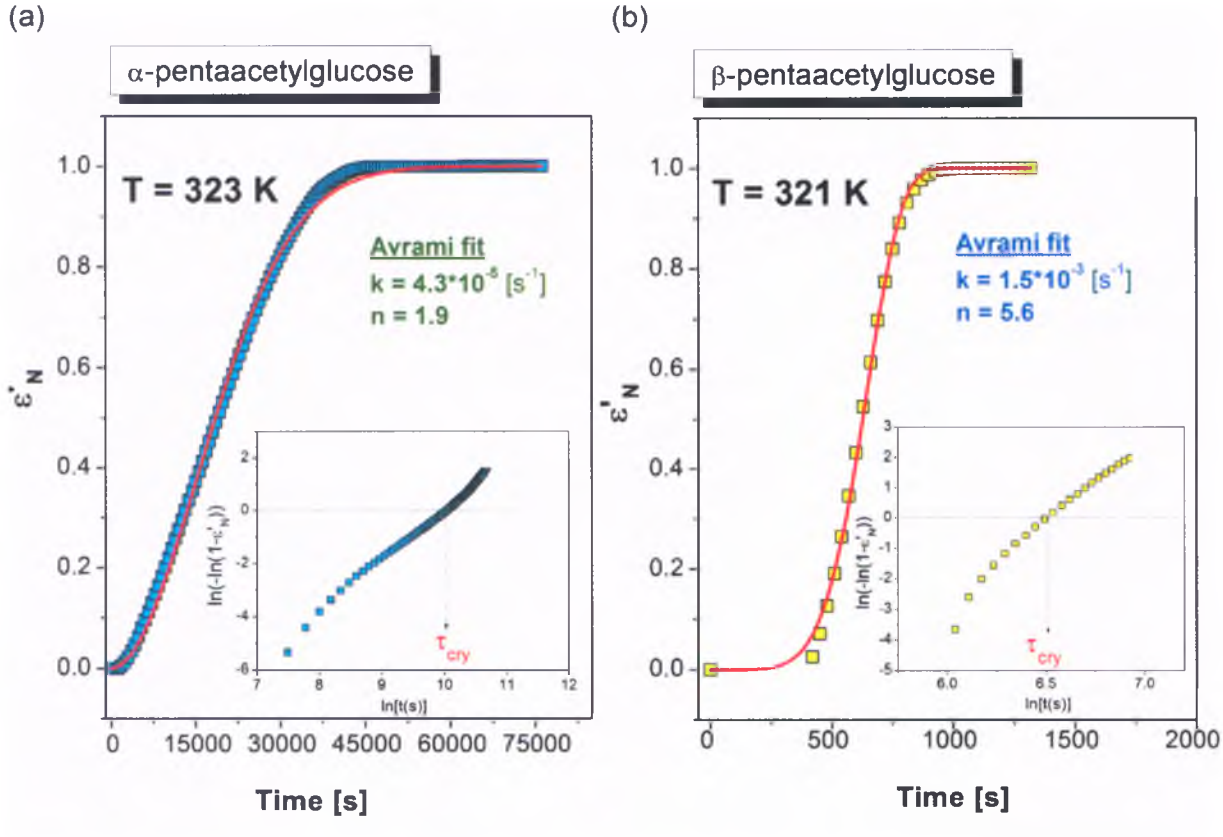

Figure 5. 22. Normalized dielectric constant ε'_N as a function of crystallization time for (a) α–pentaacetylglucose and (b) β-pentaacetylglucose at indicated temperatures, at which their molecular motions are approximately the same. Insets present same normalized crystallization data in double logarithmic units.

Interestingly, both acetyl derivatives differ in the value of Avrami parameter *n* which is believed to provide information about dimensionality or mechanism of crystal growth [140]. Again, this is quite surprising information because two practically the same chemical entities reveal completely altered mechanisms of isothermal crystallization. Indeed, snapshots taken from optical microscope while time dependent isothermal experiments (Figure 5.23) point out essential differences in nucleation and crystal growth of α- and β- pentaacetylglucoses. Firstly, there are around 1-2 and 30 centers of nucleation per 4900 μm^2 respectively in the former and the latter compound. It is worth noting that the number of nuclei and morphology of crystals were found not to change with temperature. Secondly, both modified carbohydrates form completely different structures. β-pentaacetylglucose's crystals radiate symmetrically outward from a central point in small divergent blended crystals (about 20μm diameter) without producing stellar forms in the crystallization process. On the other hand, α-acetylglucose's crystals produce stellar form and in the first stage of crystallization process

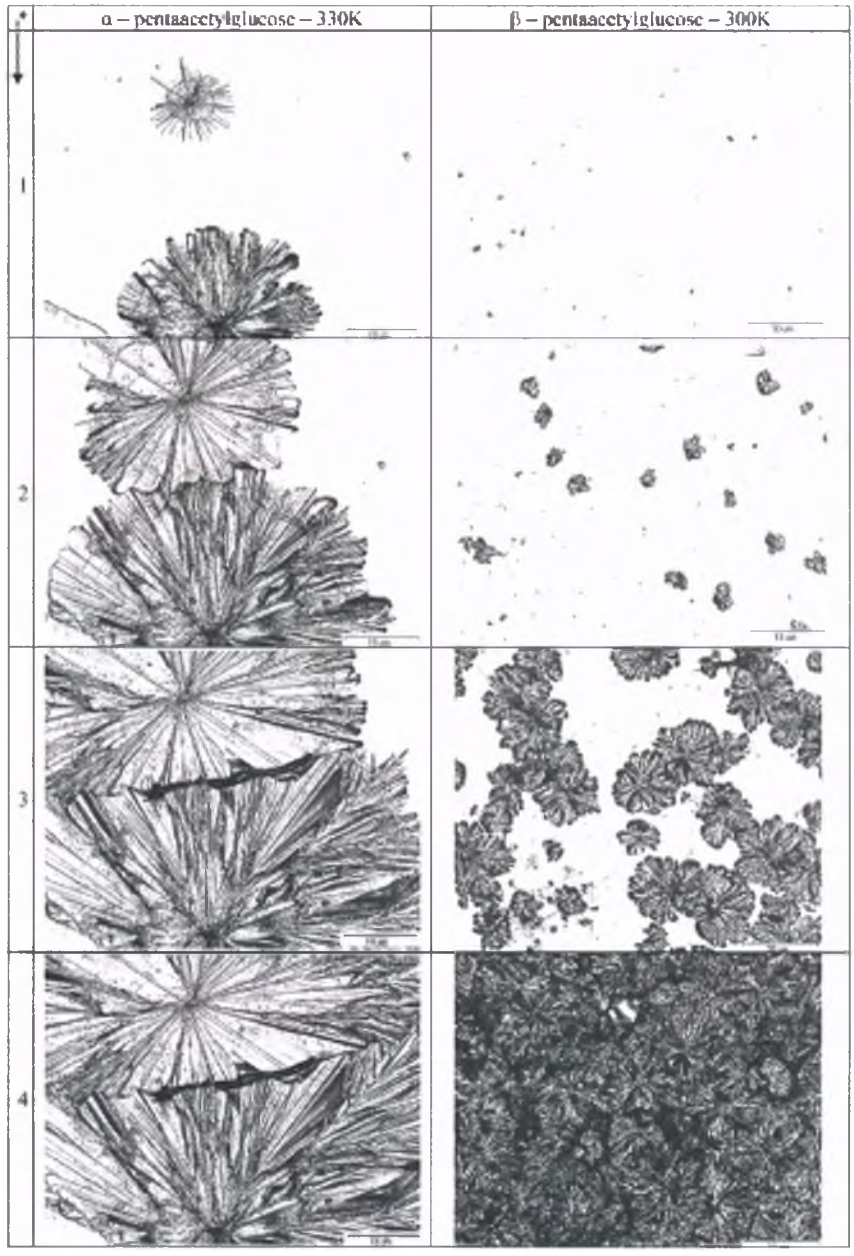

Figure 5. 23. Snapshots recorded under microscope during crystallization of α- and β- pentaacetylglucoses at indicated temperatures.

radiate in the form of relatively big (about some mm diameter) tabular or blended crystals while in the second stage as fibrous forms. Presented differences in crystal growth of pentaacetylglucoses may account for discrepancies in the values of Avrami parameters.

As crystallization abilities of glucose and its acetyl derivatives were just characterized, now their molecular dynamics will be analyzed. In Figure 5.24 superimposed dielectric loss spectra of all investigated herein carbohydrates are presented. Dielectric data for D-glucose

were taken from ref [155]. To get the same τ_α as β- pentaacetylglucose it was necessary to slightly shift spectra of two other carbohydrates. Experimental data were then fitted to the one sided Fourier transform of the KWW function and following stretching exponents were obtained β_{KWW} = 0.52 for D-glucose, β_{KWW} =0.6 for β- pentaacetylglucose and β_{KWW} =0.62 for α- pentaacetylglucose. In accordance with Shamblin et al. [138] criterion, D-glucose with the broadest distribution of structural relaxation times should be the least stable against crystallization among all studied herein compounds, which is obviously not true. A very interesting observation is also that α- and β- pentaacetylglucoses have slightly different values of stretching exponents. However, this cannot account for their different crystallization abilities.

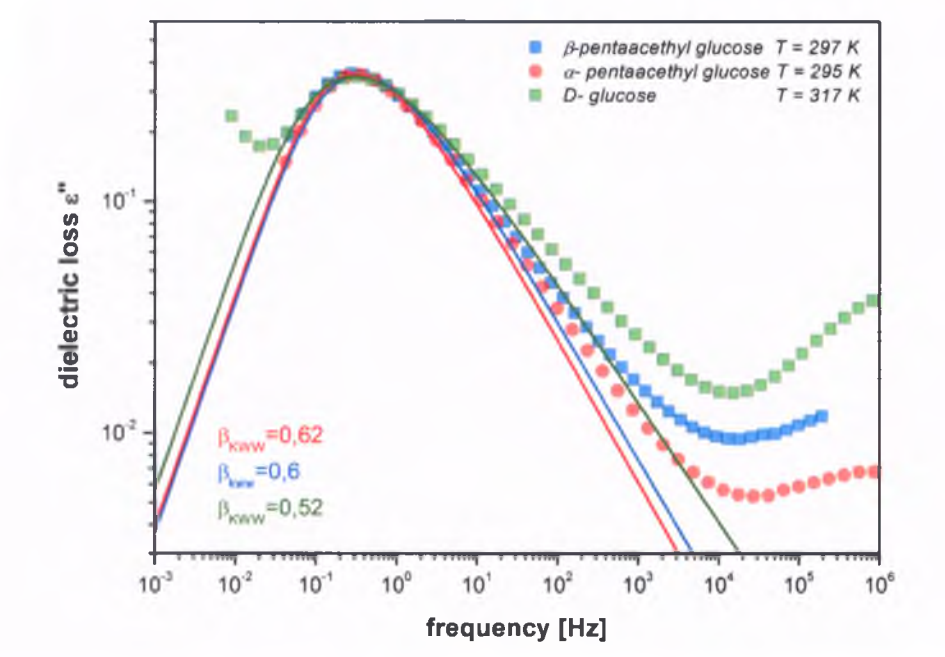

Figure 5.24. Superimposed dielectric loss spectra for D-glucose (green squares), α- pentaacetylglucose (red circles) and β- pentaacetylglucose (blue squares) at indicated temperatures at which structural relaxation times were approximately the same. Dielectric data for D-glucose were taken from [155].

In order to characterize molecular dynamics α- and β- pentaacetylglucoses, structural and secondary relaxation times were calculated and added onto relaxation map of D-glucose [155], as presented in Figure 5.25. To fit their temperature dependances VFT and Arrhenius equations were used (Eq. (3.17) and Eq. (3.18)). Extrapolation of the VFT fits to 100 seconds gives the following values of glass transition temperatures: T_g=289 K and T_g=288 K for α- and β-pentaacetylglucoses, respectively. The glass transition temperature of D-glucose equals

to T_g=307 K [155]. From Eq. (3.19) steepness indexes were also estimated to be m=96 for D-glucose [155] and m=88 for both acetyl derivatives. Thus, by changing the character of intermolecular interactions from hydrogen bonding to typical van der Waals, the glass transition temperature and fragility of glass former decrease.

It is remarkable that both pentaacetyl derivatives have practically the same values of glass transition temperatures, identical fragilities and molecular dynamics, whereas different crystallization tendencies. From that it can be concluded without any doubts that molecular mobility is not the key parameter that determines physical stability of α- and β-pentaacetylglucoses. What is even more striking, initial calorimetric measurements have shown that there is no significant differences in thermodynamic properties of glucose derivatives. For example, the values of heat capacity change at T_g were found to be very similar: ΔC_p=0.33 J/(K·g) and ΔC_p=0.32 J/(K·g) for α- and β- pentaacetylglucoses,

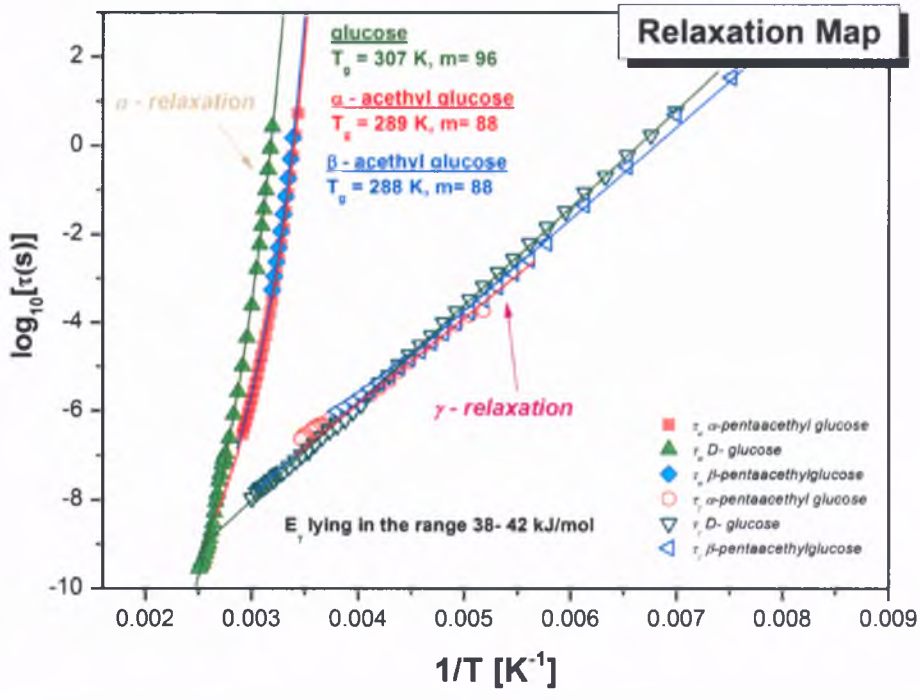

Figure 5. 25. Relaxation map of D-glucose and α-and β-pentaacetylglucoses. Temperature dependences of structural relaxation times were fitted to the VFT equation, while the temperature dependences of secondary relaxations were fitted to the Arrhenius equation. These fits are denoted as solids lines.

respectively. There is also no essential differences in the values of heat of fusion, namely, ΔH_m=89 J/g (α-pentaacetylglucose) and ΔH_m=88 J/g (β-pentaacetylglucose). This suggests

that except for kinetic and thermodynamic factors, molecular conformation may play an important role in controlling crystallization abilities of glass-formers. Moreover, as shown by the example of D-glucose strong hydrogen bonding abilities might be responsible for greater physical stability in the supercooled liquid state. In fact, the lack of crystallization tendencies were also reported for other hydrogen-bonding materials such as mono- and polyalcohols or polypropylene glycols.

5.3.3. Antibiotics

Now, the relationship between molecular mobility and physical stability will be tested for antibiotics. Azithromycin, Clarithromycin and Roxithromycin were selected for these studies because of similarities in the chemical structure, but different drive towards crystallization. In Section 5.1.2 dielectric loss spectra of antibiotics were already presented, showing that in supercooled liquid state Clarithromycin exhibits crystallization tendencies, whereas two other antibiotics not. The X-ray diffraction measurements performed in the glassy state of antibiotics (Figure 5.26) have shown that they are still physically stable even after storage at room temperature for more than one year from the preparation date. Increased temperature and humidity conditions haven't also triggered their recrystallization (85% RH, 312 K, 7 days).

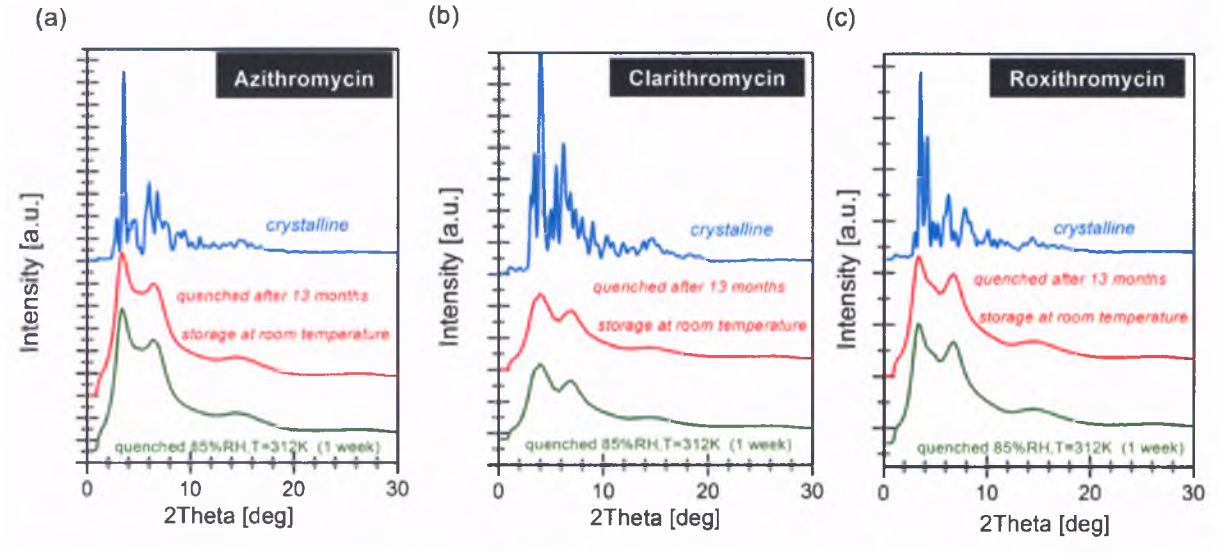

Figure 5.26 Representative X-ray diffraction patterns of crystalline and glassy antibiotics recorded at room temperature. Vitrified samples were stored at room temperature for 13 months with constant access to fresh air and subjected also to 85% RH at 321 K for 7 days. No signs of crystallizations were recorded. Panels correspond to: (a) Azithromycin, (b) Clarithromycin (c) Roxithromycin.

In Figure 5.27 the breadth of structural relaxation peaks of antibiotics was described using parameter β_{KWW}, determined by fitting α-peak in the frequency domain by the one-sided Fourier transform of the KWW function. The following stretching exponents were found: β_{KWW}=0.52 for Azithromycin and β_{KWW}=0.62 for Clarithromycin and Roxithromycin. Obtained values indicates that experimentally observed structural relaxation peaks for antibiotics are asymmetric and much broader than the classical Debye response.

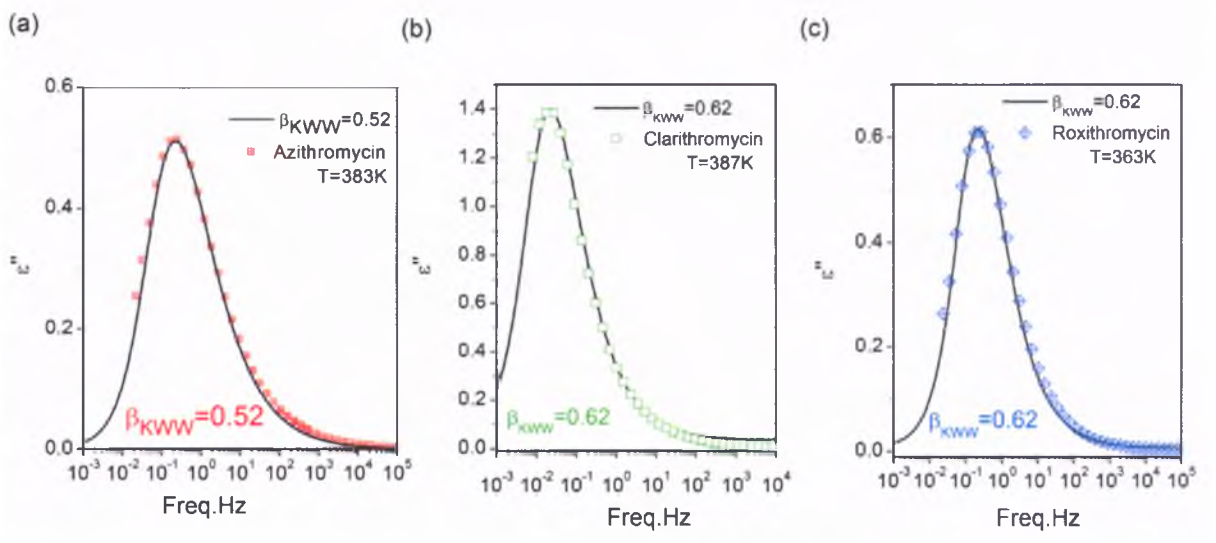

Figure 5.27. Dielectric loss spectra of antibiotics taken at (a) T=383 K for Azithromycin, (b) T=387 K for Clarithromycin and (c) T=363 K for Roxithromycin. Black solid lines represent KWW fits with β_{KWW}=0.62 for Clarithromycin and Roxithromycin and β_{KWW}=0.52 for Azithromycin.

In reference to the correlation between narrowing of the α- peak and improving stability of amorphous materials [138]. Azithromycin with the broadest distribution of structural relaxation times should be the least stable in the glassy. However, as proven experimentally amorphous Azithromycin is physically stable, same as two other compounds. This confirms that correlation between the shape of structural relaxation peak and stability below T_g doesn't work well. It cannot be applied above T_g as well. It is worth noticing that Clarithromycin and Roxithromycin are characterized by the same value of the stretching exponent, whereas above glass transition temperature only the former shows up intensified crystallization abilities.

For examined antibiotics, values of the steepness index calculated using Eq. (3.19) were found to be as follows: m=117 for Azithromycin, m=118 for Clarithromycin and m=121 for Roxithromycin. Hence, antibiotics can be classified as fragile glass-formers, which means that their temperature dependences of structural relaxation times deviate significantly from the Arrhenius law. Accordingly to TOP assumptions, large values of isobaric fragility suggest

that antibiotics should reveal great ease of crystallization. However, as confirmed by x-ray diffraction measurements they are physically stable in the glassy state, whereas during heating from the glassy state only Clarithromycin recrystallizes. This is just another conformation that there is no correlation between physical stability and fragility index.

Generally, it is believed that long-term stability of glassy materials can be achieved by storage below Vogel temperature, T_0, i.e. temperature at which molecular mobility associated with structural relaxation time approaches zero. By fitting $\tau_\alpha(T)$ dependences to the VFT equation the following values of T_0 were found: 321.5 K (Azithromycin), 324 K (Clarithromycin) and 314.3 K (Roxithromycin). Fitting parameters from the VFT equation can be found in Table 5.6. It is worth to note that the values of Vogel temperature for antibiotics lie much above room temperature, indicating that at ambient condition structural relaxation times should be negligible due to exceedingly long time scale.

In addition, the degree of global molecular mobility in the glassy state of antibiotics was estimated based on master curve approach. The structural relaxation times determined in this were added on relaxation map of antibiotics and are presented in Figure 5.28. As illustrated, for all investigated materials the time scale of molecular motions associated with structural relaxation exceed more than one year at room temperature.

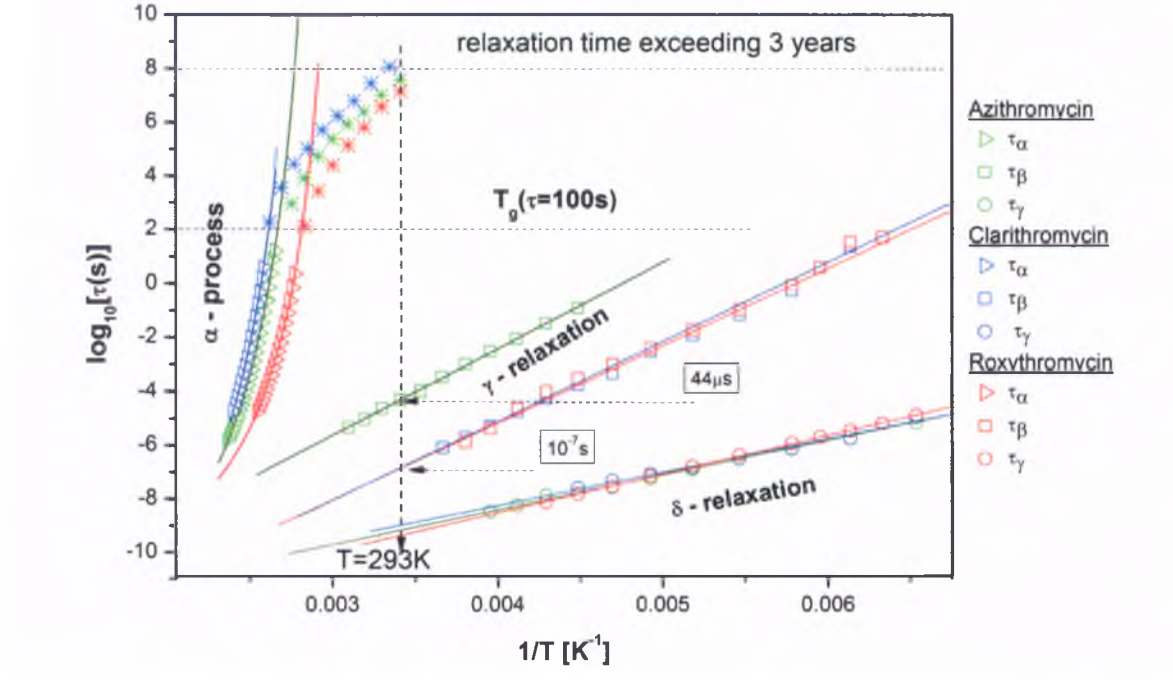

Figure 5.28. Prediction of the time scale of molecular motion in the glassy state of antibiotics. Alpha-relaxation times were estimated on the basis of the master curve approach.

Table 5.6. Fitting parameters from the VFT equation, values of the glass transition temperatures, and fragilities of antibiotics

Material	$\log_{10}[\tau_\infty(s)]$	D	T_0 [K]	T_g [K] (τ_α=100s)	Fragility m
Azithromycin	-14.6 ±0.5	2.7 ±0.3	321.5 ±1.5	375 ±1	117 ±5
Clarithromycin	-16.2 ±0.8	3.3 ±0.4	324 ±4	382 ±1	118 ±10
Roxithromycin	-12.2 ±0.1	1.8 ±0.1	314.3 ±0.5	355 ±1	121 ±2

As a final point, the degree of local mobility in the glassy state of antibiotics will be evaluated. At temperature T=293 K local motions are significantly faster than global ones i.e. τ_β= 44μs (Azithromycin) and τ_γ= 10^{-7}s (Clarithromycin and Roxithromycin). However, they cannot be treated as a source of instability, because the long-term stability of glassy antibiotics stored at room temperature is most probably due to significant reduction of the time scale of global mobility.

Concluding, results presented in this section clearly demonstrate that universal description of crystallization abilities of glass-forming liquids basing only on dynamical properties is further more complicated than expected. Firstly, there is no correlation between fragility and physical stability below as well as above T_g. Secondly, from the width of the α-relaxation peak one cannot get any valuable information concerning physical stability of antibiotics. It is also worth stressing that in view of results presented in this dissertation molecular mobility is not the dominant variable that drives glass-forming materials towards crystallization. On the other hand, significant reduction degree of global molecular mobility results in the improvement of long-term stability of amorphous APIs (glassy antibiotics at room temperature). The fact that Clarithromycin is the only one antibiotic with crystallization abilities (but only above T_g) is quite surprising. However, the situation is more complicated here, as Clarithromycin reveals hemiacetal tautomerism. Consequently, differences in crystallization tendencies of antibiotics in the liquid state might be related to the differences in hydrogen bonding patterns in 14-membered lactone ring. Nevertheless, some more detailed studies with the use of other experimental techniques, as well as quantum mechanical calculations are necessary in the future on that issue.

CHAPTER 6

ANALYSIS AND PRESENTATION OF EXPERIMENTAL RESUTS OBTAINED AT ELEVATED PRESSURE

6.1. What is the effect of pressure on molecular dynamics and crystallization kinetics of Ibuprofen?

To the best of the author's knowledge, studies of crystallization kinetics in pharmaceutically important substances as a function of pressure have been performed for the first time. The lack of such measurements is unquestionably associated with serious experimental problems arising when using a high pressure. Because of that reason the exact role of pressure on physical stability of glass-formers is not clearly understood. For example, in the past it was demonstrated, for some of non-organic glasses, that pressure can catalyze crystallization [156, 157]. On the other hand, theoretical efforts made by Gutzow et al. [158] suggest that pressure do not increase the maximal nucleation and crystal growth rate, but rather shifts it to higher temperatures. The mechanism of crystal formation from supercooled melt at reduced pressure was also considered by Tanaka et al. [159]. Based on Monte-Carlo simulations they assumed that there is a close link between crystal formation and symmetry of polymorph, as only particles compatible with crystal symmetry can join long-range translation order. Moreover, there is a stability window for metastable supercooled liquid between low and high density regions where crystal formation from supercooled liquid is not favorable. Tanaka has even postulated that pressure is the only thermodynamic variable that control crystallization process.

Crystal formation from the supercooled liquid and glassy states have been hotly debated in recent years in the world's top scientific journals (e.g.[160, 161]). Unfortunately, there is no experimental studies on the crystallization of glass-formers at elevated pressure, so it is not possible to confront all of these theoretical predictions with experimental reality.

In my studies, I have made an attempt to provide unique experimental data on crystallization kinetics under elevated pressure performed for pharmaceutical, Ibuprofen.

At the beginning molecular dynamics of Ibuprofen at elevated pressure will be characterized. Isothermal dielectric measurements were carried out at temperatures T=260 K, T=263, T= 273 K, T=280 K, T=293 K, T=378 K, while isobaric studies were performed at p=0.1 MPa, p=250 MPa, p=920 MPa and p=1750 MPa. The latter isobar was measured in order to check what is the effect of pressure on the secondary relaxations in the glassy state of Ibuprofen. For the sake of clarity in Figure 6.1 representative isothermal (panel a) and isobaric (panel b) dielectric loss spectra are presented.

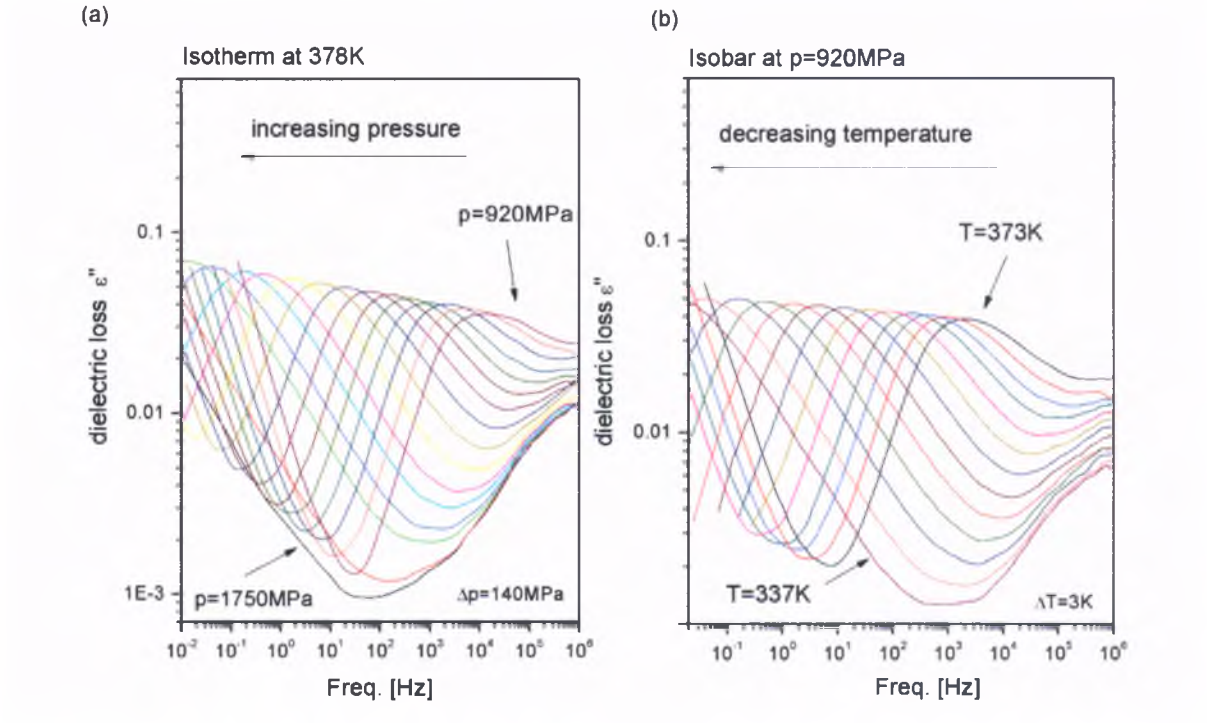

Figure 6.1. Representative dielectric loss data obtained during (a) isothermal measurements carried out at T=378 K and (b) isobaric measurements at p=920 MPa.

On both, decreasing temperature and increasing pressure the structural relaxation slows down. The α-peak exhibits strong sensitivity to pressure and less than 600 MPa is enough to move it through experimentally available frequency range. At higher frequencies (10^5-10^6 Hz) the low-frequency side of the γ-relaxation is observed. This process seems to be insensitive to applied pressure, because compression of supercooled Ibuprofen brings about a shift by many orders of magnitude of structural relaxation peak, while the position of γ-relaxation peak remains unchanged. It is worth to remind that the sensitivity to pressure is the most important criterion used to classify the secondary relaxation as a 'genuine' JG process [115]. For

Ibuprofen, the pressure-invariance of γ-peak indicates that this secondary relaxation is a non-JG process.

As shown in the past by Brás and co-workers in supercooled liquid state of Ibuprofen there is an additional relaxation process, slower than α-mode and termed as Debye relaxation [162]. It was suggested that appearance of D-process is associated with hydrogen bonded aggregates that Ibuprofen tends to form (mostly dimeric and trimeric linear or cyclic structures) [162]. However, during my studies I have found out that appearance of D-relaxation in dielectric loss spectra of Ibuprofen strongly depends on the thermal history of the sample. Depending on the temperature at which the sample was annealed to ensure complete melting and the applied cooling rate, the D-process is well-pronounced or appears only as a slight broadening of the low frequency part of α-peak. Debye-like relaxation was also not detected at elevated pressure. Thus, it is difficult to verify if pressure affects in any way hydrogen bonds in Ibuprofen and consequently cause D-relaxation to disappear, because even at ambient pressure appearance of D-relaxation is not repeatable.

In Figure 6.2 the effect of temperature and pressure on dielectric strength $\Delta\varepsilon$ of structural relaxation process is presented. As can be seen, dielectric strength behaves in different way

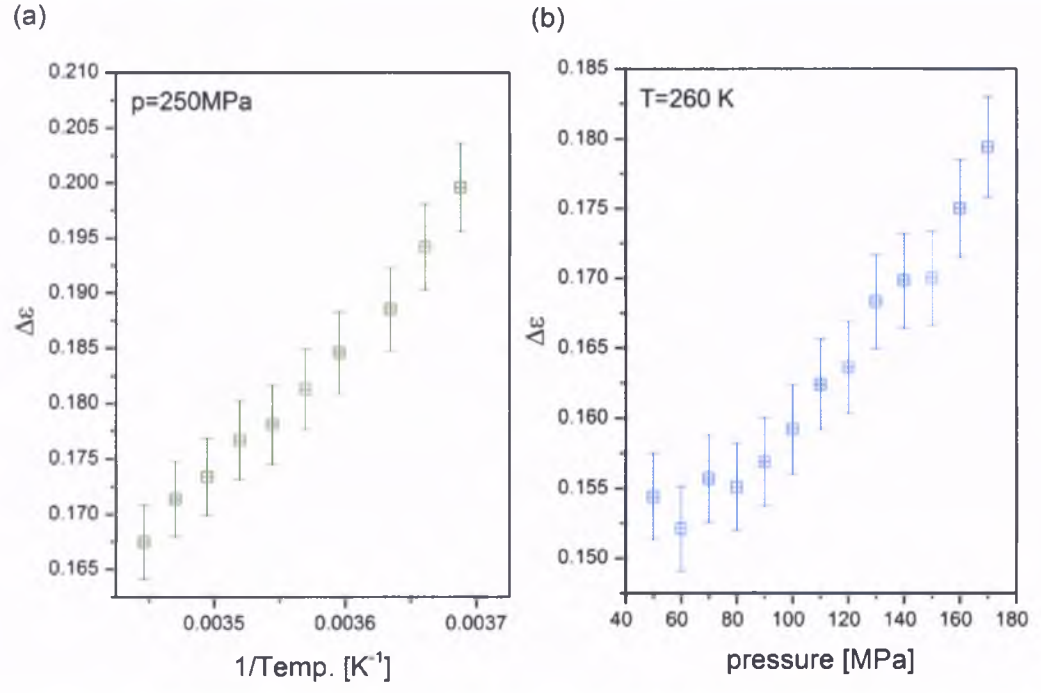

Figure 6.2. Dielectric strength $\Delta\varepsilon$ for the α-relaxation process plotted versus (a) temperature (isobar 250 MPa) and (b) pressure (isotherm at 260 K).

for isothermal and isobaric data i.e. it systematically decreases with increasing temperature (panel a) and increases with increasing pressure (panel b). Moreover, both dependences follow the linear pattern. Dielectric strength is directly proportional to density ρ (number of dipoles per unit volume) and inversely proportional to temperature T. Hence, the increase of $\Delta\varepsilon$ with increasing pressure is expected to be caused through densification of the sample. Analogous behavior as for Ibuprofen was also reported for other glass formers and polymers [163,164].

A very interesting issue observed in the case of Ibuprofen is the invariance of α-peak with increasing temperature and pressure, known as a temperature-pressure superpositining (TPS). This is illustrated in Figure 6.3, where superposed dielectric loss spectra of Ibuprofen obtained at different thermodynamic conditions, but with approximately the same structural relaxation time τ_α, are presented. Taking into account hydrogen-bonded abilities of Ibuprofen this phenomenon is quite interesting, because usually for hydrogen bonded systems (for example glycerol [165] or m-fluoroaniline [166]) TPS fails. As postulated by Roland et at. [167] the breakdown of TPS is closely related to modification of the population of hydrogen bonds at different thermodynamic conditions. However, the essential difference between m-fluoroaniline and Ibuprofen is that the former one creates complex hydrogen networks or large clusters, while the latter one only small hydrogen-bonded aggregates (dimers or trimmers). Consequently, even if their population is being modified as a result of pressure,

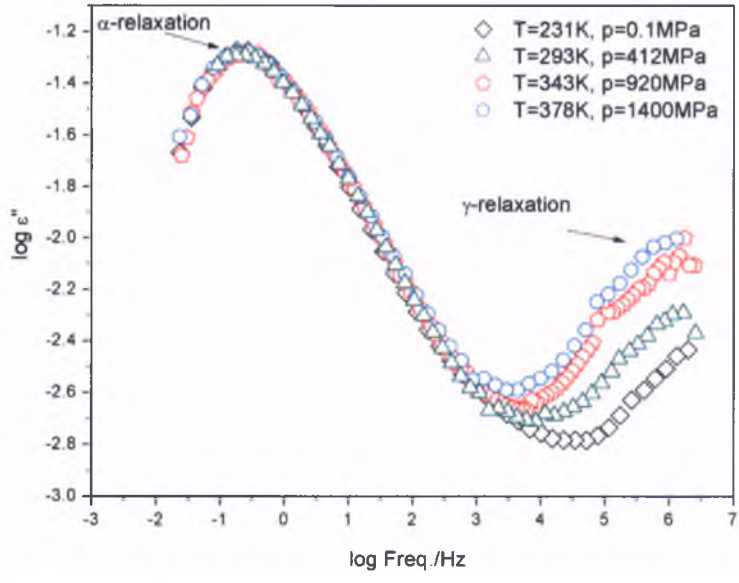

Figure 6. 3. Comparison of the dielectric loss spectra of Ibuprofen obtained for different temperature and pressure combinations, but having approximately the same structural relaxation time.

this is still not enough to alter the global dynamics of the system.

Dielectric loss spectra of Ibuprofen collected at higher temperature and pressure disclosed considerably higher amplitude of γ-relaxation, than that taken at ambient pressure and low temperature (Figure 6.3). This situation can be related to the fact that compression was carried out at higher temperature, at which the amplitude of γ-relaxation (which is thermally activated process) was also higher.

In the glassy state of Ibuprofen except for γ-relaxation, the β-process appears (Figure 6.4). However, its amplitude is significantly lower than that of the γ-relaxation. This secondary relaxation was identified by Brás et al. as the JG β-relaxation. Current studies have demonstrated its pressure sensitivity, which is an unquestionable proof that this is 'genuine' JG process.

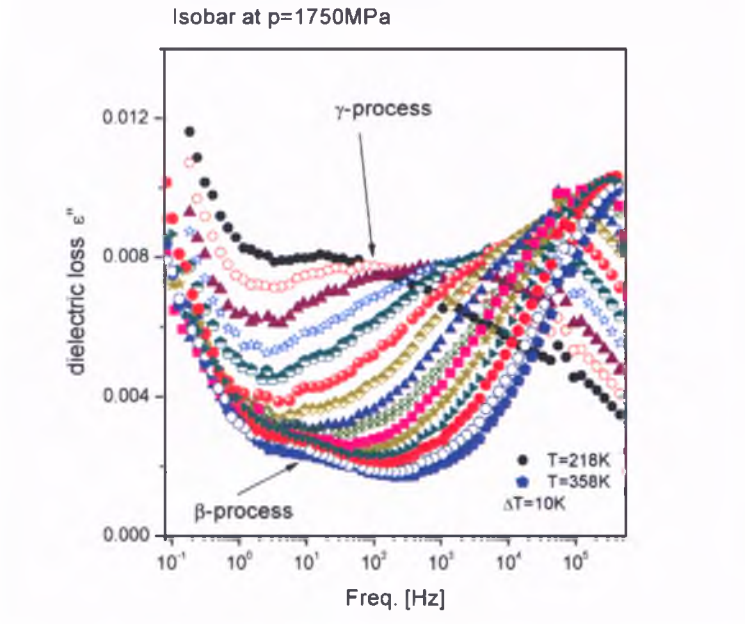

Figure 6.4. Dielectric loss spectra of Ibuprofen collected in the glassy state during isobaric measurements at p=1750 MPa.

From the analysis of ambient and elevated pressure data secondary relaxation times τ_β and τ_γ were calculated and then their temperature dependences were fitted to the Arrhenius equation (Eq. (3.17)). The values of activation barriers for isobars 0.1 MPa and p=1750 MPa can be found in Table 6.1. It is worth noticing that the activation energy of the γ-process at high pressure practically doesn't change, when compared to ambient pressure value. This is another sign of local, non-JG nature of this process. On the other hand, activation barrier for

β-relaxation increases with pressure. This situation reflects greater density of glass prepared by compression of liquid at high temperature. The β-relaxation senses the changes in the glassy structure, which is visible as an increase of its activation energy.

Table 6.1. Activation energies of the secondary relaxations for Ibuprofen at ambient pressure and 1750 MPa.

Pressure	Activation energy β-relaxation	Activation energy γ-relaxation
0.1 MPa	51 ±4 kJ/mol	27 ±0.5 kJ/mol
1750 MPa	60 ±4 kJ/mol	28 ±1 kJ/mol

In order to describe isobaric and isothermal dependences of structural relaxation times the VFT equation (Eq. (3.18)) and its pressure counterparts (Eq. (3.34)) were used. The representative fits are shown in Figure 6.5. The glass transition temperature T_g (the glass transition pressure p_g) was defined as the temperature (pressure) at which structural relaxation time is equal to 100 seconds.

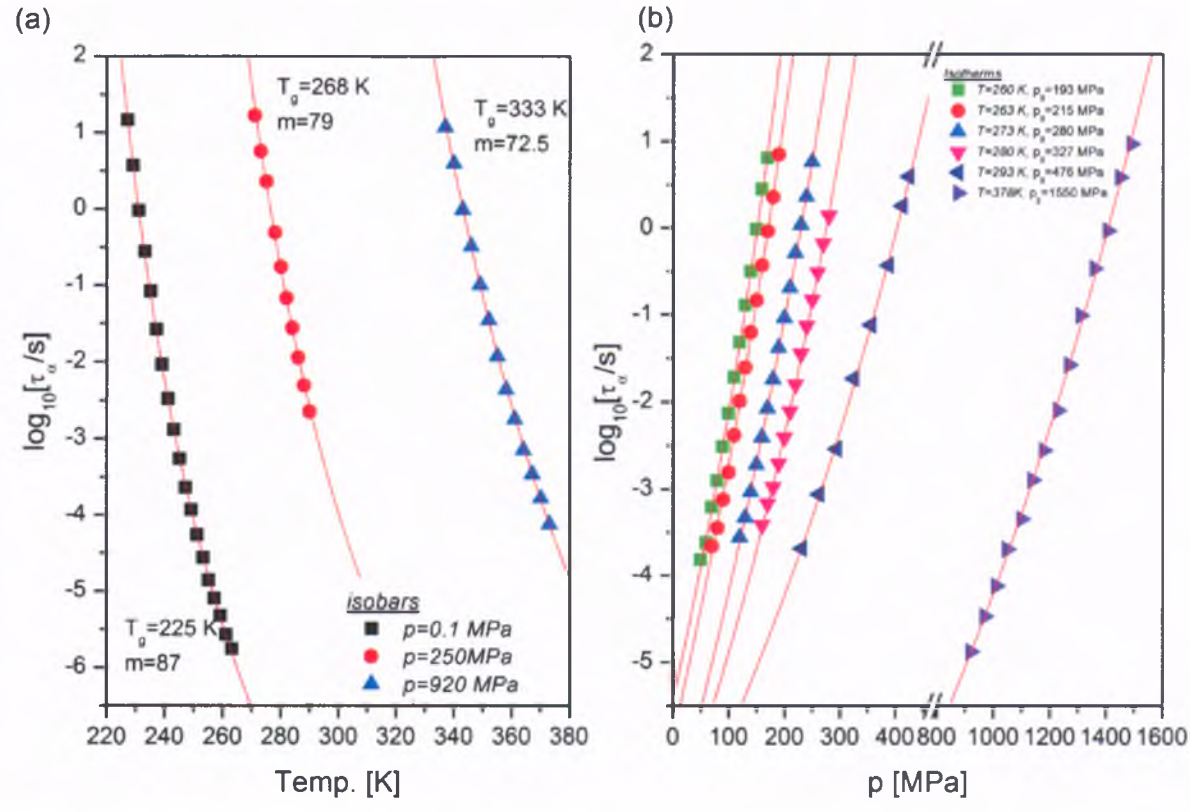

Figure 6.5. (a) Isobaric dielectric relaxation times for Ibuprofen measured as a function of temperature. (b) Isothermal dielectric relaxation times for Ibuprofen measured as a function of pressure. Solid lines represent fits of experimental data to the VFT equation and its pressure counterpart.

Next, these results were used to plot dependence of T_g versus pressure as illustrated in Figure 6.6. To describe $T_g(p)$ dependence the Andersson and Andersson equation was used (Eq. (3.35)), and then, pressure coefficient of T_g in the limit of low pressure was calculated. Interestingly, the value $\lim_{p\to 0} dT_g / dp = 0.212\pm0.021$ K/MPa obtained for Ibuprofen is much higher than those reported in the literature for strongly hydrogen-bonded systems, like glycerol (0.04K/MPa [168]), sorbitol (0.043K/MPa [169]) or propylene glycol(0.037K/MPa [170]), but rather comparable to those of typical van der Waals liquids [97].

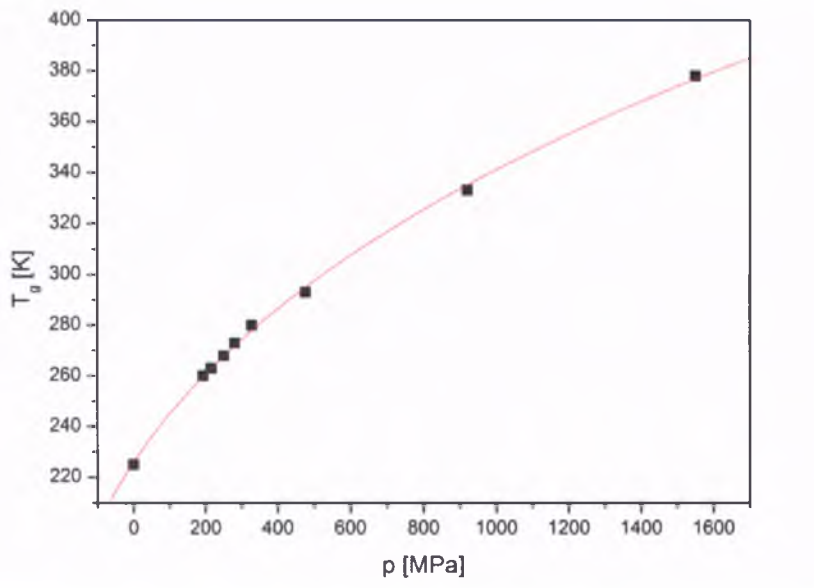

Figure 6.6. Dependence of the glass transition temperature versus pressure. The solid line represents the best fit to the Andersson and Andersson equation.

For isobaric data fragility index was also calculated in accordance with Eq. (3.19). The values m=87±5 at 0.1 MPa, m=79±3 at 200 MPa and m=72.5±5 at 920 MPa show that fragility of Ibuprofen decreases with pressure. In agreement with TOP model, the drop of fragility with compression implies that the liquid becomes stronger (more frustrated), and consequently should be more stable against crystallization. Indeed, in this case TOP model turned out to work very well, because the reduction of fragility with compression correlates with greater resistance against crystallization of considered pharmaceutical. The experimental results will be presented in the further part of this Chapter.

The essential difference in molecular dynamics of Ibuprofen at ambient and high pressure is clearly visible when the change of E_α/E_β ratio with pressure is analyzed. The relative

importance of thermal and volume effects on molecular dynamics of Ibuprofen were quantified with the use of Eq. (3.26). Thermal expansion coefficients at constant pressure and constant relaxation time were determined from isobaric together with isothermal dielectric relaxation studies and isobaric *V(T)* curves recorded in the liquid state of Ibuprofen during Pressure-Volume-Temperature (PVT) measurements and parameterized later on by means of the Tait equation of state (appropriate data and fitting parameters can be found in ref. [171]). In order to avoid significant extrapolation of the PVT data, the glass transition temperature was re-defined as temperature at which structural relaxation time is equaled to τ_α=0.1 s. Obtained values of α_P referring to dynamics of Ibuprofen at pressures varying from 0.1 MPa up to 1320 MPa, and temperatures at which τ_α=0.1 s are listed in Table 6.2.

Table 6.2. Values of α_P, E_V/E_P calculated for Ibuprofen at glass transition temperatures T_g=T(τ_α=0.1s) and pressures starting from 0.1 MPa up to 1320 MPa.

Pressure [MPa]	T_g **[K]** (τ_α**=0.1s**)	α_P **[K^{-1}] at** T_g	$\left.\frac{E_V}{E_P}\right\|_{T_g}$
0.1	235	$7.4\cdot10^{-4}$	0.54
1278	260	$5.33\cdot10^{-4}$	0.62
1466	263	$5.13\cdot10^{-4}$	0.63
201	273	$4.58\cdot10^{-4}$	0.66
245	280	$4.23\cdot10^{-4}$	0.67
250	281	$4.19\cdot10^{-4}$	0.68
328	293	$3.68\cdot10^{-4}$	0.71
920	349	$1.89\cdot10^{-4}$	0.82
1320	378	$1.32\cdot10^{-4}$	0.87

From the analysis of experimental data, the isochronal expansion coefficient was assumed to be nearly constant $\alpha_\tau(T_g)$= 8.89×10^{-4} K^{-1}, whereas the isobaric thermal coefficient decreases as pressure increases. Basing on collected values of thermal expansivities, the enthalpies ratios were calculated using Eq. (3.26) and summarized in Table 6.2.

As can be seen, at ambient pressure the value of E_V/E_P was found to be 0.54, which indicates that thermal energy as well as molecular packing are both important in controlling relaxation dynamics of Ibuprofen near the glass transition temperature. However, with increasing pressure thermal effects gains importance in governing the molecular dynamics of Ibuprofen. At pressures of around and greater than 1 GPa practically fully thermally activated

structural relaxation dynamics is expected. The increase of E_v/E_p ratio with increasing pressure is reasonable result, because pressurization of supercooled liquid increases the sample's density and at very high pressures complete reduction of free volume contribution is expected.

As a final point, the results of crystallization experiments at elevated pressure will be presented. In order to investigate what is the effect of pressure on physical stability of supercooled Ibuprofen crystallization kinetics studies were performed at different T and p combinations while keeping the structural relaxation time the same ($\tau_\alpha \approx 1 \times 10^{-5}$ s). Sample 1 was crystallized at T_1=255 K, p_1=0.1 MPa, Sample 2 at T_2=343 K, p_2=550 MP and Sample 3 at T_3=383 K, p_3=920 MPa. For all crystallization kinetics measurements the same experimental environment (1.8 GPa pressure cell, described in Experimental Section) was used. This procedure ensures the most reliable comparison between data collected at various thermodynamic conditions.

As illustrated in Figure 6.7 for representative sample, during crystallization the intensity of the structural relaxation peak gradually decrease, while in the real part of the complex dielectric permittivity this situation is reflected by a decrease of static permittivity increment. The decrease of dielectric strength with crystallization indicates that with crystallization the number of reorientating dipoles is drastically reduced.

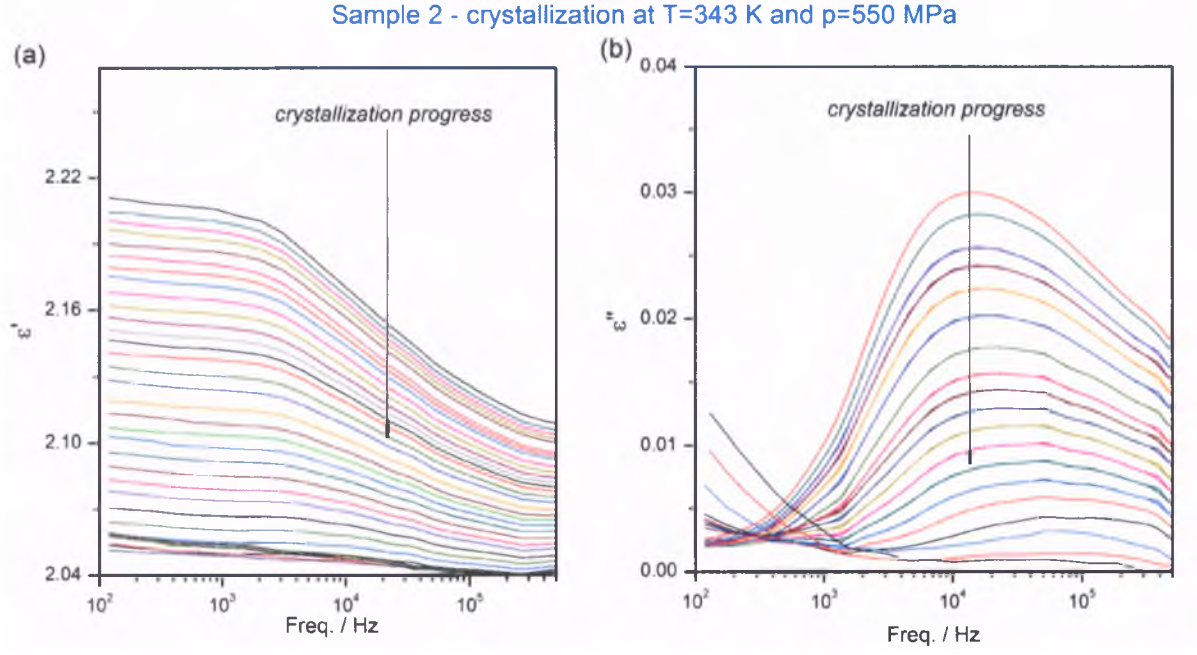

Figure 6.7. Spectra of the real (a) and imaginary (b) part of complex dielectric permittivity in the frequency domain during crystallization of Ibuprofen at T=343 K and p=550 MPa.

In order to extract the basic kinetic parameters of the crystallization, its progress was monitored in the real part of the complex dielectric permittivity. The $\varepsilon'(t)$ dependences used in further analysis were collected from the low frequency region (between 200 and 1400 Hz). For each sample the induction time of crystallization, t_0, defined as time at which dielectric constant starts to decrease, was estimated as well (Figure 6.8).

As structural relaxation times of all three samples crystallized at different T and p combinations were practically the same one, one should expect very similar onsets of crystallization if molecular mobility is really the key parameter responsible for recrystallization issue. However, experimental results have proven that the induction times of crystallization significantly extend for Samples 2 and 3. Moreover, the crystallization half-time, i.e. time at which the degree of crystallinity reaches 50% of the maximum value, was also found to be significantly extended for samples that crystallized at high pressure. Values of t_0 and $t_{1/2}$ are listed in Table 6.3.

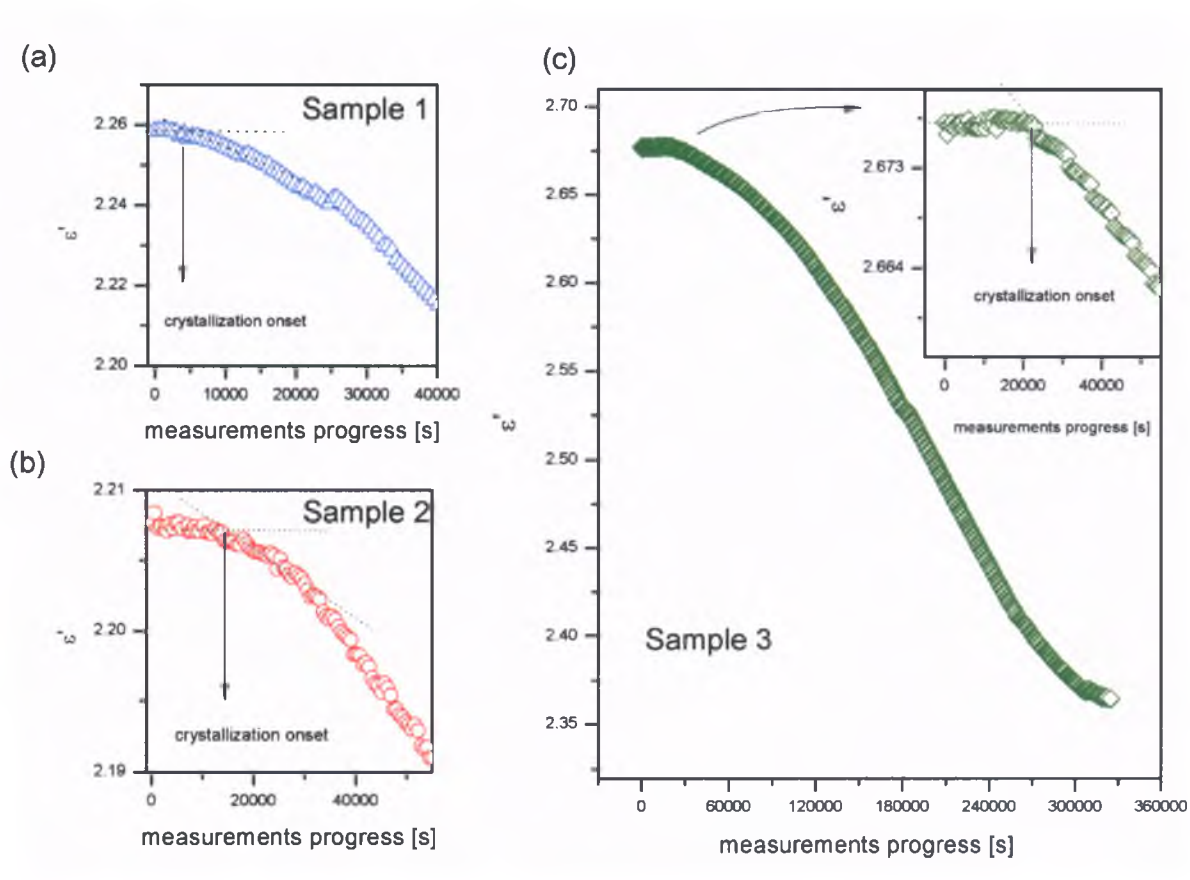

Figure 6.8. Panels a and b and inset c present the evolution of dielectric constant of α–relaxation, at the low frequency region, during the first stages of measurements, for Samples 1, 2, and 3, respectively. The main figure in panel c presents the evolution of the dielectric constant of structural relaxation throughout the whole measurement time for Sample 3.

Table 6.3. Kinetic parameters of Ibuprofen crystallized at three different combinations of pressure and temperature.

Material	Avrami			Induction time t_0 [h]	Half time $t_{1/2}$ [h]	Rate constant $k^{1/n}$ [s^{-1}]
	n	k [s^{-n}]	τ_{cry} [h]			
Sample 1 *(p=0.1MPa, T=255K)*	2.3 ±0.1	1.8×10^{-11} $\pm0.4\times10^{-11}$	13.6 ±1.4	1.2 ±0.2	12.2 ±0.2	2.1×10^{-5} $\pm0.2\times10^{-5}$
Sample 2 *(p=550MPa, T=343K)*	2.2 ±0.1	$3.\times10^{-12}$ $\pm0.3\times10^{-12}$	45 ±1.4	4 ±0.2	35.7 ±0.2	6.4×10^{-6} $\pm0.3\times10^{-6}$
Sample 3 *(p=920MPa, T=383K)*	2.2 ±0.1	1.3×10^{-12} $\pm0.2\times10^{-12}$	62 ±1.4	5.5 ±0.2	49 ±0.2	4×10^{-6} $\pm3\times10^{-6}$

In the next step crystallization data from different (T, p) combinations were normalized and presented in terms of the normalized dielectric constant ε'_N, (Eq. 5.1). Normalized curves plotted as a function of crystallization time are presented in Figure 6.9 (a). As illustrated, they shift to longer time as the crystallization temperature and pressure increase. In order to describe the time dependence of ε'_N the Avrami formula (Eq. 5.2) was applied. Avrami fits are presented in Figure 6.9 (a) as red solid lines. The dependence $\ln(-\ln(1-\varepsilon'_N))$ versus $\ln(t)$ was also plotted, as demonstrated in Figure 6.8 (b). By the projection on the x-axis the straight line for which $\ln(-\ln(1-\varepsilon'_N))=0$ the values of τ_{cry} were estimated. Obtained crystallization rate constants k, Avrami parameters n and characteristic crystallization times τ_{cry} are summarized in Table 6.3. It is very remarkable, that the values of Avrami parameter n are practically the same. This is a clear sign of non-changing mechanism and shape of growing crystals with pressure. In this case (n=2) we may expect that crystals grow as rods. However, non-integral values n of may also suggest mixed growth and surface nucleation, and/or two-step crystallization.

By taking into account all collected in Table 6.3 data one can conclude that the induction time as well as the overall crystallization time are significantly extended when crystallization if performed at high temperature and pressure (while keeping the same τ_α). The fact that

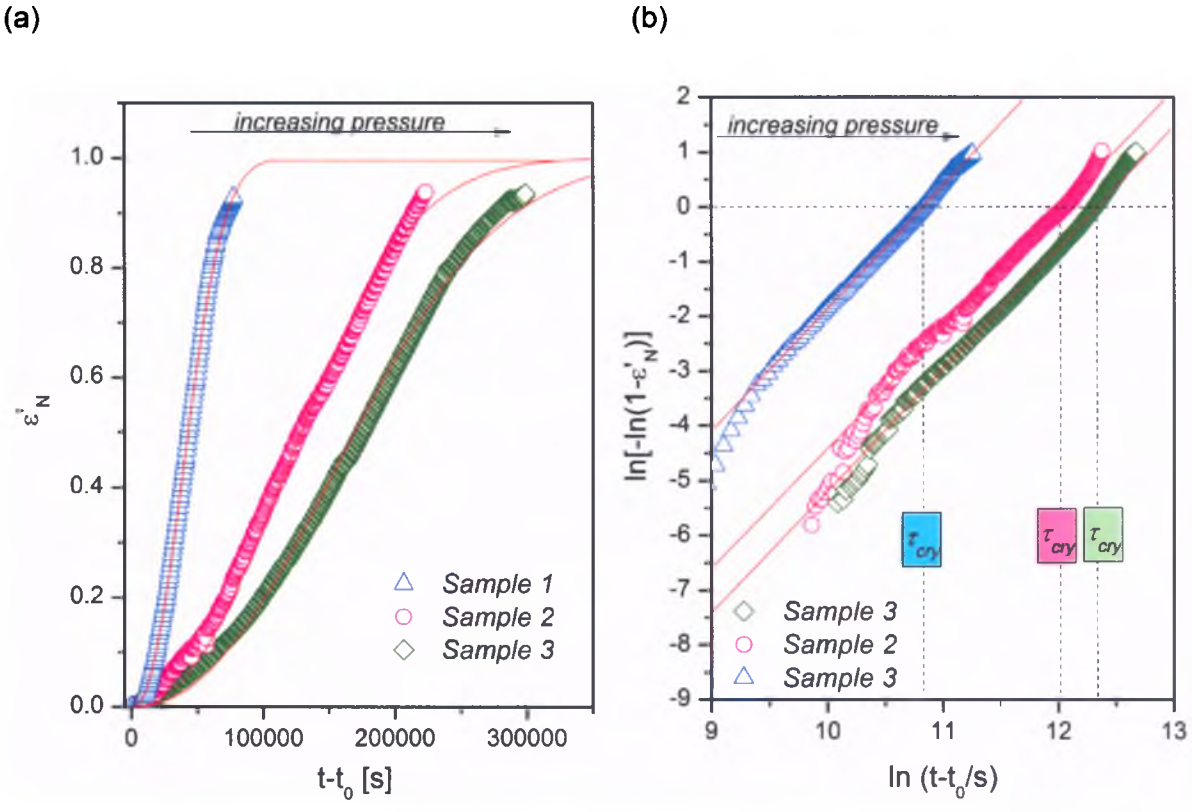

Figure 6.9. (a) Time evolution of normalized constant for crystallization carried out at p = 0.1 MPa and T= 255 K (Sample 1), p= 550 MPa and T= 343 K (Sample 2), and p=920 MPa and T= 383 K (Sample 3). Solid red lines are bets fits of experimental data to the Avrami equation, (b) Avrami plot of the normalized dielectric constant in double logarytmic scale for Samples 1-3.

crystallization of Ibuprofen slows down with pressure is very promising result regarding possible way of obtaining unusually stable against crystallization glasses. However, these results are also important from other point of view. They, unquestionably prove that molecular mobility related to structural relaxation process does not govern alone crystallization. On the other hand, it must be pointed out that at different (T, p) conditions the relative importance of molecular packing and thermal effects on relaxation dynamics near T_g were completely different. At ambient pressure both, temperature and volume govern relaxation dynamics in practically equal way, while at high pressure thermal effects become the prominent variables that control molecular mobility of Ibuprofen.

The fact that crystallization slows down with pressure can be explained more or less in terms of most of theoretical models mentioned at the beginning of this Chapter, as well as that postulated by Kanishi and Tanaka [172]. As they assumed, formation of nuclei in the liquid or glassy states induces extensional stress around it, due to volume contraction. This should provide, according to Doolittle equation, the excess of free volume to molecules

surrounding crystal, resulting in the increase of their mobility and ease of crystallization. When this explanation of the crystallization phenomenon is applied to Ibuprofen, one can suppose that it takes longer to crystallize at very high pressure because molecular mobility related to structural relaxation is governed by thermal effects, not molecular crowding. So, even if, as a result of negative pressure around crystal nuclei, additional free volume for molecules to reorientate appears, it wouldn't increase mobility and support the crystallization progress, since dynamics of compressed Ibuprofen is governed not by free volume, but almost entirely by thermal energy.

Slowing down of the crystallization with applied pressure is very optimistic result that may open up new routes in manufacturing of extraordinary stable amorphous materials. Unfortunately, at the moment there are no other experimental results which will confirm (or not) universal character of the observed effect. As crystallization abilities of glass-formers under elevated pressure are completely unexplored issue, more experimental data are certainly needed. In fact, to take full advantage from this new finding it must be confirmed for larger group of compounds, with specific as well as non-specific intermolecular interactions.

CHAPTER 7

CONCLUSION

The amorphous state is probably one of the most interesting and curious state of matter. This confirms large number of futuristic and next-generation materials that turned out to be partially or completely amorphous. However, physical properties of amorphous solids are incomprehensible in many aspects. Even the glassy formation is considered as one of the most important unsolved problems of solid state physics. Understanding what drives supercooled liquids and glasses towards crystallization is fundamental not only in the context of unexplained issues of condensed matter physics, but also many practical applications. In this Ph. D. dissertation I have made an attempt to answer the most important in recent days questions that relate to molecular dynamics of amorphous materials. The robustness of the 'universal' relationships between dynamics and crystallization tendencies of glass-formers was also uncovered.

The first raised issue concerned dynamical properties of amorphous materials depending on the preparation method. Collected results for compounds of great pharmaceutical interest, Telmisartan and antibiotics, remarkably showed that dynamical properties of amorphous substances prepared using two different amorphization routes (vitrification and cryomilling) might differ. However, observed discrepancies in molecular dynamics results only from the fact that during manufacturing they uptake different amount of water from the surroundings, and this absorbed water has critical influence on their dynamical properties. Particularly interesting here are results for antibiotics. The presence of γ-relaxation, of most probably the same molecular origin, was reported in anhydrous glassy state of Clarithromycin and Roxithromycin. In the anhydrous vitrified Azithromycin the lack of γ-relaxation was reported, while in cryomilled amorphous sample this process became suddenly activated due to the presence of water.

In the amorphous state of cryomilled material there is typically additional relaxation mode observed, but once the material passes the glass transition temperature and entered the supercooled region all differences in dynamical properties are erased. Cooling such sample in order to its re-amorphization results in relaxation dynamics of vitrified one. Moreover,

amorphous materials prepared by mechanical milling are known from the ease of recrystallization when stored at room temperature, but cryomilled Telmisartan as well as antibiotics are exceptions from this rule, because they were found to be physically long-term stable.

As second, the problem of estimation the time scale of global mobility (associated with structural relaxation time) below glass transition temperature was raised in the context of pharmaceutical, Telmisartan. From experimental point of view τ_α in the glassy state cannot be determined directly. Thus, various methods that allowed to predict structural relaxation times in the glassy state were tested, and then obtained results were confronted with each other once placed on the same relaxation map. As it turned out, methods that actually based on the simple TTS rule, i.e. the shape of the structural relaxation peak does not change while crossing the glass transition, give back almost the same dependence $\tau_\alpha(T)$ in the glassy state. In this case, more Arrhenius-like behavior is expected below T_g. However, as pointed out the invariable value of stretching parameter β_{KWW} above and below T_g is not as certain as one may suppose. Even the validity of the Coupling Model with experimental results collected below T_g (i.e. increase of τ_α and constant τ_β upon aging) requires assumption that β_{KWW} decrease in the glassy state. Thus, more studies are essential in the future to verify if the shape of the structural relaxation can be really assumed to be constant, $\beta_{KWW}(T_g)=\beta_{KWW}(T<T_g)$, so that approaches used in this work to predict structural relaxation time are indeed reliable source of information about the time scale of molecular motion in the glassy state. Interestingly, the temperature dependence of structural relaxation time in the glassy state of Telmisartan predicted by means of the modified Adam-Gibbs equation is more VFT-like and does not follow the same trend as that which is based on the aging experiment. However, it should be pointed out that the modified Adam-Gibbs formula predicts relaxation dynamics of freshly formed, non-aged glass, which makes descriptive comparison between both approaches rather impossible. Nevertheless, even if the temperature dependence of structural relaxation time below T_g of Telmisartan follows the Arrhenius pattern, the time scale of global mobility at room temperature would exceed 3 years, which actually agree with experimentally verified long-term stability of Telmisartan upon storage. Thus, the estimation of the structural relaxation time at certain temperature below T_g gives us very general information about approximate storage time within which the system shouldn't recrystallize. As molecular

mobility can only facilitate or impede crystallization progress, the greater structural relaxation time below T_g implies the greater level of protection against crystallization, and vice versa.

In this dissertation of the special interest was to evaluate the exact role of molecular mobility in governing the physical stability of amorphous materials, mainly pharmaceutically important substances. To the best of author's knowledge, such systematic and conscientious studies on the relationship between molecular mobility and instability issue have never been performed in the past, so the acquired knowledge is absolutely unique. Valuable and crucial information were achieved, as for these studies I have selected quite similar in the chemical structure and molecular conformation compounds that were prepared using same amorphization technique (vitrification).

Conducted studies have proven that global molecular mobility (associated with structural relaxation) is certainly an important parameter that controls crystallization abilities of glass-formers. In order to incorporate into crystalline lattice molecules need to rearrange and find 'proper' position, because only those which 'suits' to the lattice can be joined. However, as presented in this dissertation mobility on its own cannot 'cause' crystallization, at the most it can 'facilitate' it (above T_g crystallization proceeds faster than below T_g). Studies carried out for glassy antibiotics have confirmed that when amorphous material is stored below Vogel temperature T_0 it will exhibit maximal stability. Unfortunately, from practical standpoint storage below T_0 is not possible in many cases, and as approaching the glass transition the time scale of global molecular mobility significantly increase. In this temperature region different resistance against crystallization of nucleosides as well as glucose derivatives upon time dependent crystallization experiments, performed for the same structural relaxation time, pointed out that molecular mobility is not the key parameter that bring about crystallization of glass-formers. Thus, there must be other factors of much greater authority.

Experimental results collected in this work indicate that crystallization abilities of glass-forming liquids are certainly too complicated to be just extracted from the analysis that bases on one or two selected parameters related to relaxation dynamics, for example fragility or the width of α-relaxation. As proven, crystallization tendencies of glass-formers above and below T_g do not correlate with the distribution of structural relaxation times, neither with the value of fragility index. There is also no evident correlation between the degree of local mobility and crystallization abilities in the glassy state. Given in this work the example of nucleosides clearly demonstrates that crucial information considering stability below T_g were extracted not

from molecular dynamics studies, but the analysis of thermodynamic parameters, including configurational quantities.

In the opinion of the author, particularly interesting are results obtained for glucose and its acetyl derivatives, which reveal that by changing the character of intermolecular interactions from hydrogen bonding to typical van der Waals, the resistance against crystallization can be drastically changed. Hydrogen bonding abilities of glucose are most probably responsible for its greater stability against crystallization in the supercooled liquid state, when compared with acetyl derivatives. It is also remarkable that both pentaacetyl glucoses have practically the same values of glass transition temperatures, identical fragilities and molecular mobility, whereas different drive towards crystallization. The specific example of α- and β-pentaacetylglucoses is just another conformation that molecular mobility is not the key parameter that is responsible for recrystallization. However, the most striking thing is that the initial calorimetric measurements have shown that there is also no significant differences in thermodynamic properties of glucose derivatives. This leads to the essential conclusion that the character of molecular interaction and molecular architecture, which in fact were not taken into detailed consideration in the past, might have the crucial importance on the physical stability of glass-forming liquids.

Finally, molecular dynamics and crystallization kinetics of pharmaceutical, Ibuprofen, were investigated at ambient and elevated pressure. High pressure experiments have proven that compression of supercooled liquid at high temperature results in denser glass, which is reflected in the values of the activation energy of the secondary JG β-relaxation. Surprisingly, for hydrogen bonding Ibuprofen the TPS rule was found to be fulfilled. This finding was explained by the fact that Ibuprofen, in contrast to strongly associated liquid, creates only small dimeric or trimeric structures. So, even if their population is being modified as a result of pressure, this is still not enough to alter global dynamics of the system. In order to point essential differences in molecular dynamics of Ibuprofen at ambient and elevated pressure the change of E_v/E_p ratio with compression was analyzed. Based on collected results, it can be concluded that at ambient pressure relaxation dynamics is controlled by both variables, thermal effects and molecular packing, but with increasing pressure thermal effects gain importance in governing the molecular dynamics of Ibuprofen, and at pressures of around 1 GPa practically fully thermally activated dynamics is expected. The increase of E_v/E_p ratio with compression indicates that pressurization of supercooled liquid leads to the significant

reduction of the free-volume contribution. Consequently, free-volume models are not appropriate to describe relaxation dynamics of supercooled liquids under high pressure.

Among all results present in this dissertation the most important and promising one are those which comes from crystallization experiments at elevated pressure. To the best of author's knowledge studies on the kinetics of crystallization process of supercooled liquids under high pressure have never been conducted by anyone in the past. Thus, obtained results are absolutely pioneering. Crystallization experiments performed in the supercooled liquid state of Ibuprofen at different T and p combinations, while keeping same structural relaxation time (same degree of molecular mobility), revealed that pressure slows down crystallization progress, possibly even inhibit it. This is very novel and hopeful finding, which also clearly demonstrates that high-pressure experiments give us the most stimulating and valuable information considering dynamical properties of investigated materials.

The crucial impact of pressure, as the only one thermodynamic variable that actually have an impact on crystallization abilities of glass-formers, was even postulated by some of the world's most respected scientists that deal with crystallization phenomenon. Unfortunately, at present times there is no systematic studies on the crystallization of glass-formers at elevated pressure, which is completely unexplored issue. Because of that reason it is even impossible to confront slowing down of Ibuprofen's crystallization with pressure, with any other experimental results. Thus, universality of the effect of pressure on crystallization abilities of glass-formers remains still an open question.

At the moment some more detailed research work is in progress. Hopefully, our results will finally verify which theoretical picture of crystallization phenomenon of supercooled liquids at elevated pressure is the most appropriate one, and whether compression of liquid at high temperature can be really used as a new route of preparation extraordinary stable amorphous materials. So that, based on acquired knowledge fully aware stabilization protocol of amorphous pharmaceuticals will be finally designed in the future.

REFERENCES

[1] Lipinski,C.; *Am. Pharm. Rev.* **2002**, 5, 82–85

[2] Rasenack, N.; Müller, B.W.; *Pharmazeutische Industrie* **2005**, 67, 323–326

[3] Löbenberg, L.; Amidon, G.L.; *Eur. J. Pharm. and Biopharm.*, **2000**, 50, 3-12

[4] Serajuddin, Abu T.M.; *Adv. Drug Deliv. Rev.* **2007**, 59, 603-616

[5] Loftsson, T.; Brewste, M. E.; *J. Pharm. Sci.* **1996**, 85, 1017-1025

[6] Chaumeil, J.C.; *Methods Find. Exp. Clin. Pharmacol.* **1998**, 20, 211–5

[7] Craig, D. Q.M.; Royall, P. G.; Kett, V. L.; Hopton, M. L.; *Int. J. Pharm.* **1999**, 179, 179–207

[8] Murdande, S. B.; Pikal, M. J.; Shanker, R. M.; Bogner, R. H.; *Pharm Res.* **2010,** 27, 2704-14

[9] Hancock, B.C.; Parks, M.; *Pharm Res.* **2000**, 17, 397-404

[10] Hancock, B. C.; Carlson, G. T.; Ladipo, D.D.; Langdon, B. A.; Mullarne, M. P.; *Int. J. Pharm.*, **2002**, 241, 73-85

[11] Gupta, P.; Bansal, A. K.; AAPS *PharmSciTech* **2005**; 6 (2) Article 32

[12] Yoshioka, M.; Hancock, B. C.; Zografi, G.; *J. Pharm. Sci.* **1994**, 83, 1700

[13] Byrn, S. B.; Xu, W.; Newman, A. W.; Adv. Drug Deliv. Rev. **2001**, 48, 115-136

[14] Adrjanowicz, K.; Kaminski, K.; Grzybowska, K.; Hawelek, L.; Zakowiecki, D.; Cal, K.;, Tarnacka, M.;Mol. Pharmaceutics 2012, Just Accepted Manuscript, DOI: 10.1021/mp300067r

[15] Law, D.; Schmitt, E. A.; Marsh, K. C.; Everitt , E. A.; Wang, W.; Fort, J. J.; Krill, S. L.; Qiu, Y.; *J . Pharm. Sci.* **2004**, 93, 563-70

[16] Schmitt, E.; Davis, C. W.; Long, S. T.; *J. Pharm. Sci.* **1996**, 85, 1215-1219

[17] Bhugra, C.; Pikal, M. J.; *J. Pharm. Sci.* **2008**, 97, 1329-1349

[18] Zhou D., Geoff G., Zhang Z., Devalina Law, Grant D., Schmitt E.A. *Mol. Pharmaceutics*, **2008**, 5 (6), 927-936

[19] T. Wu and L. Yu, *Pharm. Res.* **2006**, 23, 2350-2355

[20] Zhu, L.; Wong, L.; Yu, L.; *Mol. Pharm.* **2008,** 5, 921-926

[21] Yoshioka, S.; Aso, Y.; *J. Pharm. Sci.* **2007**, 96(5), 960-81

[22] Shamblin, S. L.; Hancock, B. C.; Pikal, M. J.; *Pharm. Res.* **2006**, 23, 2254-2268

[23] Aso, Y.; Yoshioka, S.; Kojima, S. ; *J. Pharm. Sci.*, **2000**, 89, (3), 408-416

[24] Floudas, G.; Paluch, M.; Grzybowski, A.; Ngai, K. L.; 'Molecular Dynamics of Glass-Forming Systems – Effect of Pressure', Springer-Verlag **2011**

[25] Russo, J.; Tanaka, H.; 'The microscopic pathway to crystallization in supercooled liquids' submitted to *Nature*, private communication

[26] Elliott, S. R. *Nature* **1979,** 282, 560–560

[27] Demetriou, M. D.; Launey, M. E.; Garrett, G.; Schramm, J. P.; Hofmann, D. C.; Johnson, W. L.; Ritchie, R. O. *Nat. Mater.* **2011**, 10, 123–128

[28] Storey, K. B.; Storey, J. M. Annu. Rev. Ecol. Syst.**1996**, 27, 365–386.

[29] Elliot, S. R.; 'Physics of amorphous materials', Longman **1983**

[30] Zallen, R.; 'The physics of amorphous solids', Wiley **1998**

[31] http://physicaplus.org.il/zope/home/en/1223032001/stones_en

[32] Turnbull, D.; *Contemp. Phys.* **1969**, 10, 473

[33] Sesták, J. (Editor); Mares, J. J. (Editor); Hubík, P. (Editor); 'Glassy, Amorphous and Nano-Crystalline Materials Thermal Physics, Analysis, Structure and Properties Glassy, Amorphous and Nano-Crystalline Materials' (Hot Topics in Thermal Analysis and Calorimetry, Vol. 8), Springer Science & Business Media **2011**

[34] Adrjanowicz K., Kaminski K., Grzybowska K., Hawelek L., Paluch M., Gruszka I., Zakowiecki D., Sawicki W., Lepek P., Kamysz W., Guzik L., *Pharm. Res.* **2011**, 28, 3220-36

[35] De Gusseme, A.; Neves, C.; Willart, J. F.; Rameau, A.; Descamps, M..; *J Pharm Sci.* **2008**, 97, 5000-12

[36] Willart, J.F.; Caron, V.; Lefort, R., Dandède, F., Prèvost, D., Descamps. *Solid State Commun.* **2004**, 132, 693–6

[37] Lam, N. Q.; Okamoto, P. R.; Li, M.; J. Nuc. Mat. 1997, 25, 89-97

[38] Fecht, H. J. *Nature* **1992**, 356, 133-135

[39]Descamps, M.; Willart, J.F.; Aumelas A.; Complex Systems 5th International Workshop on Complex Systems. 2008, 53,61

[40] Yu, L.; *Adv. Drug Deliv. Rev.* **2001**, 48, 27-42

[41] Fukuoka, E.; Makita, M.; Yamamura, S.; *Chem. Pharm. Bull.* **1986,** 34, 4314

[42] Crowley, K. J.; Zografi, G.; *J. Pharm. Sci.* **2002**, 91, 492–507

[43] Hancock, B. C.; Zografi, G.; *Pharm. Res.* **1994,** 11, 1166–1173

[44] Gordon, J. M.; Tailor, J. S.; *J. Appl. Chem.* **1952**, 2, 493

[45] Surana, R.; Pyne, A.; Suryanarayanan, R.; *Pharm. Res.* **2004**, 21, 1167-1176

[46] Kearns, K. L.; Swallen, S. F.; Ediger, M. D.; Ye, Sun; Lian, Yu *J. Phys. Chem. B* **2009**, 113, 1579–1586

[47] Dawson, K. J.; Kearns, K. L.; Sacchetti, M.; Zografi, G.; Ediger, M. D. *J. Phys. Chem. B* **2009**, 113, 2422–2427

[48] Dawson, K. J.; Kearns, K. L.; Yu, L.; Steffen, W.; Ediger, M. D.; *PNAS* **2009**, 106 (36), 15165-15170

[49] Ediger, M. D.; Angel, C. A.; Nagel, S. R.; *J. Phys. Chem.* **1996**, 100, 13200-13212

[50] Debenedetti, P. G.; Stillinger, F. H. *Nature*, **2001**, 410, 259-267

[51] Moynihan, C. T.; Easteal, A. J.; Wilder, J.; Tucker, J.; *J. Phys. Chem.* **1974**, 78, 2673–2677

[52] Torquato, S.; *Nature* **2000**, 405, 521-523

[53] Santen, L.; Krauth, W.; *Nature* **2000**, 405, 550-551

[54] Gibbs, J. H.; diMarzio, E. A.; *J. Chem. Phys.* **1958**, 28, 373

[55] Cohen, M. H.; Grest, G. S.; *Phys. Rev. B* **1979**, 20, 1077

[56] Doolittle, A. K., *J. Appl. Phys.* **1951**, 22, 1471–1475

[57] Williams E.; Angell, C. A.; *J. Phys. Chem.* **1977**, 81,232-237

[58] Adam, G.; Gibbs, J. H.; *J. Chem. Phys.* **1965**, 43, 139–146

[59] Yamamuro, O.; Tsukushi, I.; Lindqvist, A.; Takahara, S.; Ishikawa, M.; Matsuo,T.; *J. Phys. Chem. B* **1998**, 102, 1605–1609

[60] Dyre, J. C; *Rev. Mod. Phys.* **2006**, 78 953-972

[61] Tanaka, H.; *J. Non-Cryst. Solids* **2005**, 351, 3371–3384

[62] Feldman, J.; The Physics of Dielectrics 83887, Lecture 1 Introduction into the physics of dielectrics.

[63] Kremer, F.; Schönhals, A.; Broadband Dielectric Spectroscopy, Springer-Verlag Berlin Heidelberg New York **2002**

[64] Kaminski, K.; Kaminska, E.; Hensel-Bielowka, S.; Pawlus, S.; Paluch, M.; Ziolo, J.; *J. Chem. Phys.* **2008**, 129, 084501

[65] Fröhlich, H.; Theory of Dielectrics: Dielectric Constant and Dielectric Loss – 2nd Edition, Oxford University Press **1958**

[66] Havriliak, S.; Negami, S.; *Polymer* **1967**, 8, 161

[67] Kohlrausch, R.; *Ann. Phys.* (Leipzig) **1847**, 72, 393

[68] Williams, G.; Watts, D.C.; *Trans. Faraday Soc.*, **1970**, 66, 80 – 85

[69] Wojnarowska, Z.; Adrjanowicz, K.; Wlodarczyk, P.; Kaminska, E.; Kaminski, E.; Grzybowska, K.; Wrzalik, R.; Paluch, M.; Ngai, K. L. *J. Phys. Chem. B* **2009**, 113, 12536–12545

[70] Stickel, F.; Fischer, E. W.; Richert. R.; *J. Chem. Phys.* **1996**, 104, 2043

[71] Casalini, R.; Ngai, K. L.; Roland, C. M.; *Phys. Rev B* **2003**, 68, 014201

[72] Wang, L. M.; Richert, R.; *Phys. Rev B* **2007**, 76, 064201

[73] Richert, R.; *J. Non-Cryst. Solids* 1994, 172-174, 209 - 213

[74] Richert, R.; *J. Phys.: Condens. Matter* **2002**, 14, R703 - R738

[75] Kawasaki, T.; Tanaka, H.; *PNAS* **2010**, 107, 14036 –14041

[76] Jäckle, J.; Richert, R.; *Phys. Rev. E* **2008**, **77**, 031201

[77] Wagner, H.; Richert, R.; *Polymer*, **1997**, 38, 255-261

[78] Glasstone, S.; Laider, K. J.; Eyring, H.; The theory of rate processes, McGraw-Hill Book Company, New York, **1941**

[79] Vogel H.; *Physikalische Zeitschrift* **1921**, 22, 645-6

[80] Fulcher, G.; *J. Am. Cer. Soc.* **1925**, 8, 339 – 355

[81] Tammann, G.; Hesse, W.; *Zeitschrift für anorganische und allgemeine Chemie*, **1926**, 156, 245 – 257

[82] Schönhals, A.; Kremer, F.; Hofmann, A.; Fischer, E. W.; Schlosser, E.; *Phys. Rev. Lett.* 1993, 70, 3459 - 3462

[83] Stickel, F.; Fischer, E. W.; Richert, R.; *J. Chem. Phys.* **1995**, 102, 6251

[84] Novikov, V. N.; Sokolov, A. P.; *Phys. Rev. E* **2003**, 67, 031507

[85] Casalini, R.; Ngai, K. L.; Roland, C. M.; Phys. Rev. B **2003**, 68, 014201

[86] Angell, C. A., Strong and fragile liquids, Relaxations in Complex Systems, edited by K. L. Ngai and G. B. Wright (U.S. GPO, Washington, D.C) pp. 3–11, 1985

[87] Böhmer, R.; Ngai, K. L.; Angel, C. A.; Plazek, D. J.; *J. Chem. Phys.* **1993**, 99, 5899

[88] Wang, L. M.; Velikov, V.; Angel, C. A.; *J. Chem. Phys.* **2002**, 117, 10184-10192

[89] Wang, L. M.; Angel, C. A.; *J. Chem. Phys.* **2003**, 118, 10353-10355

[90] Lubchenko, V.; Wolynes, P. G.; *J. Chem. Phys.* **2003**, 119, 9088-9105

[91] Roland, C. M.; Santangelo, P. G.; Robertson, C. G.; Ngail, K. L.; *J. Chem. Phys.* **2003**, 118, 10351-10352

[92] Ngai, K. L.; Yamamuro, O.; *J. Chem. Phys.* **1999**, 10403-10406

[93] Paluch, M.; Casalini, R.; Roland, C.M.; *Phys. Rev. B* **2002**, 66, 092202

[94] Roland, C.M.; Paluch, M.; Pakula, T.; Casalini, R.; *Phil. Mag. B.* **2004**, 84, 1573-1581

[95] MacKenzie, J. D.; *J. Chem. Phys.* **1958**, 28, 1037

[96] Casalini, R.; Roland, C.M. *J. Chem. Phys.* **2003**, 119, 4052

[97] Roland, C.M.; Hensel-Bielowka, S.; Paluch. M.; Casalini, R.; *Rep. Prog. Phys.* **2005**, 68, 1405–1478

[98] Roland, C.M.; Casalini, R. *Macromolecules* **2005**, 38, 8729-8733

[99] Hodge, I.M..; Macromolecules 1987, 20 2897

[100] Shamblin, S. L.; Tang, X.; Chang, L.; Hancock, B. C.; Pikal, M. J.; *J. Phys. Chem. B.* **1999**, 103, 4113-4121

[101] Gupta, P.; Chwala, G.; Bansal, A. K.; *Mol. Pharm.* **2004**, 1, 406-413

[102] Casalini, R.; Roland, C. M. *Phys. Rev. Lett.* **2009**, 102, 03501

[103] Struick, L.C.E.; *Physical Aging in Amorphous Polymers and Other Materials*, Elsevier, Amsterdam **1978**

[104] Ngai, K. L.; Rendell, R. W.; *Supercooled Liquids, Advances and Novel Applications* (ACS Symposium Series 1997 vol 676) ed. Fourkas J. T.; Kivelson, D.; Mohanty, U.; Nelson, K.; (Washington, DC: American Chemical Society) chapter 4, **1997**

[105] Ngai, K.L.; Casalini, R.; Capaccioli, S.; Paluch, M.; Roland, C. M.; *Dispersion of the Structural Relaxation and the Vitrification of Liquids*, pp. 79-138, volume in monograph "Fractals, diffusion and Relaxation in disordered Complex Systems", Advances in Chemical Physics, 133, (ISBN: 0-471-72507-2), Kalmykov, Y. P.; Coffey, W. T.; Rice, S. A.; Willey, New York **2006**

[106] K. L. Ngai, *J. Phys.: Condens. Mat.* **2003**, 15, S1107

[107] Floudas, G.; Paluch, M.; Grzybowski, A.; Ngai, K.L.; Molecular Dynamics of Glass-Forming Systems – Effect of Pressure, Springer-Verlag **2011**

[108] Forsman, H.; Anderson, P.; Bäckström, G.; *J. Chem. Soc. Faraday Trans.* **1986**, 2, 857

[109] Paluch, M.; Grzybowska, K.; Grzybowski, A.; *J. Phys.: Condens. Matter* **2007**, 19, 205117

[110] Hong, L.; Novikov, V.N., Sokolov, A. P.; *J. Non-Cryst. Solids* **2011**, 357, 351–356

[111] Paluch, M.; Rzoska, S. J.; Habdas, P.; Ziolo, J.; *J. Phys.: Condens. Matter* **1996**, 8, 10885-10890

[112] Andersson, S. P.; Andersson, O. *Macromolecules* **1998**, 31, 2999-3006

[113] Johari, G. P.; Goldstein, M.; *J. Chem. Phys.* **1970**, 53, 2372

[114] Johari, G. P.; *J. Chem. Phys.* **1973**, 58, 1766

[115] Ngai, K. L.; Paluch, M.; *J. Chem. Phys.* **2004**, 120, 857

[116] Kudlik, A.; Benkhof, S.; Blochowicz, T.; Tschirwitz, C.; Rössler, E.; *J. Molec. Struct.* **1999**, 479, 201

[117] Dixon, P. K.; Wu, L. Nagel, S. R.; Williams, D.; Carini, J. P.; *Phys. Rev. Lett.* **1990**, 65, 1108

[118] Lunkenheimer, P.; Wehn, R.; Riegger, Th.; Loidl, A.; *J. Non-Cryst. Solids* **2002**, 307–31, 336–344

[119] Gainaru, C.; Kahlau, R.; Röossler, E.;. Böhmer, R.; *J. Chem. Phys.* **2009**, 131, 184510

[120] Hensel-Bielowka, S.; Paluch, M.; Ngai, K. L.; *J. Chem. Phys.* **2005**, 123, 014502

[121] Kudlik,A.; Tschirwitz, C.; Benkhof, B.; Blochowicz, T.; Rössler, E.; *Europhys. Letter* **1997**, 40, 649

[122] Ngai, K. L.; Capaccioli, S.; *Phys. Rev. E* **2004**, 69, 031501

[123] Paluch,M.; Pawlus, S.; Hensel-Bielowka, S.; Kaminski, K.; Psurek, T.; Rzoska, S. J.; Ziolo, J.; Roland, C. M.; *Phys. Rev. B* **2005**, 72, 224205,

[124] Alpha and Beta Analyzers, NovoControl User's Manual 2004,

[125] Gao, N.; Starink, M. J.; Langdon, T. G.; *Mat. Sci. Tech.* **2009**, 25, 687-698

[126] Brown, M. E.; Introduction to Thermal Analysis Techniques and Application, Hot Topics in Thermal Analysis and Calorimetry, Vol. 1, Ed. Simon, J.; Kluwer Academic Publishers, New York 2001

[127] Starink, M. J.; Int. Mat. Rev.; 2004, 49, 191-226

[128] He, B. B.; Two-Dimmensional X-ray Diffraction, Wiley & Sons, New Jersey (2009)

[129] Kumar, S.; Liquid Crystals, Experimental Study of Physical Properties and Phase Transitions, Cambridge University Press, Cambridge (2001)

[130] http://frontpage.okstate.edu/nanotech/Assignments/Readings/XRD/XRD-Basics.pdf

[131] Descamps, M.; Amorphization and manipulation of the amorphous state by milling of molecular materials, 6th International Discussion Meeting on Relaxations in Complex Systems Rome, 2008

[132] Carpentier, L.; Descamps, M.; Influence of the preparation method (thermal quench, ball-milling, dehydration and freeze-drying) on the dynamical properties of glassy trehalose, Private Communication

[133] Capaccioli, S.; Ngai, K. L.; Shinyashiki, N.; *J. Phys. Chem. B* **2007**, 111, 8197-8209

[134] Ermolina I, G. Smith,. *J. Non-Cryst. Solids* **2011**, 357, 671-676

[135] Adrjanowicz K., Grzybowska K., Kaminski K., Hawelek L., Paluch M., Zakowiecki D., *Phil. Mag.*, **2011**, 91, 1926-1948

[136] Williams, G.; Watts, D. C.; *Trans. Faraday Soc.* **1971**, 67, 1971

[137] Capaccioli, S.; Prevosto, D.; Kessairi, K.; Lucchesi, M.; Rolla, P.; *J. Non-Cryst. Solids* **2007**, 353 3984–3988

[138] Shamblin, S.L.; Hancock, B.C.; Dupuis, Y.; Pikal, M. J.; *J. Pharm. Sci.* **1999**, 89,417–427

[139] Avrami, M.; *J. Chem. Phys.* **1939**, 17, 1103

[140] Wunderlich, B. ; Macromolecular Physics. Crystal Nucleation, Growth, Annealing ; Academic Press: London, **1976**; Vol. 2.

[141] Hikima, T.; Hanaya, T.; Oguni, M.; *J. Mol. Struct.* **1999**, 479, 245

[142] Hikima, T.; Hanaya, T.; Oguni, M.; *Bull. Chem. Soc. Jpn.* **1996**, 69, 1863

[143] Alie, J.; Menegotto, J.; Cardon, P.; Duplaa, H.; Caron, A.; Lacabanne, C.; Bauer, M.; *J. Pharm. Sci.* **2004**, 93, 218

[144] Xi, H.; Sun, Y.; Yu, L.; *J. Chem. Phys.* **2009**, 130, 094508

[145] Sun, Y.; Xi, H.; Ediger, M. D.; Richert,R.; Yu, L.; *J. Chem. Phys.* **2009**, 131,074506

[146] Hoffman J.D.; Weeks J.J.; *J. Chem. Phys.* **1962**, 37, 1723

[147] Bhugra, C.; Pikal, M. J.; *J. Pharm. Sci.* **2008**, 97, 1329-1349

[148] Kaushal, A. M.; Bansal, A. K.; Eurp. *J. Pharm. Biopharm.* **2008**, 69, 1067-1076

[149] Zhou, D.; Zhang, G. G. Z.; Law, D.; D. J. W. Grant, E. A. Schmitt, *J. Pharm. Sci.* **2002**, 91, 1863-1872

[150] Cangialosi, D.; Alegria, A.; Colmenero, J.; *J. Chem. Phys.* **2006**, 124, 024906

[151] Scopigno, T.; Cangialosi, D.; Ruocco, G.; *Phys. Rev. B* **2010**, 81, 100202 (R)

[152] Sidebottom, D. L.; *Phys. Rev. E* **2007**, 76, 011505

[153] Roos, Y. H.; Phase transitions in foods, Academic Press, London, **1995**

[154] Napolitano, S.; Wubbenhorst, M. *J. Phys.: Condens. Matter* **2007** , 19 , 205121

[155] Kaminski, K.; Wlodarczyk, P.; Hawelek, L.; Adrjanowicz, K.; Wojnarowska, Z.; Paluch, M.; Kaminska, E.; *Phys. Rev. B.* **2011**, 83, 061506

[156] Matsuoka, S.; *J. Pol. Sci.*, **2003**, 42, 511 – 524

[157] Fuss , T.; Ray, C. S.; Kitamura, Makihara, N. M.; Day, D. E.; *J. Non-Cryst. Solids*, **2003**, 318, 157–167

[158] Gutzow, I.; Durschang, D.; Russel, C.; *J. Mat. Sci.*, **1997**, 32, 5389-5403

[159] Russo, J.; Tanaka, H.; Soft Matter, 2012, 8, 4206-4215

[160] Shintani, H.; Tanaka, H.; *Nature Physics*, **2006**, 3, 200-206

[161] Kawasaki, T.; Tanaka, H.; *PNAS* **2010**, 107, 14036-14041

[162] Brás, A.R.; Noronha, J. P.; Antunes, A. M.; Cardoso, M. M.; Schönhals, A.; Affouard, F. Dionísio, M.; Correia, N. T.; *J. Phys.Chem B* **2008**, 112, 11087-99

[163] Paluch, M.; Hensel-Bielowka, S.; Ziolo, J.; *Phys. Rev. E* **2000**, 61, 526-533

[164] Pawlus, S.; Rzoska, S.J.; Ziolo, J.; Paluch, M.; Roland, C.M. *Rubber Chem. Tech.* **2003**, 76, 1106-1115

[165] M. Paluch, S. Casalini, S. Hensel-Bielowka, C. M. Roland, *J. Chem. Phys.*, 2002, Volume 116, Issue 22, pg. 9839-9845

[166] Hensel-Bielowka, S.; Paluch, M.; Ngai, K. L.; *J. Chem. Phys.*, **2005**, 123, 014502

[167] Roland, C. M.; Casalini, R.; Paluch, M.; *Chem. Phys. Lett.*, **2003**, 367, 259-264

[168] O'Reilly, J. M.; *J. Polym. Sci*, **1962**, 57, 429-444

[169] Atake, T.; Angell, C. A.; *J. Phys. Chem.*, **1979**, 83, 3218-3223

[170] Casalini, R; Roland, C. M.; , *J. Chem. Phys.*, **2003**, 119, 11951-11957

[171] Adrjanowicz K., Grzybowski A., Kaminski K., Paluch M., *Mol. Pharmaceutics* **2011** *8* (5), pp 1975–1979

[172] Konishi, T.; Tanaka, H. *Phys. Rev. B* **2007**, 76, 2200201